University of Washington
Department of Civil and Environmental Engineering

ATTENUATION OF RANDOM DEEP WATER WAVES BY A POROUS WALLED BREAKWATER

E. P. Richey
D. B. Morden
B. J. Hartz

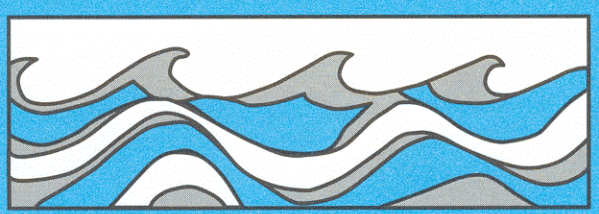

Water Resources Series
Technical Report No. 36
August 1973

Seattle, Washington
98195

Department of Civil Engineering
University of Washington
Seattle, Washington 98195

ATTENUATION OF RANDOM DEEP WATER WAVES BY A POROUS WALLED BREAKWATER

E. P. Richey
D. B. Morden
B. J. Hartz

Water Resources Series
Technical Report No. 36

August 1973

TECHNICAL REPORT STANDARD TITLE PAGE

1. Report No.	2. Government Accession No.	3. Recipient's Catalog No.

4. Title and Subtitle

ATTENUATION OF RANDOM DEEP WATER WAVES BY A POROUS WALLED BREAKWATER

5. Report Date
March 1974

6. Performing Organization Code

7. Author(s)
Richey, E.P., Morden, D.B., Hartz, B.J.

8. Performing Organization Report No.
C.W. Harris Hyd. Lab Report #36

9. Performing Organization Name and Address
Department of Civil Engineering
University of Washington
Seattle, Washington 98195

10. Work Unit No.

11. Contract or Grant No.
Y-1307

12. Sponsoring Agency Name and Address
State of Washington
Washington State Highway Commission
Department of Highways
Olympia, Washington

13. Type of Report and Period Covered
09/25/70 to 09/30/73

14. Sponsoring Agency Code

15. Supplementary Notes
in cooperation with the United States Department of Transportation
Federal Highway Administration

16. Abstract

The porous walled resonating chamber, a type of breakwater, is investigated as a means of reducing reflected waves from structures subjected to random wind generated waves in deep water. Extending laboratory monochromatic studies to a full-scale apparatus appended to a floating bridge allows assessment of scale factors and the effects of random waves on the predicted performance of the device as a linear damped oscillator. The full-scale device is shown to be frequency selective at a frequency precisely corresponding to the predicted resonance of the system. The forces, measured on the porous wall, are lower than predicted and the device completely eliminates the problem of wave runup onto the bridge roadway.

The method of evaluating the energy attenuation by the breakwater incorporates spectral analysis of digitized data recorded at fixed locations equidistant in front of the chamber and at a remote station away from the influence of the breakwater. Analysis demonstrates that the time average energy density at a fixed location where incident and reflected waves co-exist is influenced not only by the wave amplitudes, as expected, but also by the product of the amplitudes and a function of the phase angle. The chamber effects a change in the random phase angle during reflection, producing a different effective distance of wave travel to the fixed location and thus negating quantitative analysis of the energy dissipation.

17. Key Words	18. Distribution Statement
Wave attenuation, breakwater	

19. Security Classif. (of this report)	20. Security Classif. (of this page)	21. No. of Pages	22. Price
Unclassified	Unclassified	247	

Form DOT F 1700.7 (8-69)
HWY FORM 341-004 6/72

ACKNOWLEDGEMENTS

The research presented in this report was sponsored by the State of Washington, Washington State Highway Commission, Department of Highways, Olympia, Washington in cooperation with the United States Department of Transportation, Federal Highway Administration under Agreement Y-1307 for the project beginning date of 9/25/70, and subsequent amendments, acting by and through the Director of Highways under and by virtue of RCW 43.27.020, RCW 47.08.070, RCE 47.28.140. Contract administration was provided by the Office of Grant and Contract Services, University of Washington, Seattle, Washington.

The contents of this report reflect the views of the authors who are responsible for the facts and the accuracy of the data presented herein. The contents do not necessarily reflect the official views or policies of the Washington State Department of Highways or the Federal Highway Administration. This report does not constitute a standard, specification, or regulation.

TABLE OF CONTENTS

LIST OF FIGURES

LIST OF SYMBOLS

A_j, A_{jet}	total contracted pore jet area
A_p	total geometric area of pores
Attn	Attenuation
A_w, A_{wall}	total porous wall area (including A_p)
a	surface wave amplitude
a_i	incident wave amplitude
a_r	reflected wave amplitude
BW	station in front of the breakwater
b	breakwater chamber width
C	wave celerity
C_D	Discharge coefficient
D	distance from wall to gage
d	depth of water at S.W.L.
E_L	non-conservative energy converted during reflection process
$\overline{E}$	average total energy density per unit area of sea surface
$\overline{E}_K$	average kinetic energy density
$\overline{E}_p$	average potential energy density
e	natural logarithm base
f	frequency
g	acceleration due to gravity
H	wave height
H_i	incident wave height
H_r	reflected wave height
h	breakwater chamber depth
i	incident

j	index
k	wave number = $2\Pi/L$
L	wave length
m	effective breakwater porosity
m'	geometric porosity
$\overline{PE}$	average potential energy density
$\overline{KE}$	average kinetic energy density
R	reflection coefficient, H_r/H_i
S	reflection coefficient for a solid vertical wall
S.W.L.	still water level
T	wave period
t	time measurement
x	horizontal coordinate
z	vertical coordinate, + upward
γ	specific weight of water
δ	effective length of pore
η	wave surface elevation
η_i	incident wave surface elevation
η_r	reflected wave surface elevation
η_{max}	monochromatic wave envelope relative maximum surface elevation
η_{min}	monochromatic wave envelope relative minimum surface elevation
η_t	surface elevation resulting from the sum of η_i and η_r
θ_i	phase angle of incident wave
θ_r	phase angle of the reflected wave
Π	dimensionless constant, 3.1416

ρ	mass density of water
Σ	summation
σ	wave angular frequency = $2\pi f$. Also, variance.
τ	time lag
ω	chamber natural frequency
∞	a fixed measuring location in front of a solid vertical barrier; not influenced by the breakwater, but subject to the same average incident conditions.

CHAPTER I

INTRODUCTION

The present study investigates the response of a porous walled breakwater to random, wind generated, deep water waves, with the particular focus on the characteristics of waves reflecting from it. As shown in the sketch below, the porous wall breakwater is an L-shaped device which, when appended to a solid wall, forms a chamber with a porous front wall, a solid back wall and a solid but removable bottom. When attached to a barrier, such as a floating bridge, the chamber operates as an energy loss system reducing reflected wave energy while also reducing the structural loads on the barrier.

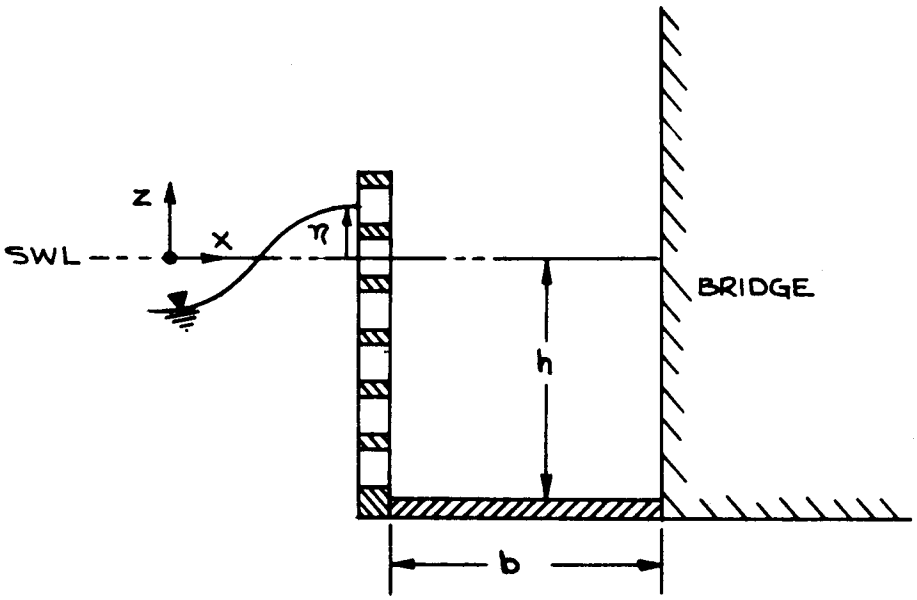

Incident waves impacting the device produce a pressure differential across the porous wall. A portion of the incident energy is reflected and the remainder enters the pores where the potential energy associated with wave height is converted to kinetic energy in the form of jets passing through

sharp edged orifices. Inside the chamber, the kinetic energy of the jets is dissipated through turbulent mixing and diffusion. When the level inside the chamber is sufficient to overcome the incoming momentum, the process reverses and again energy is lost through the non-conservative mixing and diffusion process. A laboratory and analytical model study had demonstrated that the system, when exposed to monochromatic waves, acted as a linear damped oscillator or resonator with a maximum efficiency at one discrete frequency, with the efficiency decreasing continuously on both sides of the dominant frequency. The laws for scaling breakwater performance under the monochromatic wave input to the prototype subjected to a random incident wave system are not well defined, so a field study was undertaken to obtain data for a critical assessment of the full-scale breakwater.

To monitor the efficiency of the full-scale breakwater, two stations are established to measure the sum of the incident and reflected wave heights. One station is in front of the breakwater and the second, or remote station, in front of the solid reflector (vertical pontoon wall) away from the influence of the breakwater. Small amplitude wave theory demonstrates that wave energy is related to the square of the wave height and that the sub-surface pressure fluctuations are functions of the surface disturbances. Over a period of time, the total incident energy of both stations will be the same. For the ratio of wave length to pontoon width under investigation, no waves are transmitted under the floating bridge. Thus, any difference in energy between the two stations can be attributed to a difference in reflected wave energy. Spectral analysis allows the superposition of waves of different frequencies to describe wave

height in a random sea. The energy is proportional to the squares of these superimposed components. Using spectral analysis, the random wave (subsurface pressure) records are analyzed and the time average total energy density at the remote station is compared with the total energy in front of the breakwater. The breakwater is also instrumented with force gauges to ascertain the maximum resultant force exerted by waves on the porous walls.

Porous walled resonating chambers can be tuned to create maximum energy dissipation at dominant incident wave conditions, resulting in a reduction of reflected waves and at the same time, reducing the loads on the floating structure.

Though the initial objectives and theory presume to acquire a quantitative evaluation of the amount of energy dissipated by the chamber, the analysis demonstrates a dependence of the time averaged energy density, for coexisting incident and reflected wave system, upon the product of the wave amplitudes, the physical distance to the barrier, and the phase angle. The chamber alters the phase angle during reflection. This results in the distance to the two measuring stations being effectively different in front of the breakwater and at the solid wall and thereby negating the desired comparison. Fortunately, the other objectives are independent of this problem.

Background and Literature Review

General:

Breakwaters have long been used to protect coastlines and vessels within harbors and marinas from storm damage. Traditionally they are constructed of rubble piled to a sufficient height and width to minimize the transmission of energy over or through the structure. Due to its relatively low cost and high efficiency, most shallow water installations still incorporate variations on the rubble mound concept including various interlocking concrete components.

The complex wave-rubble breakwater interaction in shallow water remains the topic of many recent publications.

The amphibious assaults and vessel damage repair requirements during the Second World War introduced the need for temporary and portable breakwaters. Hudson[1](1) conducted model tests on portable concrete caissons for use during the beach landings on D-Day. At the same time, the use of temporary floating breakwaters to reduce transmitted wave energy was investigated by Minikin(2).

In each of the preceding cases the breakwaters were used to reduce transmitted energy and the amount of reflected or dissipated energy was of little consequence. Most investigations dealt exclusively with devices placed in relatively shallow water where the characteristics of the incident waves were affected by the sloping bottom.

As water depth increases, rubble breakwaters become impractical. An early device used in deep water was the pneumatic breakwater which incorporated a submerged pipe emitting compressed air producing currents that reduce the transmission of wave energy through turbulent mixing and partial or complete breaking. Patented by Philip Brahser(3) in 1907, and in use in Dover, England for protection of boats since 1904, this device was the subject of several investigations during the 1950's.

Another device using the principle of an opposing current is the hydraulic breakwater, introduced in the mid 1950's. Nece, Richey, and Rao(4) investigated the use of the hydraulic breakwater to reduce the height of waves in deep water. Analytical work by Garrison(5) has demonstrated that a rigid

---

[1]NOTE: Superscripted numbers refer to number in reference section.

plate with zero draft reflects ninety percent of the wave energy incident upon it for wave length to bridge width ratios of 2.4:1. Ordinarily a breakwater is used to reduce transmitted energy. However, there are certain structural installations, such as piers, floating bridges, bulkheads, etc., where waves reflecting from the structure can be a concern if they should impinge on a site or shoreline sensitive to a new, or changed wave climate. A mechanism that would increase the losses in the reflection process would not only reduce the site interaction problem but at the same time could reduce the loadings on the structure and anchor system and thereby effect savings in construction and maintenance costs. The hydraulic breakwater lends itself well to this application. The submerged pipe can be run along the structure with the water jet aimed away from it. Unfortunately, the efficiency of these devices is quite low[4] and the power requirements are high. Other types of deep water energy reduction devices have been studied which require no power to drive them. Various types of floating breakwaters have been tested, including surface and subsurface rafts of various size, complexity and porosity. Investigations concentrate on reflection transmission, and energy dissipation through wave interference, forced instability of waves, and turbulent action and energy dissipation by porous and deformable surface membranes, as well as the breakwater motions and forces on the anchor cables.

Two energy attenuation concepts which can be attached directly to a floating platform and require no power to drive them are horizontal hollow cylinders and porous walled chambers. In 1964, Lawson[6] and Kirkham reported on various model studies including stacks of horizontal hollow cylinders to absorb waves within a rectangular ship mooring basin. The cylinders were placed longitudinally in stacks at the end of the basin, and were qualitatively

reported to show promise for reducing reflected waves. In 1968, Bourodimos and Ippen[7] reported on horizontal open tubes aligned with the direction of the wave travel. Tests of floating and fixed arrays of tubes of various lengths were shown to attenuate periodic wave energy by de-tuning the energy through currents induced within the tubes and by generating turbulence at both ends of the tubes. Unfortunately this interesting concept is primarily studied with relation to reducing transmitted energy. Peak energy dissipation was shown to occur for pipe lengths of approximately half of the design wave length. Application in a random wave system was not discussed. Possible applications of this device to floating bridges would require that the array of tubes be held some distance away from the solid structure. Research would have to be conducted on the interaction between the reflection wall of the bridge and the array. An alternative use would be to attach the tubes directly to the bridge forming an array of closed pipes of different lengths. This concept may also function as a de-tuning device but its efficiency would undoubtedly be much less than the open tube concept. Even if the open tube concept could be cantilevered from a reflecting surface of the bridge and still function well, pressures exerted on the horizontal surfaces of the tubes would result in large forces which would be exaggerated by the cantilever distance resulting in very large moments being transmitted to the bridge. Thus this design would reduce the reflected wave problem at the expense of additional structural loading on the bridge.

The porous walled breakwater, on the other hand, readily lends itself to incorporation in a floating bridge structure comprised of a porous wall set parallel to the solid wall of a floating bridge to form a chamber. The porous walled breakwater dissipates wave energy through turbulence and

diffusion mixing of the jets passing through the porous wall. This dissipation process reduces the reflected wave energy without transmitting the energy to the structure, which, combined with its ease of incorporation, justifies careful consideration of this device for application to floating bridge structures. The subject of this investigation is the extension of the knowledge about porous walled breakwaters, as based upon linear and monochromatic theory and model studies, to the full-scale wind/wave case, with emphasis on the reflected wave components.

Evolution of Porous Walled Breakwaters:

Studies relating to the effects of porosity on rubble breakwaters have been conducted for years primarily to define the effects of porosity on wave transmission and breakwater structural stability. In 1961, Jarlan[8] introduced a porous walled breakwater similar to that being considered in this investigation. A chamber was created by a porous front and solid back wall and a solid bottom. Jarlan presented experimental data for a fixed breakwater in shallow water but did not relate the importance of the various breakwater parameters. In 1965, Jarlan[9] applied acoustic theory to analyze the effects of holes in a vertical concrete breakwater which absorbed wave energy by dissipation in voids behind the porous wall. His major concern was with the construction of dikes and protection against shoreline erosion. From his shallow water studies and analytical work, Jarlan concluded that the wave chamber and wall porosity affect the efficiency of the breakwater but the width of the chamber was unimportant and the device was not frequency selective.

In 1966, Marks[10] investigated a mobile porous walled breakwater for fixed or floating application in shallow water. In comparing this device to a solid caisson-type structure he recorded approximately 50% less total force on the porous walled breakwater. Sloping the porous face 30° produced a six

fold increase in vertical forces. Interested primarily in bottom scouring and forces, Marks drew no conclusions about the wave reflections.

In 1968, a joint study by Marks and Jarlan[11] reviewed the effects of irregular wave trains on model porous walled breakwaters fixed to pilings and set on a shallow bottom. Their major concern was with force reduction and breakwater effects on scouring the bottom. The back wall was perforated as well as the front and a perforated interior wall was added to further reduce the forces on the structure. The interior wall was shown to be less effective than the perforated back wall. No information was given on wave reflection. Incidentally, an artificial island in the North Sea is presently being built (12,13) with a protective outer ring wall of the perforated "Jarlan" type.

The concept of resonating chambers is discussed by James[14] as rectangular cavities built into rubble breakwaters. Applying to shallow water and harbor entrances the optimum resonator geometry was shown to depend on harbor entrance width. Though the paper does not apply directly to the present investigation it does illustrate the importance of viewing chambers as frequency selective devices. Another demonstration of frequency selection occurs with double curtain wall chambers, which are composed of two solid vertical walls where the front wall is set slightly below still water level. Tonaka[15] demonstrated that the transmission coefficient for this device peaks at one frequency (the resonant frequency) and falls off with increasing or decreasing frequency. Tonaka did not record the characteristics of the reflected waves. Ricey and Sollitt[16] observed that the reflection coefficient of the double curtain wall devices obtains a minimum at the same resonant frequency that the maximum for the transmission coefficient occurs. The frequency sensitivity of the reflected wave energy has also beeen demonstrated for rubble type permeable breakwaters[17] where the reflection

coefficient decays as a damped oscillation with increasing wave frequency.

The porous walled breakwater was shown by Richey and Sollitt[16] to have similar optimum performance at a natural frequency. The natural frequency was shown to depend on the chamber characteristics of porosity, width, depth, and pore geometry as well as wave length and steepness. Results of model studies in single frequency waves suggest that the optimum porous walled device has the following characteristics:

Vertical porous wall.

Porosity: A uniform porosity, m´, between .2 and .3.

Chamber depth: Efficiency increases as depth increases to a depth of one half wave length.

Pore geometry: Circular holes provide an effective length of fluid mass accelerated through the pores to be equal to four-thirds the pore diameters[18].

Chamber width: Design variable.

Chamber width is selected as the method of tuning the breakwater to the dominant wave conditions at the location where the structure is to be used. Theory and model studies show that the chamber width controls the resonant frequency of the breakwater. The relationship between chamber width and incident wave length is dependent on all other breakwater parameters. Burrows[19] demonstrated that the forces on a porous wall (porosity = .196) in front of a solid wall were as little as 65% of the force calculated for a solid plate submerged to the same depth.

Objectives

The present investigation extends the model work of Richey and Sollitt[16] by testing a full-scale porous walled breakwater subjected to

wind generated random waves. The chamber width is varied with and without the solid chamber bottom to test the efficiency of the breakwater in an attenuating reflected wave energy over a wide range of wind speeds for each configuration. The force upon the porous wall is measured for each configuration.

The program initially focused on two aspects of the design extension, namely, the forecast for the breakwater performance and the omission of the bottom from the chamber. The forecast involved conventional modeling laws, and also the assumption that the reflection coefficient was a linear function of wave frequency, even though the analysis had shown it to be nonlinear and to depend upon other wave parameters as well. A key question is whether the breakwater responds in random wind-wave exposure in a manner similar to its performance as a linear damped resonator in model studies exposed to monochromatic waves. The extent to which scale factors relate the model and full-scale hardware will be analyzed.

Laboratory experimental data showed that if the chamber bottom were left off, the main effect was to shift the optimum performance toward the shorter wave lengths with only a nominal reduction in reflection coefficient. A second objective is therefore to check these laboratory results in random wave systems; the omission of the chamber bottom would simplify some field installations considerably.

A basic test section designed to accomplish the two objectives above would also contribute additional data of importance to the project as a whole and to the general subject of wave-structure interaction such as:

1. Data on the actual wave spectrum in Lake Washington as a function of wind speed and duration.

2. Extend the value of existing experimental and theoretical work by providing experimental links between the systems.
3. Force measurements to be compared with other prototype data and model results.
4. The reduction in wave overtopping onto the bridge roadway, a phenomenon not amenable to model analyses.
5. A measure of the scale effects between model and prototype.

Test Apparatus

A breakwater (Figure 1) section 38 feet long and having the cross section illustrated in Figure 2 is used for the basic full-scale test unit. A 3.3 foot, central portion of the vertical porous wall is mounted so that force data can be obtained from strain gages on cantilever beam which support the test panel. The width of the unit can be set at 3,5, or 7 feet, but is set at 5 feet initially; the bottom is removable.

Specific Application:

The effects of random, wind-generated, deep water wave systems on a porous walled breakwater are investigated by appending the full-scale prototype to the south side of Evergreen Point Floating Bridge traversing Lake Washington to join Seattle and Bellevue, Washington (Figure 3). The breakwater, attached near the midspan, has been exposed for a period of two years to the various wave conditions developed over a 2.8 mile effective fetch by dominant wind from the southern sector.

The sixty foot bridge pontoon width is sufficiently large compared with wave lengths present that transmitted wave energy is eliminated for all wind conditions. Thus, any incident energy produced over the fetch and not dissipated by wave breaking--or losses at the bridge becomes a reflected wave

system proceeding from the bridge. The floating pontoon span, 7580 feet long, traverses the typically 200 foot deep lake, 12° off from an east-west crossing. Thus, a southerly wind produces a progressive wave system which reflects from the vertical pontoon walls and proceeds toward the western shore at an approximate angle of 24°. For some wind conditions reflected waves impinge on the western shore 4,000 feet south of the bridge[20].

Wind roses show winds from the southerly sector to be dominant in frequency and magnitude followed by those from the north. Winds from the east or west seldom occur and are of short duration. Previous investigations[20] have shown that steady eight to twelve mph winds are required to form a significant reflected wave system. Wave breaking exists when wind conditions exceed 25-30 mph. Wave systems produced by winds in excess of 30 mph contain sufficient energy upon impact with the solid pontoon wall that runup overtops the guard rail eleven feet above still water level.

The overtopping water is windblown onto the windshields of traffic on the four lane, 50 mph roadway. Wind driven wave peaks resulting from wind conditions above 40 mph contain sufficient momentum to cross all four lanes of traffic. Though wind conditions in excess of 40-45 mph are rare, winds are high as 60 mph, gusting to 75 mph, have been recorded during the test period (March 26, 1971).

Design Constraints

To create a reasonable scope for the investigation and minimize the expenditure, the prototype breakwater was made of a length sufficient only to eliminate end-effects on a central force-instrument panel and at a pressure monitoring station in front of the breakwater. The presence of a high traffic density roadway immediately adjoining the test sight required that the

units be constructed in a modular form and transported for attachment to the bridge without modifications to the pontoon assembly. This was accomplished using a straightforward steel and wood modular construction, assembled at the University of Washington and transported to the bridge by barge where they were appended to the bridge using hooks over the guard rail and held rigidly in place by cables running under the bridge to the guard rail on the opposite side. It was necessary that the breakwater be capable of withstanding exposure to wind and wave conditions produced by 60 mile an hour winds, and remain operational for an unspecified period of months. Thus, the structure was carefully designed to provide an appropriate tradeoff between strength and economy.

CHAPTER II

THEORY, APPLICATION, AND PREDICTION

Overview

Wind blowing over a body of water imparts energy to the surface producing a random wave system. If the resulting progressive wave system impacts a barrier, conservation of energy requires that the energy either be transmitted, dissipated, or reflected. If the wind speed is sufficiently high instability will occur and some energy will be dissipated through the turbulence losses associated with wave breaking. Once reflected, the wave train traveling against the wind contains significant amounts of energy which are slowly consumed by viscous shear. Previous investigations[20] have shown impingement of reflected waves on the shoreline 4000 feet from the bridge (25% of the fetch length).

The bridge pontoons form a semi-immersed, rectangular floating breakwater with a width nearly equal to the longest incident wave length. This eliminates any significant transmission of energy to the lee side of the bridge. The use of solid vertical walls on the pontoons results in a nearly perfect reflection barrier. Thus, almost all of the energy imparted by the wind to the incident wave train is reflected and proceeds upwind. A reduction of reflected wave energy can most efficiently be accomplished by converting energy to non-conservative forms using a breakwater device at or near the barrier. The condition of deep water which necessitates the construction of a floating bridge also restricts the type of breakwater which can logically be incorporated for increasing losses.

The porous walled resonating chamber being investigated lends itself readily to incorporation with a floating structure. The device converts the

potential energy of the incident wave into kinetic energy as jets of water passing through sharp edged orifices where non-conservative turbulent mixing and diffusion dissipate a portion of the energy. An advantage of this loss mechanism, besides requiring no power to drive it, is that the energy does not affect the structure. The result is a device that reduces the reflected waves while reducing the loading on the structure. The load reduction can result in structural design and operating cost reductions.

The measurement of the efficiency of the porous walled chamber is a problem. Small amplitude wave theory demonstrates that the average total energy per unit surface is proportional to the square of the wave height. Though the wave heights in a wind generated sea surface are quite complex, they can be treated as a linear summation of sinusoidal waves of various amplitudes, frequencies, and phase angles. A wave height sensor is mounted in front of the chamber to measure the combined field of incident and reflected waves. The net force experienced by the porous wall is monitored at the center of the structure. A second (remote) station in front of the solid vertical bridge wall and away from the influence of the breakwater is used to establish the wave height without the chamber.

Surface piercing gages, available at the outset of the investigation, were found to lack the resolution necessary to function in fresh water. Small amplitude wave theory also establishes the sub-surface pressure fluctuations as a unique function of the surface waves. Therefore, sub-surface pressure transducers are used to monitor the vertical pressure at a constant depth in front of the chamber and at the remote station. The pressure is proportional to the wave height which, in turn, is proportional to the square root of the total energy.

In principle, the efficiency of a given chamber configuration is established by analyzing the pressure fluctuations due to the sum of the incident and reflected waves in front of the breakwater and at the remote station away from the influence of the breakwater. For all conditions of interest, at the particular test site studied, transmitted energy is zero[20]. Over a period of minutes the total incident wave energy at the two stations, separated by 150 feet, is the same. Thus any difference in the total energy monitored at the two stations can be attributed to a change in the reflected wave energy.

Over the period of minutes during which a record is taken, the wind generated waves are approximately stationary Gaussian random processes with zero averages. As such, the relevant statistical properties are contained in the autocovariance function and the power spectrum. The exact computation of the spectrum would require a record of infinite length. The acquisition of analog records twenty to sixty minutes in length allows calculation of spectral estimates for digitized sections of the data using the window closing technique of Jenkins and Watts[21].

Small Amplitude Wave Theory

A classical and basic simplified description of wave motion is described by small amplitude wave theory. Small amplitude or linear wave theory is developed in detail in numerous texts, i.e., Lamb[22] and Ippen[23]. The theory, based on mathematical potential flow analysis of an ideal fluid, provides a useful treatment of wave motion and forces for real waves of finite height. The theory is not applicable in conditions where there is wave breaking. Sinusoidal wave profiles predicted from the theory provide an equal distance from the still water level to the crest of the trough. In

actuality, the crest is somewhat higher than the trough. The fundamental relationship between the wave period, T, wave length, L, and the wave speed, C, for the sinusoidal wave is

$$T = \frac{L}{C} \qquad 1$$

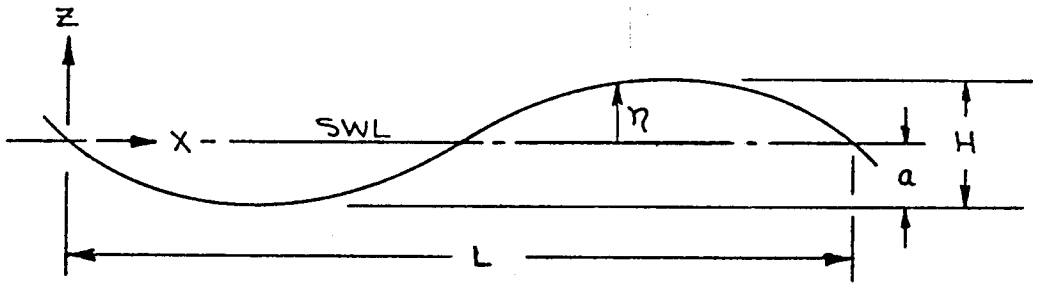

In general, the theory relates the wave speed to wave length and depth, d, by

$$C^2 = \frac{gL}{2\pi} \tanh \frac{2\pi d}{L} \qquad 2$$

but $$\frac{L^2}{T^2} = C^2$$

Therefore, combining the above equations yields

$$L = \frac{gT^2}{2\pi} \tanh \frac{2\pi d}{L} \qquad 3$$

Thus, for a known water depth each wave period corresponds to a unique wave length. For depths greater than one-half of the wave length, the hyperbolic tangent function approaches unity, making the wave speed independent of depth. For deep water conditions, the basic relationship between wave velocity and wave length is

$$C^2 = \frac{gL}{2\pi} \qquad 4$$

Substituting the square root of Equation 4 into the fundamental relationship, speed equals length divided by period gives

$$C = \frac{gT}{2\pi} = \frac{gT}{2\pi} = 5.12T \qquad 5$$

This can also be rewritten as

$$L = 5.12T^2 \qquad 6$$

A table demonstrating the relationship between the various deep water parameters relevant to the present investigation is shown in Figures 4 and 5.

Conservation of energy requires that energy transmitted by wind and the progressive wave system incident to the vertical wall on the floating bridge must either be transmitted, reflected or dissipated through losses. Though the losses due to breaking of the waves cannot be accounted for by small amplitude wave theory, the linear theory will provide a relationship between wave height and energy. The average potential energy density, $\overline{PE}$, of a single frequency progressive wave per unit area of sea surface (energy density) is due to the displacement of the water surface and is shown by linear theory to be equal to

$$\overline{PE} = \frac{\gamma}{4L} \int_0^t \eta^2 \, dt = \frac{\gamma a^2}{4} \qquad 7$$

where a is the wave amplitude and γ is the specific weight of water.
The kinetic energy, KE, of the water particles per unit area of sea surface averaged over a wave length is equal to

$$\overline{KE} = \frac{\gamma a^2}{4} e^{4\pi nL} \approx \frac{\gamma a^2}{4} \qquad 8$$

Thus, the average energy per unit area of sea surface for a progressive wave contains equal contributions from the kinetic and potential energy. The resulting average energy density is

$$\overline{E} = \frac{\gamma a^2}{2} = \frac{\gamma H^2}{8} \qquad 9$$

For the case of a complex surface the superposition of linear components provides the result that

$$\overline{E} = \frac{\gamma}{8} \sum_{j=1}^{n} H_j^2 \qquad 10$$

Loss Mechanism of a Porous Walled Breakwater

As progressive incident waves strike the porous wall, the difference in head between the incident wave and the water inside the chamber creates a pressure differential across the porous wall. Some of the wave energy is reflected from the wall and the remainder enters the pores, or square-edged orifices. Potential energy of the incident wave height is converted to the kinetic energy of jets passing through the orifices (Figures 6 and 7). As the jets mix with the fluid inside the chamber, the kinetic energy is lost due to non-conservative turbulent mixing and diffusion. When the level inside the chamber is sufficient to overcome incoming momentum, the process reverses and the jets exiting the chamber again have kinetic energy converted to losses through further turbulent mixing and diffusion. The outgoing energy results in the generation of another reflected wave.

Measurement of Wave Height

Initial attempts to measure the wave height with a fixed surface piercing gage showed insufficient resolution in fresh water with the equipment available at the beginning of the test. An alternate method was chosen using sub-surface pressure transducers. The sub-surface pressure fluctuations can be shown to be a direct function of the surface waves. Small amplitude wave theory shows that the pressure beneath the surface is equal to

$$P = \gamma[\eta \frac{\cosh(\frac{2\pi}{L}(d + Z)}{\cosh(\frac{2\pi}{L} d)} - Z] \qquad 11$$

For our investigation, d = 200 ft., Z = - 5 ft. (Z up defined as positive). Therefore the variables are L and η. Contributions of the hyperbolic cosine terms for wave lengths of 20 and 40 ft. are shown as follows:

$$L = 20: \quad \frac{\cosh \frac{2\pi(195)}{20}}{\cosh \frac{2\pi(200)}{20}} = .992 \qquad 12$$

$$L = 40: \quad \cosh \frac{2\pi(195)}{40} = .993$$

Thus, the primary variable is

$$\eta = \frac{H}{2} \sin (\frac{2\pi x}{L} - \sigma t) \qquad 13$$

Therefore, time dependent pressure fluctuations are directly related to wave height and, through equation 10, can be used to obtain the wave energy. The above is shown for a single harmonic, while the actual sea state contains many components which are treated by linear superposition during analysis. The pressure is shown to be a unique function of the wave height and in turn the energy differences at the two measuring stations, one in front of the

breakwater, the other away from the influence of the breakwater are derived from the spectral analysis of the squared pressure fluctuations. The pressure sensors were at the same depth (five feet) beneath the water surface and the concern was with the difference in energy between stations, so the conversion from pressure at depth to equivalent wave height need not be performed. The $-\gamma Z$ contribution to the pressure (equation 11) due to hydrostatic pressure on the transducer is 2.16 p.s.i. The output signal of the data acquisition amplifier establishes the 2.16 psi a zero output to allow the entire recorded data signal to be wave induced pressure fluctuations.

Wave Reflection; Reflection Coefficient and Energy Dissipation

In the laboratory experiment on the porous walled breakwater (16) waves of a single frequency (monochromatic) were used, so the reflection coefficient R, defined as the ratio of reflected wave height (H_r) to the incident wave height (H_i) can be obtained from

$$R = H_r/H_i = \frac{\eta_{max} - \eta_{min}}{\eta_{max} + \eta_{min}} \qquad 14$$

wherein η_{max} and η_{min} are the maximum and minimum amplitudes of a wave envelope developed by traversing a height gage through the standing wave which developed in front of the model breakwater. The technique inherent in the statement of Eq. 14 can be applied when only two components are present, so it cannot be used to reduce a random wave field to its components.

The premise assumed in planning the full-scale experiment was that the energies in a composite wave system could be expressed as proportional to sum of the squares of the wave heights (Eq. 10) of the individual waves composing the system, and that pressure (height) measurements at two stations, one (designated ∞) at a depth of 5 feet and a horizontal distance of 7 feet in

front of the vertical wall of the bridge and another (designated B.W.) the same depth and distance in front of the porous breakwater could be analyzed to determine the difference in energy between the two locations. Practically no energy is transmitted by the Evergreen Point Bridge at any of the wave frequencies encountered on Lake Washington; the vertical plane wall of the bridge is nearly a perfect reflector until wave breaking and overtopping occur, so the difference between the energies at the two stations is attributable to the energy dissipation introduced by the breakwater. By locating the two gages identically with respect to depth and distance from the walls of concern, the need for correcting the pressure data to surface heights and accounting for secondary effects to the two locations can be eliminated by focussing on the differences in energy between the two locations, i.e.:

$$E_{\infty} = E_i + E_{r\infty} \qquad 15$$

$$E_{BW} = E_i + E_{rBW} \qquad 16$$

The energy at B W should be equal to or less than that at the remote station (∞). The reflection process from the vertical wall is an efficient one, so, until breaking and overtopping develop, $E_i \tilde{=} E_{r\infty}$ and

and $$E_{\infty} = 2\, E_i \qquad 17$$

$$E_{r_{BW}} = E_{BW} - [E_{\infty}]/_2 \qquad 18$$

$E_{r_{BW}}$ is the energy in the wave system reflected from the porous wall.

The average energy densities, $\bar{E}_{\infty}$ and $\bar{E}_{BW}$, can be determined from spectral analyses of the pressure data from the two gages, the energy in

reflected system computed from Eq. 18, and the effectiveness of the breakwater as a ratio of $E_{r_{BW}}/E_{\infty}$.

In the lab study[16], the reflection coefficient $R = H_r/H_i$, as determined from model data, was used to predict energy spectrum for the reflected wave, and then the energy loss due to the breakwater was found as the difference between the predicted incident and reflected spectra.

The energy dissipation due to porous breakwater is a very basic notion, and can be used alone to compare the relative effectiveness of different breakwater geometries and incident wave conditions. Although, the reflection coefficient is a convenient concept, and was used in the lab study to predict the energy loss dissipation by the breakwater, it cannot be found directly from the pressure data at the two sites. It can be predicted, by computing an incident height-frequency curve from the pressure data at station ∞, and predicting a reflected height-frequency curve by using the computed energy E_{BW} by the method used to predict the reflected wave spectrum in (16, p. 58). It should be pointed out again, that the concern is to evaluate the energy reduction accomplished by the breakwater--the reflection coefficient is a convenience term.

The reflection coefficient has been shown by dimensional reasoning (ref. 16, p. 35) to depend upon the set of variables

$$R = f(m, H_i/L, b/h, h/L, \delta b/mLh) \qquad 19$$

wherein m is the porosity, L is the wave length, b the breakwater width, h its depth, and δ the effective pore length. A key question is whether the breakwater responds in the random wind wave exposure in a manner similar to its performance as a linear, damped oscillator in the model basin where

the input waves were monochromatic. The measures of its response will be the sensitivity of the reflection coefficient (or energy loss) to the terms in Eq. 19, particularly to the last term. An alternative form for this term is σ^2/ω^2, where $\underline{\sigma}$ is the wave angular frequency and $\omega^2 = mgh/\delta b$, the breakwater width is changed and measurements are taken over a range of input wave conditions so the wave parameters containing wave height and length (or frequency) will vary. The bottom of the breakwater is removed for another set of conditions. Though no theoretical analysis of performance was made in (16) with the bottom out, the empirical data from the lab experiment provides a basis for a similarity comparison between the model and the prototype.

The reflection coefficient can be related to the amount of energy dissipated during the reflection process. Conservation of energy requires that

$$E_i = E_r + E_t + \text{dissipation losses} \qquad 20$$

For the present investigation the transmitted energy is zero. Thus the amount of potential and kinetic energy dissipated (converted) to non-conservative energy such as turbulence or heat is

$$E_D = \text{Dissipation losses} = E_i - E_r \qquad 21$$

From small amplitude theory $E = \frac{\gamma H^2}{8}$

$$E_D = \frac{\gamma}{8}\left[H_i^2 - H_r^2\right] \qquad 22$$

As a ratio of the energy not recovered during reflection to the available incident energy the

$$\text{Energy dissipation ratio} = \frac{E_D}{E_i} = \frac{\frac{\gamma}{8}\left[H_i^2 - H_r^2\right]}{\frac{\gamma}{8} H_t^2} \qquad 23$$

$$\% \text{ energy dissipated} = (1 - R^2)\ 100 \qquad 24$$

The percentage of energy dissipation represents the efficiency of a device in converting incident energy into non-conservative forms and thereby reducing the reflected wave energy. For example, perfect reflection (R = 1) results in zero dissipation during reflection, while the total elimination of reflected waves (R = 0) corresponds to a 100% energy dissipation (see Figure 8).

Method of Evaluating Energy Dissipation

To evaluate the effectiveness of the full-scale porous walled breakwater in reducing reflected wave energy from a solid vertical barrier, two stations are established to measure the sum of the incident and reflected wave height. The presence of a continuous floating structure at the test site eliminates transmitted wave energy, and also negates the possibility of obtaining incident or reflected wave signals individually. Thus, the method proposed at the outset of the investigation for determining the reflected energy reduction by the breakwater exposed to random incident waves requires the following steps.

1) Time histories of the summations of the random waves are simultaneously acquired over periods of at least twenty minutes at each station, one in front of the breakwater and the second an equal distance in front of the solid reflector (bridge pontoon wall) away from the influence of the breakwater (See Figure 1).
2) Small amplitude wave theory demonstrates that the energy in a progressive wave is proportional to the square of the wave height and that the wave

heights of waves progressing in opposite direction add linearly.

Under the linear assumption a random wave can be described by the superposition of a Fourier series of sinusoidal waves of different frequencies and associated amplitudes. Using spectral analysis the time average total energy density, calculated from the variance, is obtained at each station.

3) Over a period of minutes the incident energy at the two stations is the same. Thus, any difference in the average total energy density at the two locations must be due to a difference in reflected wave energy.

Following this line of reasoning the wave height at the fixed station in front of the solid vertical wall (∞, denoting the conditions without a breakwater) is the superposition of the incident (i) and reflected (r) components

$$\eta(t)_{\infty} = \eta(t)i_{\infty} + \eta(t)r_{\infty} =$$

$$[\sum_j \frac{H_j}{2} \cos(-2\pi f_j t + \phi_j)]_{i\infty} + [\sum_k \frac{H_k}{2} \cos(+2\pi f_k t + \phi_k)]_{r\infty} \qquad 25$$

where ϕ_i and ϕ_k are the phase angles associated with the various random components likewise the wave height in front of the breakwater (B W) are

$$\eta(t)_{BW} = \eta(t)_{iBW} + \eta(t)_{rBW}$$

$$= [\sum_j \frac{H_j}{2} \cos(-2\pi f_j t + \phi_j)]_{i_{BW}} + [\sum_k \frac{H_k}{2} \cos(+2\pi f_k t + \phi_k)]_{r_{BW}} \qquad 26$$

The average energy content in a random wave is found from spectral analysis to be proportional to the variance, σ^2. The variance for a series of cosine waves of different frequencies, f, and amplitudes, a_j, equals $\sigma^2 = \sum_j \frac{1}{2} a_j^2$. Thus, recalling equation 10, the average energy density of the incident and reflected waves in front of the solid wall and in front of the breakwater

can be expressed by the specific weight, γ, times the respective variances. The average total energy density in front of the breakwater,

$$\bar{E}_{BW} = \gamma\sigma^2_{BW} = \gamma(\sigma^2_{i_{BW}} + \sigma^2_{r_{BW}}) \qquad 27$$

and the corresponding average total energy density in front of the solid wall is

$$\bar{E}_{\infty} = \gamma\sigma^2_{\infty} = \gamma\ (\sigma^2_{i_{\infty}} + \sigma^2_{r_{\infty}}) \qquad 28$$

The variance is obtained over a sufficient period of time (5.6 minutes) that the average incident energy to the two locations is the same, i.e.,

$\gamma\sigma_{i_{\infty}}{}^2 = \gamma\sigma_{i}{}^2_{BW} = \gamma\sigma_i{}^2$. Therefore,

$$\bar{E}_{BW} = \gamma\sigma^2_{BW} = \gamma(\sigma_i{}^2 + \sigma^2_{r_{BW}}) \text{ and} \qquad 29$$

$$\bar{E}_{\infty} = \gamma\sigma^2_{\infty} = \gamma(\sigma^2_i + \sigma_{r_{\infty}}{}^2). \qquad 30$$

Subtracting equation 29 from 30 results in the average energy density difference at the two stations due to the presence of the breakwater

$$\bar{E}_{\infty} - \bar{E}_{BW} = \gamma(\sigma^2_{r_{\infty}} - \sigma^2_{BW_{\infty}}) \qquad 31$$

This amount of energy decrease cannot be expressed as a percentage of the incident energy because $\gamma\sigma^2_i$ cannot be obtained independently. Though the wave spectra for the incident wave alone cannot be measured, the method described by (16, pg. 58) provides a means of predicting a reflected height-frequency curve. Alternatively, the energy can be ratioed to the average total energy density in front of the solid wall, σ^2_{∞}. This ratio is defined as attenuation

$$\text{ATTENUATION} \equiv \frac{\text{Average Reflected Wave Energy Decrease Due to the Breakwater}}{\text{Average Total Energy without the Breakwater}}$$

$$= \frac{\bar{E}_\infty - \bar{E}_{BW}}{\bar{E}_\infty} = \frac{\gamma(\sigma_\infty^2 - \sigma_{BW}^2)}{\gamma\sigma_\infty^2} =$$

$$\therefore \text{ATTENUATION} = 1 - \frac{\sigma_{BW}^2}{\sigma_\infty^2} \qquad 32$$

Example of Reduction in Energy by a Linear Damped Oscillator. The oscillator, or resonator, can only affect the amplitude and phase of the incident wave not the frequency. The complex wind generated incident wave can be decomposed into a number of sinusoidal waves each having a different frequency, random phase, and an associated wave height. For this illustration the incident wave has a peak frequency of .3, that is .3 is the frequency of the component wave assigned the greatest wave height. Suppose, for example, the square of the non-dimensional incident and reflected wave height vs. frequency distribution in front of the breakwater is that shown in the figure below.

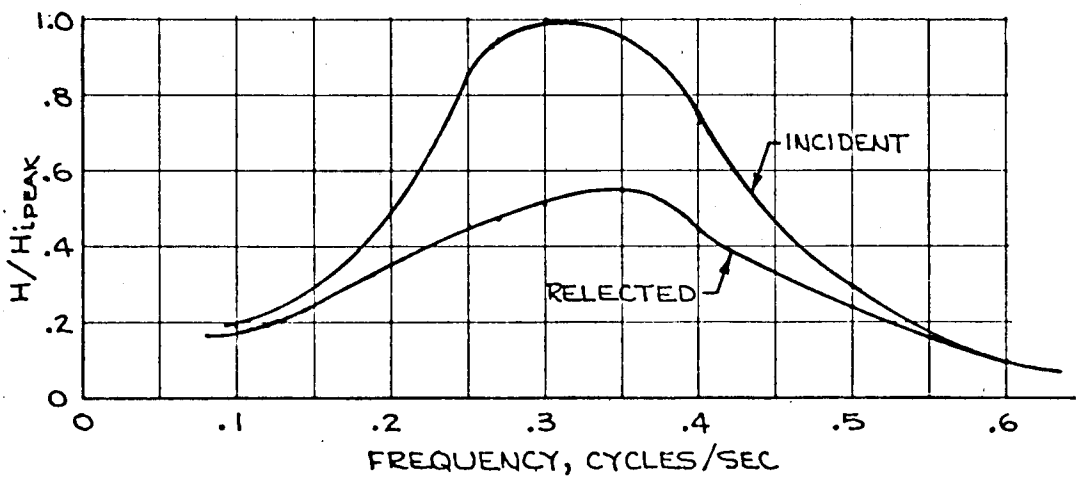

The breakwater, operating as a resonator reduced the amplitude of the incident wave at every frequency below .6. The maximum reduction occurred at f = .27. The peak reflected energy occurred at .35. The knowledge that the system models as a linear resonator provides the information that the difference in reflected wave height at the frequencies .27 and .35 is solely due to a selective reduction in the incident wave height by the breakwater for the two distinct frequencies. None of the reduction in wave height at f = .27 was accomplished by the reassignment of incident wave height at that frequency to reflected wave height at a different frequency.

The reflection coefficient for this example would be the ratio of H_r/H_i for each increment of frequency.

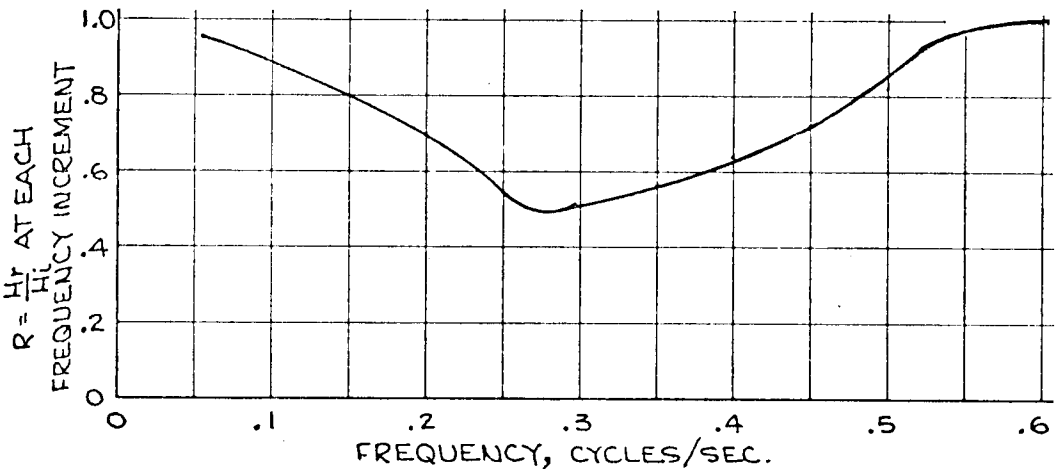

The associated non-conservative energy conversion is

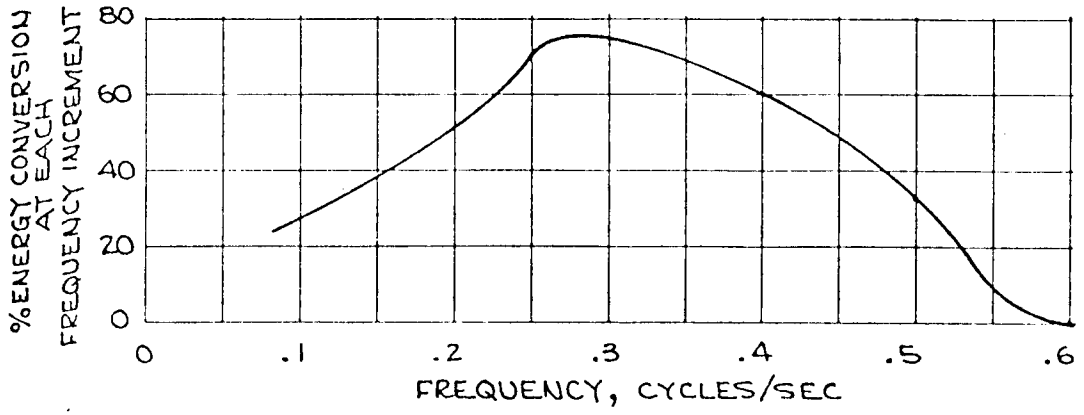

Expected Conditions at Test Site

The model studies of the porous wall breakwater subjected to monochromatic waves by Richey and Sollitt [16] produced the following results. The chamber is frequency dependent upon the wave frequency and steepness as well as the chamber characteristics of porosity, depth, pore geometry and chamber width. The chamber was shown to act as a linear damped oscillator or resonator, having a natural frequency

$$\omega = \sqrt{\frac{mgh}{\delta b}} \qquad 33$$

where m is the effective porosity, h - the chamber depth, δ - the effective core length, taken as 1.3 times the diameter of the orifice, and b is the chamber width.

The ratio of the model chamber depth to the full-scale requirement of 6.4 feet provides a scale ratio of 1:12. Figure 9 shows the model experimental reflection coefficient for a breakwater that would scale to a four foot chamber width, have a geometric porosity of .196 using one foot diameter holes uniformly spaced on two foot centers, and include a solid bottom. Figure 10 presents the corresponding experimental reflection coefficient for a chamber with the only variable change being an increase in geometric porosity to .333. Comparison of the two figures indicates that the minimum reflection coefficient is shifted to higher wave numbers as the porosity increases and the range of wave numbers over which the chamber is effective increases. The theory [16] predicts a decreasing reflection coefficient with increasing porosity up to an optimum porosity, and the experimental results indicate that the optimum occurs between .2 and .3 (16, Figure 3). Based on the model results for the full-scale investigation m' is chosen as .293, produced by one foot diameter holes uniformly spaced on eighteen inch centers.

Figure 11 displays the shift in minimum reflection coefficient with variations in chamber widths for the model chamber with .196 geometric porosity. From the discussion above, the minimum reflection coefficient corresponding to each chamber width should be shifted to higher wave numbers (smaller wave lengths) for the prototype due to the increased porosity.

Removal of the bottom from the breakwater shifts the occurrence of the minimum reflection coefficient to higher wave numbers and produces a higher minimum reflection coefficient as shown in Figure 12.

Having established an appropriate prototype porosity the variable remaining to tune the breakwater is the chamber width. For maximum energy dissipation the chamber width must be chosen to produce a minimum reflection coefficient near the frequency for which the wave energy at the test site is a maximum. The natural frequency can be determined from equation 33.

$$b = \frac{mgh}{\delta\omega^2} \tag{34}$$

Experimental results indicate the maximum energy dissipation occurs near $\sigma^2/\omega^2 = 1.2$. Thus

$$b = \frac{mgh(1.2)}{\delta\sigma^2} = \frac{1.2mgh}{\delta(2\pi f)^2} = \frac{1.2mhL}{2\pi\delta} \tag{35}$$

where m is the geometric porosity times an appropriate jet discharge coefficient[16][25] of approximately .77. The prototype chamber width can thus be expressed as a function of incident wave length

$$b = \frac{1.2(.77)(.293)(6.4)(L)}{2\pi\ (4/3)} = .207L \tag{36}$$

or as a function of wave frequency

$$b = \frac{1.2(.77)(.293)(32.174)(6.4)}{16/3\pi^2\ f^2} = 1.06/f^2 \tag{37}$$

where the wave length or frequency should correspond to the maximum energy condition at the test site.

The calculated effective fetch for the test sight on the Evergreen Point Floating Bridge is 2.8 miles (calculation Figure 13). An annual wind rose for the area, Figure 14, indicates that winds from the southerly section are dominant in frequency and magnitude. Maximum wind speeds and duration expected are approximated by Figure 15. Previous investigations[20] have shown that steady eight to twelve mph winds are necessary to create a significant reflected wave system. Thirteen to thirty mph winds often occur. Forty mph storms lasting up to five hours occur at the test site during the winter. The short duration maximum recorded during the two years test period was 60 mph gusting to 75 mph. The significant wave height and frequency as a function of the windspeed at the test site is shown in Figure 15 (predicted by the method presented in (24).

Though the breakwater must be capable of withstanding the extreme wave conditions, the chamber width is selected to produce maximum energy dissipation for wave conditions which produce the maximum total reflected energy. Windspeeds of 8-12 mph are required to produce a noticeable reflected wave system[20]; thus, even though Figure 14 shows that the majority of the time incident winds speeds are below 12 mph, it is of no value to tune the chamber to these conditions. As shown in Figure 16, the increase in wave height at the test site is approximately linear with increasing windspeed. Since energy is proportional to the square of the wave height, a dramatic increase in reflected energy occurs with increasing windspeed. Though the reflected energy during a given period of time is much greater at higher windspeeds, the total length of time each condition exists during the year rapidly decreases for windspeeds above twenty mph. Wave breaking begins to help dissipate energy at the test site for wind speeds in excess of 25-30 mph.

a three second period for a chamber configuration similar to the present investigation except for the porosity. Assuming a linear relationship between the force and the area of the porous wall, the ratio between Burrows porosity and that of the present investigation would suggest an expected force of 205 pounds on the solid wall of the full-scale breakwater at a windspeed of about 40 mph.

The porous walled caissons investigated by Jarlan [13] use a porosity, m', of approximately .3. For the system, including porous front wall and solid back wall, Jarlan demonstrates a seventy percent reduction in force relative to that acting on a solid wall alone. Marks [10] also measured the forces exerted on both walls of a porous walled chamber. Being concerned with much longer wave lengths and shallow water conditions, the scale of the chamber is ten times that of the present test. Making the scale conversion the chamber would correspond to a 3.4' wide chamber at the present test site designed for a forty-four foot wave with a three second period and a 1.5 foot wave height. With a porosity, m', of about .25, Marks recorded a 69% reduction in the sum of the horizontal forces on the porous and solid wall relative to the force on the same size solid wall alone.

The present investigation makes no attempt to develop an analytic prediction for the wave forces against a porous wall. Rather, the maximum forces on the porous wall and the frequency distribution of the force for the matrix of wind generated wave conditions and chamber configurations are obtained experimentally. Establishment of the force reduction obtained by incorporating the breakwater could allow substantial reduction in the design load requirements and maintenance costs of a floating structure.

Experimental Force Evaluation

The chamber created by the porous walled breakwater includes a porous front wall and solid back wall. Because the device was appended to an existing floating bridge the back chamber wall was formed by the bridge pontoon. The force against the back wall is not measured but can be calculated, because the major component of water movement inside the chamber is the level change due to the influx and emptying of the chamber. Runup and the shock pressure due to breaking waves are non-existent at the back of the chamber. Thus the maximum force on the solid chamber wall can be calculated simply as the hydrostatic force due to the maximum level within the chamber.

The wave system in front of the breakwater and the level within the chamber result in forces against the porous wall. As detailed in the next chapter, central 3.3 feet of the porous wall form an instrumented test section allowing the acquisiton of the representative maximum force free from end effects and provides a porosity representative of the entire porous wall. The use of a short test section also assures the force is not averaged by the limited crest length of the waves.

The vertical force on the thin porous wall is assumed to be insignificant. For use primarily as a design input for fatigure loading the frequency distribution of the force is acquired using the same spectral analysis program used to analyze the wave data. Though the resulting spectral amplitudes are not an expression of pounds of force, the plots indicated the frequency at which the peak force occurs and provide information regarding secondary peaks, if any.

The portions of the prototype breakwater subjected to the most force are the chamber end plates. These solid walls, required to provide two dimensionality within a reasonable length for the experiment, are subjected to a

This range of uncertainty, both in the frequency corresponding to the optimum performance of a given chamber width and the windspeed which produces the most total energy at the test site during the year, suggests that a range of chamber widths be tested. Figure 16 is used to establish the relationship between windspeed and the significant frequency (at the test site) and Figure 4 to relate this frequency to the corresponding dominant wave length. This wave length can then be related to the desired chamber width through equation 34 for the resonant frequency and equation Eq. 36 for laboratory predicted optimum performance. Choosing chamber widths that correspond with a wind range of 12 to 25 mph results in a reasonable choice of chamber widths being five and seven feet. The test apparatus is built to also allow a three foot width in case the full-scale device reacts to a frequency lower than predicted. A table demonstrating the predicted characteristics is shown below.

Chamber Width (feet)	Predicted Natural Frequency of, ω (eq. 34) (HZ)	Approximate Windspeed at Test Site Associated with with ω (mph)	Frequency Predicted from eq. 36	Approximate Corresponding Windspeed (mph)
3	.545	12	.63	<10
5	.435	15-20	.48	15
7	.365	20-25	.38	22

Summary of Prototype Breakwater Specifications

Porous walled resonating chamber.

- Porous vertical front wall: porosity (m′) = .293
- Solid vertical back wall (bridge pontoon wall)
- Solid, removable chamber bottom
- Solid end plates (to establish two dimensionality with the minimum chamber length)
- Chamber depth: 6.4 feet
- Pore geometry: one foot diameter round sharp edge orifices uniformly spaced on 18" centers.
- Chamber width: design variable: 3, 5 and 7 feet.

Forces

The forces exerted on a solid vertical wall by the various wave forms have been the subject of numerous investigations and as a result are reasonably predictable.

Existing methods can be used to calculate the approximate maximum force exerted on the solid wall of the floating bridge pontoon. On the other hand, literature examining the maximum forces on a porous wall in front of a solid wall exposed to random deep water waves is very limited. A laboratory investigation by Burrows [19] indicated that the force on a vertical porous wall used to form a chamber in front of a solid vertical reflecting wall was less than the force exerted on a solid wall immersed to the same depth. For a porosity, m′, of .196 and a depth of immersion scaled to the present investigation a reduction in force of 65% was obtained relative to the theoretical value for a solid plate extending to the same depth. Burrows further predicts a full scale force of 236#/lineal foot of wall due to a three foot wave height with

maximum pressure differential near the pontoon when a wave outside the chamber is overtopping the guardrail at the same time the chamber level is low. This effect is amplified when the waves crests are not parallel to the bridge as evidenced by wave runup onto the roadway near one side of the chamber for wind conditions too low to produce overtopping anywhere else along the bridge. The forces exerted on these panels were not measured because permanent breakwater would likely span the entire length of the structure and have porous end plates to reduce the loading.

CHAPTER III

APPARATUS AND INSTRUMENTATION

General Description of Equipment

The experiment required construction of a full-scale porous walled breakwater and the associated instrumentation to monitor the forces upon the breakwater and wave characteristics in front of and inside the attenuator as well as those beyond its region of influence. The apparatus, assembled at the University of Washington, C. W. Harris Hydraulic Laboratory, is attached to the south side of the second Lake Washington Floating Bridge near the center of the lake (400 feet west of the drawspan).

The breakwater, shown in Figures 17-20, is a chamber created by the solid wall of the bridge, a removable solid bottom, and a movable, porous vertical wall. The water can pass into and out of the chamber through uniformly spaced, round holes (orifices). The chamber extends three feet above and 6.4' below still water level, the dimensions of the chamber are maintained by securing the bottom and porous wall panels to steel superstructure attached to the side of the bridge. The characteristics of the breakwater are determined by evaluating the difference between the sea state (pressures) immediately in front of the breakwater and at a remote location along the bridge where the breakwater does not influence the sea state. The breakwater is of sufficient length, thirty-eight feet, only to eliminate end effects on the limited region where force and pressure measurements are obtained. The chamber is enclosed on each end by solid end panels attached to the steel superstructure. The apparatus is constructed to allow chamber widths, b, of three, five, and seven feet and can be tested with or without the bottom panels.

The central 3.3 feet of the porous wall is held in position at the top and bottom by pairs of cantilever beams. The output of strain gages attached to the beams are monitored to establish the resultant horizontal force "felt" by the porous wall. Two tripods house pressure transducers which are used to measure the pressure five feet below S.W.L. One tripod extends seven feet nine inches out from the side of the bridge 150 feet east of the breakwater to monitor the pressure due to waves away from the influence of the breakwater. The second tripod is attached to a porous wall and measures the pressures due to waves seven feet nine inches in front of the breakwater. The outputs of each of the calibrated pressure and force sensors are amplified and recorded onto analog tape for periods of at least twenty minutes per run. The various components of the apparatus are treated in detail in the following sections.

The Breakwater

Steel Superstructure (Figure 21):

Two modules of steel trusses and cross bracing attach to the bridge using hooks over the bridge railing eleven feet above S.W.L. to sustain loading down and away from the bridge. Seven feet below S.W.L. horizontal extensions of the trusses extend underneath the bridge to prevent upward motion. From the center truss extension of each module 75' cables run under the bridge to the north side where they are attached to hooks over the north bridge railing. Turnbuckles are used to hold the modules rigidly against the bridge. Steel bracing welded between the modules maintain the required spacing for the test section. The modules contain all the installation hardware required to create three, five, or seven foot wide enclosed chambers. Overall dimensions of the superstructure are: height = 19 feet, width = 8 feet, and length = 38 feet.

Porous Walls (Figure 22):

Four porous walls, each eight feet long, ten feet high and seven inches thick are set into slots at the base of steel trusses and bolted to truss crossmembers at the top. Each wall contains thirty, one-foot-diameter holes spaced on eighteen inch centers. Each hole is lined with sheet metal to provide a seven-inch-long sharp-edged orifice. The ratio of the geometric area summation of all holes to the total wall frontal area (porosity) is .293. The walls are of wooden construction incorporating 3/4 inch plywood sandwiched over two-by-sixes to transmit loads vertically to pairs of $2\frac{1}{4}$ inch angle iron edges at the top and bottom. The angle iron transmits the forces horizontally to the trusses and in turn to the bridge. Seven feet of porous wall extend below and three feet above still water level. One row or orifices is above S.W.L., one row has centers coincident with the S.W.L., and the remaining four rows are uniformly spaced beneath the S.W.L.

Test Section:

A 3.3 foot wide by ten foot high wall with the same thickness and porosity as the porous walls is suspended between the two steel modules. Constructed in a manner identical to the porous walls, the resultant forces on the wall are transmitted vertically by the sandwiched wood construction to horizontal angle iron edges at the top and bottom. The angle iron is rigidly mounted to 3"X3"X16" inch sections of mild steel each with machined sections of steel extending 12 inches from each end to form cantilever beams (Figure 23). A two inch diameter steel cylinder is welded to the free end of each beam. The cylinder is placed into receptacles on the steel superstructure which allow free rotation while minimizing horizontal motion. The machined surfaces on each beam are fitted with strain gages. Thus, the resultant force on the test section is transmitted through upper and lower instrumented cantilevered beams

of precise dimension. The test section is always placed at the same chamber width as the rigid porous walls. The dimension of the chamber is sufficient to insure that the forces registered on the test section are representative of the maximum value which would occur for a chamber extending the length of the bridge; i.e., end effects are not felt by the test section. The calculated force corresponds to an infinite crest length, and thus is greater than the average value that would occur on a long wall.

Chamber Bottom (Fig. 24)

A solid removable bottom is provided for the chamber. The bottom is divided into sections of corresponding dimension to the three chamber widths and may also be removed completely. The panels are of sandwiched wooden construction incorporating $\frac{1}{2}$ inch plywood over 2 x 8's on twelve inch centers. The bottoms are held in place on top of the lower steel truss I-beams by welded studs. A diver can remove a section of bottom by removing nuts and an angle iron retainer allowing the section to float to the surface. Due to bottom thickness, the depth from S.W.L. to the bottom of the chamber is 6.4 feet while the corresponding distance to the bottom of the porous wall is seven feet. The porosity of the chamber is calculated based on the 6.4 foot chamber depth. The uniformity of hole locations also takes into account the physical chamber depth of 6.4 feet.

End Panels:

To provide reasonable economics the length of the prototype breakwater is only sufficient to reasonably assure two-dimensional flow characteristics at the test section and pressure gages and thus the chamber must be solidly closed at both ends. The end panels are of wooden 3/4" plywood sandwich

construction with the loads being carried by vertical 2 x 8's on two foot centers to the top and bottom where the panels are bolted securely to plates welded to the steel truss I-beams on the superstructures. Each end panel extends from seven feet below S.W.L. to three feet above S.W.L. and is divided into three sections to allow end panels which are flush with the front of the breakwater for each chamber width. Due to the extreme forces created by wave runup the end panels nearest the bridge must be much stronger than the others. The additional problem of wave runup propagating along the bridge, was not accounted for in the original analysis and failure of these panels on two occasions resulted. The final configuration required doubled 2 x 8's on twelve inch centers sandwiched by sheets of 3/4 inch plywood.

Miscellaneous:

Due to the eleven foot distance from the bridge railing to S.W.L. a ladder and work platform were installed. The platform is three feet above still water level and directly behind the test section. From the platform, adjustments and inspection of the test section locator receptacles are possible.

A 14 foot A-Frame (Fig. 25) built from $2\frac{1}{2}$ inch pipe is used in conjunction with winches to provide a self-sufficient means of changing chamber widths. The base of the frame fits into specified locations on adjoining pairs of trusses. The vertex of the frame is thus centered over a porous panel. Using one winch from the porous wall to the vertex and a second from the vertex to the module cross-members on the bridge railing, any needed combination of height and distance from the bridge is possible.

Sensor and Instrumentation Enclosures

Pressure Sensor Tripod in Front of Breakwater:

The sea state is monitored using pressure transducers. To allow

measurement of the summation of incident and reflected waves over a wide range of wave height the pressure transducers were placed five feet below the still water level. The transducers were mounted seven feet nine inches away from the nearest surface to avoid affecting the pressure records by the jet velocity from the breakwater pores or wave runup. To avoid pressure readings due to instrument motion it was necessary to build rigid mounting devices.

A tripod constructed of 2.5 inch galvanized pipe is bolted to and extends from the porous panel beside the test section (recall Figure 18). The transducer is housed within a machined, water-tight plug which, in turn, screws into the vertex of the tripod. A 1/4 inch inside diameter pipe extends horizontally from the transducer diaphragm, through the plug and horizontally away from the assembly for twelve inches, where it terminates in a 1/4 inch ID., 90° elbow with the opening facing upward. The end result is a rigid, water-tight pressure sensing device exposed to the vertical pressures existing at a location seven feet nine inches in front of the porous wall and five feet below S.W.L. Because it is attached directly to one of the porous walls, the distance between the chamber and pressure measuring station is constant regardless of breakwater chamber width. One leg of the tripod is water-tight to allow passage of wiring from the transducers to the surface without sealing problems or danger of debris fouling in the wires.

Remote Pressure Sensor Tripod: (Figure 18)

In order to monitor the sea state at a control station beyond the influence of the breakwater another transducer measures the pressure seven feet nine inches out from the bridge, 150 feet east of the breakwater and

five feet beneath S.W.L. The transducer mounting including the 1/4 inch pipe and 90° elbow extension are identical to those used in front of the breakwater. 2.5 inch pipe is used to form a hook over the guard rail, extends eighteen feet from the rail to the bottom of the bridge, where it connects to a cable from a hook over the opposite guard rail. A turn-buckle attached to the cable is used to place sufficient tension in the cable to hold the pipe rigidly against the bridge. A horizontal 2.5 inch pipe, containing the transducer, extends from a tee in the vertical member to form a water-tight passage to allow wiring to be run from the transducer to the roadway without exposure to debris or sealing problems. The horizontal pipe is rigidly positioned by angle iron bracing.

Pressure Sensor Receptacle Inside Breakwater:

To monitor vertical pressure components within the chamber, a receptacle was constructed of 2.5 inch galvanized pipe welded to a large flat base allowing it to be placed on the floor of the chamber at the chamber centroid. The transducer was fitted into a machined plug sealing the top of the pipe. From the transducer diaphragm a 1/4 inch inside diameter plug extends to a point five feet below the S.W.L.

Instrumentation Enclosure: (Figure 19)

The presence of a 50 mph freeway within three feet of a test set-up presents a rather unique problem with regard to placement of power supplies, amplifiers, and recording instrumentation near the weather. This problem is circumvented by centering the breakwater over one of the bridge pontoon access panels. Wiring from the various pressure and force sensors are routed over the guard-rail and through the access panel into the bridge pontoon.

Due to the common presence of a few inches of water within the pontoon, scaffolding was erected to form a safe working platform. Extreme humidity and condensation within the pontoon further required that a sealed box be built on top of scaffolding to provide a controlled environment for the various instruments. The box, constructed of plywood, contains the required electrical outlets and is of sufficient size to enclose and protect all of the instrumentation. The front cover of the box opens up to form a protective cover from road debris during data acquisiton, and is weather stripped to provide a water-tight seal when closed. A 40 watt light remains on to provide heat and eliminate moisture inside the box.

Instrumentation for Data Acquisition (Figure 26)

Force Sensors:

The resultant horizontal force on the porous walls of the breakwater due to the differences between the pressures exerted on the inner and outer surfaces are monitored by sets of strain gages affixed to cantilever beams at the top and bottom of the test section. As shown in Fig. 27 a net force toward the bridge causes the strain gages on the front of the beam to be in compression while the gages on the back of the cantilevers are placed in tension. The four gages form a bridge such that the change in resistance due to the tension and compression on the strain gages result in a positive voltage output for the net force toward the bridge. Similarly, a net force away from the bridge results in a negative signal. The output, linear over the entire range of interest, is the same for both beams and periodic calibrations during the test have substantiated repeatability. The beams are constructed of one by three inch 44,000 psi. hot rolled steel machined to close tolerances in the region of the strain gages. The use of two-inch

round cylinders at the end of each beam provides an accurate method of maintaining precisely twelve inch long cantilever beams.

Pressure Sensors:

The resultant pressure fluctuations due to the incident and reflected surface waves are measured five feet below the still water level by pressure transducers. Three similar transducers are used, one each inside and in front of the porous walled chamber and the other as a control station in front of the solid bridge wall away from the influence of the breakwater. Inside the breakwater the transducer was mounted vertically at the chamber centroid. The others monitored pressure fluctuations at a 1/4" diameter, upward facing circular opening 93 inches (seven feet nine inches) in front of the porous wall of the breakwater and at the same distance in front of the solid bridge wall.

Initially Viatran Model 218 transducers were incorporated to monitor pressure fluctuations over zero to five psig. range. An integral amplifier produced a five volt maximum output signal which eliminated the need for a separate carrier amplifier. A 2/1 and 4/1 reduction in signal before submittal to the 1.4 volt maximum P.I. tape recorder allowed two ranges of voltage yielding better resolution on low wind condition records. Unfortunately, the individually shielded six strand wiring, including a 28 volt supply and self-contained calibration circuit, between the transducer and the instrumentation enclosure had sufficient capacitance that the two hundred feet of wiring required for the remote gage resulted in occasional erratic output signals.

To increase the output signal reliability the Viatran unit with self-contained amplifiers were replaced by Viatran PTB 101 transducers having a

millivolt output signal with a 0-15 psi range. The transducer linearity is within ± 0.75% F.S., hysterisis less than 0.25%, and repeatability within 0.1%.

Power Supply:

Electricity is supplied to the floating portion of the bridge from the eastern shore to operate various functions including lights and the drawspan mechanisms. The nearest outlets available for test instrumentation are two hundred feet from the instrumentation enclosure and the same circuit supplies a series of lights within the pontoon. The losses within the wiring and the variation in circuit load creates a variation in voltage beyond the acceptable range of the test instrumentation. Therefore, a transformer and voltage regulator are placed into the supply line to provide a constant 117 volts to the data acquisition instrumentation. The voltage regulator is a Superior Electric Co. Stabiline 1 KVA. maximum unit which produces 110-120 volts, 60 cycle, from an allowable input range of 95-135 volts, 60 cycle.

The associated transformer is a General Radio Variac Adjustable Transformer, Type 100, set to maintain 117 volts. Because of an initial 50 volt ground variation, the incoming ground line is now common to all instruments and metal structures.

Amplifier:

A six channel Honeywell carrier amplifier is used to amplify the millivolt strain gage and pressure transducer outputs from millivolts to a maximum of 1.4 volts for input to the Precision Instrument (P.I.) tape recorder. Each channel

incorporates variable capacitance and resistance potentiometers which allows zeroing of output signal for steady state input signals. Thus, the millivolt output of the pressure transducers due to a still water depth of five feet (2.6 psi) can be zeroed out allowing the entire amplified signal to be pressure fluctuations due to wave action.

Each channel includes a step variable attenuation switch. Calibrations made over the applicable range for each setting allow full-scale output from smaller input values and thus increase the resolution for lower windspeed conditions. Voltage and milliampere gages are visually monitored to confirm that transient, temperature-induced, zero shifts, within the amplifier during warmup, have been removed prior to data recording.

Tape Recorder

Analog data are recorded onto one inch tape using a fourteen channel Precision Instrument reel to reel recorder. All data are recorded at 3.75 inches/second using the associated factory installed carrier frequency and observing the 1.4 volt maximum peak input requirement to assure a linear input/output relationship.

Oscilloscope:

On-line pressure and force fluctuation, are monitored with a Hewlett-Packard 1224 twin sweep oscilloscope. Real time monitoring is used to assure that sensors are operational and that sensor output appears reasonable and peak values are observed to establish the appropriate amplifier attenuation setting.

Anemometer:

The nominal windspeed and direction are acquired from existing instrumentation on top of the bridge tower (Z approximately forty feet) a few

hundred feet from the breakwater. A hand-held Dwyer anemometer is used to supplement the wind speed data from the tower gage. The Dwyer model consistently provides readings five mph lower than the tower gage.

Junction Box and Calibration Voltage:

A junction box, in-line between the amplifier and the tape recorder, contains a monitoring switch allowing selection of channels for oscilloscope viewing. The junction box also provides an easy means of disconnecting the amplifier output and signal to allow a constant 1.35 volt calibration signal to be put onto the tape prior to each data record. The calibration voltage is supplied by mercury cells which provide a constant 1.35 volts until the onset of rapid and noticeable deterioration, when a new cell is installed.

Data Reduction Instrumentation (Figure 28)

Ampex Tape Recorder

For convenience the P.I. recorder remains on the bridge and a fourteen channel Ampex recorder is used for analog playback. Originally, the two machines operated at different carrier frequencies (for the same tape speed). The Ampex was modified to make the units compatible. The resulting configuration allows the analog tape to be recorded and played back at 3.75 inches/second (Using the Ampex carrier frequency corresponding to the factory installed frequency for 1-7/8 inches/second). The ordering of channels was opposite on the two machines (P.I. channel 1 = Ampex channel 14; 2 = 13; etc.). For convenience, the arbitrary factory numbering of channels on the Ampex is reversed to allow data, originally recorded on channel one, for example, to be referred to as channel 1 data throughout the reduction and analysis.

Low Pass Filters:

High frequency noise is eliminated from the signals of interest by low pass filters. Analog force data passes through a one Hz filter which begins to effect the data at .8 Hz. Analog pressure data, containing pertinent information at frequencies to 1.5 Hz, is passed through a 2.5 Hz filter.

Systron Donner:

The analog data both filtered and unfiltered is digitized on a Systron Donner recorder/digitizer. The analog data is scanned at equal time intervals to produce a discrete value for each channel at each time increment. The sampling rate being used throughout the data reduction is .328 second (sample frequency resolution .0030 cycles/second). The Systron Donner unit digitizes data into records of 512 points each. The records are taken in pairs of 512 point records immediately adjoining one another on the analog tape. Digital values are automatically coded onto magnetic computer tape compatible with the CDC 6400.

CDC 6400:

Digitized data is processed on the CDC 6400 digital computer at the University of Washington.

Cal-Comp Plotter

Final spectral plots, such as the figures shown in the appendices are machine plotted using a Cal-Comp plotter.

Installation Technique

Modular components of the porous wall breakwater were assembled on the Oceanography Dock at the University of Washington (Figure 29).

Following assembly the 2730 pound units were crane-lifted onto a barge in the Lake Washington Ship Canal. The barge was towed to the south side of the Evergreen Point Bridge where a crane, operated from the roadway, hung the units onto a bridge guard railing. Cables, attached to the bottom of each module, were connected through turn-buckles to hooks over the bridge railing on the north side of the pontoons. Sufficient tension was put into the cables to assure a rigid attachment. A similar installation technique was employed to mount the remote pressure transducer station.

Calibration Techniques

Strain Gages:

Prior to installation of the pairs of cantilever beams on the test section, the linearity of the strain gage bridge output with applied force was determined on a calibrated press at ore Hall, University of Washington. The outer ends of the beams were grounded and the load applied on the rigid 3x3x16 inch center section, as shown in Figures 30 and 31. The beams, deflected in both directions, demonstrated repeatability within 0.6% for range 0-3000 pounds with a maximum non-linearity of less than 1% (maximum 0.9% at 1200 pounds). The output for both pairs of beams was virtually identical with scatter for both being within the same 0.6% bandwidth.

The stiffness of the 3x3x16 inch sections from which the cantilevers extend was assessed by comparing the result of point loading at the center and distributing the load over the 3x16 inch surface. The maximum calibrated output difference corresponded to 12 pounds in 3000 (0.4%). The increase in stiffness due to the method of attachment to the test section assures that the beams are truly cantilevers.

Force Sensors:

Following attachment of the cantilever beams to the test section, the entire assembly was installed into the receptacles provided between the two rigid breakwater modules. Periodically, on calm days, a hydraulic ram including a calibrated pressure gauge, is placed between the bridge and the test panel. With known pressures applied the amplifier output voltage can be calibrated for various amplifier attenuation settings. Typical calibration curves are shown in Figures 32 and 33.

Pressure Transducer Calibration:

Pressure transducers were originally calibrated by recording the amplifier outputs for various elevations of a water column within a clear plastic hose (0 - 12 feet). Following installation into the fixed receptacles, five feet below still water level, the amplifier was set to produce zero output at the five foot depth. Plastic tubing connected to the transducer inlet allows static water columns above SWL to be used to calibrate the transducer outputs for various amplifier attenuation settings. Periodically this technique is used to check transducer and amplifier output. The linearity, originally demonstrated out of the water, is assumed to exist for the distances between the gauge and still water level. The approximate linearity is finally verified by removing the transducers from the fixed receptacles and calibrating the amplifier output as a function transducer distance below still water level in one foot increments from zero to eleven feet below S.W.L. Calibration curves are shown as Figures 34-36, for each of the transducers.

Tape input/output calibration:

Prior to each data record the amplifier input to the tape recorder is momentarily replaced by a constant 1.35 volt calibration signal from a mercury cell. Inserted for each channel, the plus and minus signal provides the known input needed to calibrate the voltage output of the tape playback.

CHAPTER IV

TEST PROCEDURES, DATA ACQUISITION AND PROCESSING

Test Requirements

To adequately establish the performance of the porous walled breakwater subjected to random wind conditions a range of data is required for reasonably steady wind conditions between eight and at least thirty-five m.p.h. At each wind condition the assessment of performance requires an analog record of force and pressure fluctuations for at least twenty minutes. During the twenty minute record the wind produced wave system should neither be building, declining nor changing direction. For a given breakwater configuration, a data set is complete when records meeting the above criteria are acquired for windspeed increments of approximately five m.p.h. Complete data sets are acquired for four breakwater configurations; five and seven foot chamber widths each with and without a solid chamber bottom.

Data Acquisition

Prior to each record all equipment is warmed up for a period sufficient to remove temperature induced signal transients. During this period the windspeed and direction must remain substantially constant.

The $\pm$ 1.35 volt calibration signal is recorded onto the analog tape and the oscilloscope monitored to check that the pressure and force output signals are reasonable and that the choice of amplifer attenuations produces a peak output less than 1.4 volts. The attenuation and wind conditions are logged and a minimum twenty minute record is recorded. The record is aborted if the average wind increases, decreases or changes direction noticeably or if an extraneous signal is monitored on the oscilloscope;

i.e., saturated transducer output, amplifier mean voltage shift, or the superposition of boat-created waves.

Data Processing

The analog data tapes containing continuous wave (pressure) and force records are processed at the University of Washington. The procedure is shown schematically in Figures 37 and 38.

Segments of the twenty to sixty minute analog pressure and force records are converted to digital records containing 1024 discrete values taken at equal (0.328 second) time increments resulting in a Nyquist frequency of 1.52 Hz. Each digital record represents 5.6 minutes of analog data satisfying the criteria that the total incident energy at the chamber equals that at the solid wall (remote station) 150 feet away. Analog tapes are played back on an Ampex recorder. The channel assignments of raw data are always:

Channel #	Sensor
1	top force gages
2	bottom force gages
3	pressure transducer away from the influence of the breakwater (or remote transducer)
4	pressure transducer in front of porous wall (near transducer)
5	Pressure transducer inside of chamber

The ± 1.35 volt calibration signals recorded on the P.I. before each data record is played back on the Ampex and on an ouput/input calibration factor is acquired for each channel; individually.

The output of the Ampex is branched for each channel. One branch is directly input to the digitizer, the other branch goes through a low pass filter and then into the digitizer. Thus, the digitizer receives ten channels of input; 1-5 being raw analog data and 6-10 the corresponding filtered analog data.

The filters are incorporated to eliminate noise which occurs at frequencies above the Nyquist frequency (1.52 cycles/sec) and thus prevent possible aliasing problems in the final spectral analysis. Care is taken to avoid filtering data which are part of the phenomena being investigated. Originally both one Hz. and 2.5 Hz. low pass filters were applied to the early data. The resulting force data were identical indicating that all pertinent data occurs at frequencies less than one Hz and hence the use of a one Hz filter assured the elimination of extraneous signals without a loss of real information. The response function of the filter starts to drop off at 0.8 Hz. Comparison of filtered and low noise unfiltered data also indicates no significant error in force data using the one Hz. filter. Pressure transducer data, on the other hand, indicate a significant amount of energy existing at frequencies up to 1.5 Hz. For each of the pressure channels the high frequency equipment noise is removed without loss of desired data by incorporating a 2.5 Hz. filter.

The five unfiltered and five filtered channels of data are input to the Systron Donner digitizer. The analog data is scanned to produce a discrete value for each channel at equal time increments. The sampling rate used throughout the data reduction is .328 sec. The Systron Donner digitizes data into records of 512 points each. For most of the data reduction, adjoining pairs of these records are used to create digital records of 1024 (2^{10}) data points. The digital values are automatically recorded onto

magnetic computer tape compatible with the CDC 6400.

Thus, segments of analog data records twenty to sixty minutes in length are converted into digital records each corresponding to approximately 5.6 minutes (1024 points x .328 seconds/point) of the original record. Comparison of the different digitized data lengths for the same data record demonstrates that 1024 points provide sufficient duration to validate the assumption that the total incident energy at the two pressure stations (150 feet apart) is the same. The relative lengths of the digitized and analog records allow the reduction of at least three digitized records from each analog case. Eventual comparison of the analyzed data at the beginning and end of an analog record provides a check on the stationarity of the process.

The sampling rate and the use of low pass filters are sufficient to assure that the energy belonging to sinusoids calculated to pass through these equally spaced points will not belong to a high frequency wave being assigned to a lower frequency (its alias).

The second step in data processing involves the conversion of the digital tape to punched computer cards containing 10 digital values per card. A Fortran program (HOOD5, undocumented) is used on the CDC 6400 computer to make the conversion and calculate maximum, minimum and mean raw values for each channel. The program printout lists the complete raw digital data and the maximum, minum and mean values. Perusal of the printout allows recognition of incomplete or erroneous data (the Systron Donner is subject to occasional saturation which appears on the raw data printout as groups of a constant value).

The Systron Donner digitizes groups of 512 data points, with a lag of .640 seconds between records, a continuous 1024 point record is synthesized

by averaging the last value in one 512 point record with the first value on the 512 point record immediately following it. The average value is punched on the card as a 513th point and the two records are placed together and input as one continuous record containing 1025 points for the remainder of the data analysis.

Spectral Analysis

Digitized records which appear to be complete and correct are resubmitted to the CDC 6400 in puched card form. Though bulky, the intermediate step of card production allows analysis of any record or individual channel merely by selective stacking of groups of cards. The data is reduced using the lag product method of spectral analysis. The computer program used is the Numerical Spectral Analysis Program (NSAP). The procedure is basically that given by Jenkins and Watts [21].

The original digital data is first shifted to a zero mean value. The P.I./Ampex correction factor to account for any amplitude differences between the originally recorded data and the playback values, and the scale calibration factors for the sensors based on the slope of the linear feet of water vs. millivolt or pounds of force vs. millivolt curves are combined to give a final scale factor for use on the data. The calibration is applied to the zero mean raw data and a listing of discrete calibrated data points is printed out along with the associated calculated maximum, minimum and mean values, as well as the variance.

A numerical DC filter subroutine is applied to the data to eliminate erroneous energy contributions introduced during the initial data recording by slight, temperature induced, amplifier and transducer transients. These transients occurred over a period of minutes and would be interpreted during spectral analysis as an apparent DC shift in the data.

The autovariance function for the first 57 lags of 1024 data points is calculated, listed, and plotted. The variance of zero lag product value is listed. A factor of two is introduced into the program so that the variance, proportional to the total energy per unit horizontal area at the sensor for the period of the record, automatically becomes the mean-square of differences of all possible pairs of values.

The Tukey window is applied to the autocovariance function and the A.C.V.F. is transformed. Smoothed spectral estimates are then calculated and plotted for 20, 40, 50, 60 and 80 lags. For each case the variance (area) and peak spectral ordinate value and frequency are tabulated. Histograms for ten divisions of data points are also calculated and presented for each record.

Careful perusal of the spectral estimate plots allows the selection of the number of lags required to minimize both the bias and the instability. The smoothed spectral estimate plot for the minimum bias and instability, typically 50 lags, was then placed on magnetic tape for use to create final Cal-comp plots. For convenience and uniformity in presentation the ordinates on Cal-Comp plots are non-dimensionalized (normalized) by the variance creating a plot with unit area under the curve. The plot scales are held constant for all plots and thus allow easy overlay of curves. The ordinate has a range of normalized smoothed spectral estimate values from 0 to 9.6 while the abscissa includes frequencies from zero to 1.5 cycles/sec., approximately the Nyquist frequency.

CHAPTER V

ANALYSIS

The premise upon which the full scale test was based assumes the following:

1) Virtually no energy is transmitted to the lee side of the bridge. Therefore, the incident wave energy must be either reflected by the bridge or dissipated (converted to a non-conservative form of energy).
2) Linear wave theory can be used to relate energy to wave height and sub-surface pressures.
3) Time histories of the summations of incident and reflected random wave heights, taken simultaneously in front of the breakwater and at a station away from the influence of the breakwater, can be analyzed using spectral analysis to yield the average total energy at the two locations.
4) Over a period of minutes the average incident energy is the same at the two locations.
5) Therefore, differences between the calculated average total energy at the two stations are due to differences in the average reflected wave energy. This difference must be caused by energy dissipation at the breakwater.

To conveniently relate the amount of dissipation occuring for different wave conditions and breakwater configurations, the term attenuation was introduced. Attenuation proports to ratio the energy dissipated by the chamber to the sum of the incident and reflected energy in front of the solid bridge pontoon (remote station). Incorporating

spectral analysis (equations 26-32) the attenuation is given by the difference in variance at the two locations divided by the variance at the remote station, Attn $\equiv 1 - \sigma^2_{BW}/\sigma^2_{\infty}$.

The vertical wall of the bridge pontoon (remote station) is nearly a perfect reflector below windspeeds causing wave breaking and overtopping. Thus, the denominator in the attenuation should represent almost twice the incident wave energy. Under these conditions, the expected range of values for attenuation is between 0 (no energy dissipation) and .5 (total dissipation of incident energy, no reflection). Early in the course of data reduction attenuation values beyond the expected range appeared. Immediately suspecting a calibration error, the instrumentation was recalibrated and program calibration inputs checked. Finding no discrepancies, but still suspecting a measurement error, the transducers and amplifiers were changed completely. New data continued to produce unexpected attenuation values. The use of sub-surface pressure transducers to monitor surface fluctuations was examined as a source of error. Higher order pressure terms, not accounted for by the small amplitude analysis, were shown to be too small to contribute the amount of discrepancy being observed. The influence of the jets (exiting the breakwater pores) on the pressure readings was demonstrated to produce less than a one percent error in calculated energy. Consultation with other researchers in the field failed to provide a plausible solution.

Having reasonably established the validity of the data records it is necessary to assume that either the attenuation values being observed are real, or there is an error in the assumptions, or an error in the method used to reduce the data to acquire the attenuation. Negative

attenuation values are calculated from some data records suggesting that there is more energy in front of the breakwater than at the remote location. Negative attenuations are calculated at windspeeds below that required for wave breaking or overtopping, suggesting the creation of energy by the chamber. This creation being physically impossible allows one to safely assume that attenuation, as calculated, does not represent the desired ratio of energies as defined in equation 32.

The inconsistency is introduced by the assumption that the average energy calculated from spectral analysis of the time history of the sum of the incident and reflected wave heights is the same as the sum of the average energies calculated for the incident and reflected waves individually. At this time, the author cannot quantitatively evaluate the extent of this difference and therefore cannot calculate the amount of energy dissipated by the breakwater as originally intended.

The following sections enumerate the subtle error in the original assumptions and demonstrate, as presently understood, the complex nature of the difference between attenuation and the actual energy dissipation. Methods which may serve to relate the two quantities are suggested but not presently pursued. The attenuation is recorded for the various wind/wave conditions and chamber configurations in the appendices in hope that the author or another investigator will relate the quantity to actual energy dissipation at a future date. Fortunately, other objectives of the investigation are independent of this problem.

Evaluation of the Attenuation of a Monochromatic Wave Using Wave Envelope Traverses

An initial appreciation for the problem of evaluating the energy

can be obtained by examining a monochromatic incident wave and the associated monochromatics reflected wave. The incident wave surface can be represented by

$$\eta_i = a_i \sin(kx - \sigma t + \theta_i) \qquad 39$$

and the reflected wave surface can be represented by

$$\eta_r = a_r \sin(kx + \sigma t + \theta_r) \qquad 40$$

Richey and Sollitt (16, p. 41-45) demonstrate that the incident and reflected wave height, H_i and H_r, can be obtained directly for superimposed monochromatic waves by traversing the envelope of the resulting standing wave. Linear wave theory relates the energy to the square of the wave height and therefore, for this case the reduction in energy during reflection is

$$E_i - E_r = \frac{\gamma}{8}(H_i^2 - H_r^2) \qquad 41$$

To calculate the attenuation for the above case, the wave characteristics in front of the breakwater and in front of a vertical solid reflecting barrier must be known. Throughout the present investigation the transmitted wave energy is virtually zero. Also, the breakwater responds as a linear resonator only acting upon the phase and amplitude of a wave and not affecting the frequency during reflection. Thus, incident and reflected wave heights for a monochromatic wave system can be

obtained by traversing the standing wave in front of the breakwater to give $H_{i_{BW}}$ and $H_{r_{BW}}$. Similarly, the wave heights in front of the solid barrier can be obtained and designated H_{i_∞} and H_{r_∞}. The calculation of attenuation requires that the average incident conditions at both locations be the same; thus, $H_{i_{BW}} = H_{i_\infty} = H_i$.

$$\text{Attenuation} = \frac{\bar{E}_\infty - \bar{E}_{BW}}{\bar{E}_\infty} \tag{42}$$

From equation 9, $\bar{E}_\infty = \frac{\gamma}{8}(H_i^2 + H_{r_\infty}^2)$ and $\bar{E}_{BW} = \frac{\gamma}{8}(H_i^2 + H_{r_{BW}}^2)$. Therefore

$$\text{Attenuation} = \frac{H_{r_\infty}^2 - H_{r_{BW}}^2}{H_{i_\infty}^2 + H_{r_\infty}^2} \tag{43}$$

Recalling the reflection coefficient, $R = \frac{H_{r_{BW}}}{H_i}$, in front of the breakwater and defining the reflection coefficient at the solid wall as S, where

$$S = \frac{H_{r_\infty}}{H_i} \tag{44}$$

and substituting R and S into the attenuation, yields

$$\text{Attenuation} = \frac{S^2 - R^2}{1 + S^2} \tag{45}$$

The solid wall is nearly a perfect reflector until wave breaking occurs. Assuming a perfect reflector, $H_{r_\infty} = H_i$ or $S = 1$. Therefore, for the

approximation of perfect reflection at the solid wall for monochromatic waves

$$\text{Attenuation} = \frac{1 - R^2}{2} \qquad 46$$

The range of values expected for attenuation under these conditions is between zero, when no dissipation occurs at the breakwater, and .5 when all the incident energy is dissipated by the chamber.

Evaluation of the Attenuation of a Monochromatic Wave Monitored at a Fixed Location

For comparison, the same monochromatic wave system analyzed in the last section will be re-evaluated with the constraint that data must be acquired at a fixed location. As in equation 39, the incident wave surface is represented by

$$\eta_i = a_i \sin(kx - \sigma t + \theta_i)$$

For convenience, the fixed measuring station is established so that the initial phase angle, $\theta_i = 0$. Therefore,

$$\eta_i = a_i \sin(kx - \sigma t) \qquad 47$$

The reflected wave surface is

$$\eta_r = a_r \sin(kx + \sigma t + \theta_r) \qquad 48$$

where θ_r is, for this case, the phase angle between the incident and reflected wave and is equivalent to $\sigma\tau$ where τ is the time lag. Thus, by superposition, the resulting surface is

$$\eta_T = \eta_i + \eta_r = a_i \sin(kx - \sigma t) + a_r \sin(kx + \sigma t + \theta_r) \qquad 49$$

but $\sin - \sigma t = -\sin \sigma t$; therefore

$$\eta_T = \underbrace{[(a_i + a_r \cos \theta_r) \sin kx + a_r \sin \theta_r \cos kx]}_{A(x)} \cos \sigma t \qquad 50$$

$$+ \underbrace{[(-a_i + a_r \cos \theta_r) \cos kx - a_r \sin \theta_r \sin kx]}_{B(x)} \sin \sigma t$$

Ippen (23, p. 58) points out that this is not a progressive wave and that the average potential energy per unit surface area is a function of x.

$$\overline{PE}(x) = \frac{\gamma}{4}[A^2(x) + B^2(x)]$$

$$= \frac{\gamma}{4}\{[(a_i + a_r \cos \theta_r) \sin kx + a_r \sin \theta_r \cos kx]^2 \qquad 51$$

$$+ [(-a_i + a_r \cos \theta_r) \cos kx - a_r \sin \theta_r \sin kx]^2\}$$

expanding

$$\overline{PE}(x) = \frac{\gamma}{4}[a_i^2 \sin^2 kx + 2a_i a_r \cos \theta_r \sin^2 kx + a_r^2 \cos^2 \theta_r \sin^2 kx$$

$$+ 2a_i a_r \sin kx \sin \theta_r \cos kx + 2a_r^2 \cos \theta_r \sin kx \sin \theta_r \cos kx$$

$$+ a_r^2 \sin^2 \theta_r \cos^2 kx + a_i^2 \cos^2 kx + a_r^2 \cos^2 \theta_r \cos^2 kx \qquad 52$$

$$- 2a_i a_r \cos \theta_r \cos^2 kx + 2a_i a_r \cos kx \sin \theta_r \sin kx$$

$$- 2a_r^2 \cos \theta_r \sin \theta_r \sin kx \cos kx + a_r^2 \sin^2 \theta_r \sin^2 kx]$$

combining terms and making use of trigonometric identities the time average potential energy per unit surface area at x becomes

$$\overline{PE}(x) = \frac{\gamma}{4}(a_i^2 + a_r^2 - 2a_i a_r \cos(\theta_r + 2kx))$$
$$\overline{PE}(x) = \frac{\gamma}{16}(H_i^2 + H_r^2 - 2H_i H_r \cos(\theta_r + 2kx)) \qquad 53$$

The average total energy density at x, being twice the sum of the constituent potential energies, is

$$\overline{E}(x) = \frac{\gamma}{8}(H_i^2 + H_r^2 - 2H_i H_r \cos(\theta_r + 2kx)) \qquad 54$$

It is noted that if the time average potential energy density at x, equation 53, is integrated over x for one wave period and averaged,

$$\overline{PE} = \frac{\gamma}{16L} \int_0^L (H_i^2 + H_r^2 - 2H_i H_r \cos(\theta_r + 2kx))dx \qquad 55$$

the resulting average potential energy is

$$\overline{PE} = \frac{\gamma}{16}(H_i^2 + H_r^2) \qquad 56$$

and the associated average total, being twice the sum of the components by linear wave theory, equals

$$\overline{E} = \frac{\gamma}{8}(H_i^2 + H_r^2) \qquad 57$$

It is this result that was assumed throughout the development of the theory. Thus, if the wave system is traversed, as done in the laboratory studies, the assessment of the average energy is directly proportional to the sum of the squares of the wave heights which are easily obtained from traverse data by equation 14.

The effect of a fixed measuring location on the calculated average energy of a monochromatic wave system in front of the solid bridge wall can be calculated from examination of equation 54. By setting $x = 0$ at the measuring station the energy varies as the cosine of the phase angle between the incident and reflected wave, which, in turn, is a function of the ratio between the wave length and twice the distance, D, to the barrier. Ippen (23, p. 49) points out that though an imperfect reflection can be represented by the superposition of a standing wave and a progressive wave, the resulting surface is itself a "standing wave" because the resulting wave envelope is stationary. Thus, the average total energy per unit surface area monitored at a fixed point is a function of not only the incident and reflected wave heights, but also the location of the measuring station and the phase angle between the incident and reflected wave. Small amplitude wave theory can be incorporated to define the time required for an incident wave to travel from the fixed measuring location, be reflected at the solid wall, and return to the measuring station as a reflected wave. By setting $x = 0$ at the measuring station, the phase angle becomes that which is required by the wave of frequency $\sigma = \frac{2\Pi}{T} = \sqrt{\frac{2\Pi g}{L}}$, to travel a distance 2D. Thus, at a given measuring station, each wave frequency produces a constant phase relationship between the incident wave and that reflected from a

solid barrier.

The phase relationship between the incident wave and that reflected from a porous walled breakwater is complicated by the fact that a portion of the wave is reflected at the porous wall and the remainder is operated on by the chamber, resulting in a different phase angle.

Attenuation can be calculated from the surface fluctuations at the same distance in front of a solid wall and a porous walled breakwater. From equation 32 attenuation equals the difference in the average total energies at the two locations divided by the average total energy at the solid wall.

Substituting the energy from equation 54 using subscripts ∞ at the station in front of the solid wall, and BW in front of the breakwater, and requiring that the incident wave be the same at the two locations, the attenuation (ATTN) becomes

$$ATTN = \frac{\bar{E}_\infty - \bar{E}_{BW}}{E_\infty} = \{\frac{\gamma}{8}[H_i^2 + H_{r_\infty}^2 - 2H_i H_{r_\infty} \cos(\theta_{r_\infty} + 2kx)]$$

$$- \frac{\gamma}{8}[H_i^2 + H_{r_{BW}}^2 - 2H_i H_{r_{BW}} \cos(\theta_{r_{BW}} + 2kx)]\} / \{ \frac{\gamma}{8}[H_i^2 \qquad (58)$$

$$+ H_{r_\infty}^2 - 2H_i H_{r_\infty} \cos(\theta_{r_\infty} + 2kx)]\}$$

$$ATTN = \frac{H_{r_\infty}^2 - H_{r_{BW}}^2 - 2H_i[H_{r_\infty} \cos(\theta_r + 2kx) - H_{r_{BW}} \cos(\theta_{r_{BW}} + 2kx)]}{H_i^2 + H_{r_\infty}^2 - 2H_i H_{r_\infty} \cos(\theta_{r_\infty} + 2kx)}$$

again employing the reflection coefficient, $R = \frac{H_{r_{BW}}}{H_{i_{BW}}} = \frac{H_{r_{BW}}}{H_i}$, in front

of the breakwater and $S = \frac{H_{r_\infty}}{H_i}$, for the reflection coefficient at the solid wall the attenuation becomes

$$ATTN = \frac{S^2 - R^2 + 2R\cos(\theta_{r_{BW}} + 2kx) - 2S\cos(\theta_{r_\infty} + 2kx)}{1 + S^2 + 2S\cos(\theta_{r_\infty} + 2kx)} \qquad 60$$

Comparison of equation 60 with 45 demonstrates that the value of the attenuation can be different if the surface fluctuations are monitored at a fixed point rather than obtained by the wave height traverses of the wave envelope.

Random Waves

Random waves can be represented by the summation of a series of sinusoidal waves each with their own amplitude, frequency, and initial phase angle. In front of a solid wall an incident and reflected wave exists for each frequency. Thus, by superposition, the resulting surface is,

$$\eta_T = \eta_i + \eta_r = \sum_j (a_{i_j} \sin(k_j x - \sigma_j t + \theta_{i_j})) \qquad 61$$

$$+ \sum_j (a_{r_j} \sin(k_j x + \sigma_j t + \theta_{r_j}))$$

At each frequency the contribution to the average energy at a fixed unit surface area could be described by equation 54 except for the further constraint that in a random system the incident phase angle cannot be set to zero. Thus, the attenuation calculated from the random fluctuation

of the surface at a fixed point involves not only the Fourier components of the incident and reflected wave heights but also terms due to the product of the incident and reflected waves and the associated random phase angles.

The recorded signal is only $\eta_T(t)$. Fourier analysis of this signal provides component wave heights and phase angles as though η_T were a single series of sinusoidal waves. Spectral analysis computes a variance for the series of sinusoidal waves so that the variance is the average sum of the squares of each component amplitude $(\sigma^2 = \sum \frac{1}{j2} a_j^2)$ and the average energy is $\gamma\sigma^2$. The fact that η_T includes both incident and reflected components each including the summation of a series of sinusoids with random phase angles may well mean that analysis of the η_T signal results in a different calculated average energy than the sum of the energies calculated for η_i and η_r individually, if they could be obtained.

The introduction of extraneous terms or the elimination of existing ones is even more likely during spectral analysis of the η_T in front of the breakwater due to the additional phase relationship introduced between the random incident and reflected wave components by the fluctuation of the chamber.

At this place in time the author can only express caution that the variance calculated from the surface fluctuations of superimposed random incident and reflected waves does not directly relate the average total energy of the wave system.

Alternatives

The present study does not resolve the apparent discrepancy between

the average total energy and that calculated from the variance obtained from spectral analysis of the surface fluctuations at a fixed location. Though they are not pursued at this time, two alternative methods of data analysis show promise as a means to separate the incident and reflected wave energy.

A recent paper by Thornton and Calhoun [26] presents a method of separating the incident and reflected wave energy spectra using in-line pressure transducers. To obtain the required records, in the present experiment, two additional transducers were mounted five feet further away from the porous wall and the solid wall. Thus, for the final few data records, pressure fluctuations at a constant depth were obtained at two distances in front of the breakwater and at a matching set of distances in front of the solid pontoon wall. At this time, only a sample data reduction has been accomplished. The results show promise. Due to the limited length of the prototype breakwater, diffraction from beyond the chamber could be affecting the surface fluctuation at the gage furthest in front of the breakwater.

It should be noted that if this process works it will only separate incident and reflected spectra for that portion of the investigation using the extra transducers. It is possible, however, that the understanding acquired for those records could provide a basis for better evaluating the remainder of the data.

A second method of evaluating the data could be adapted from an extension of spectral analysis originated by Tukey called Power Cepstrum [27]. Though intended for an entirely different subject, it assumes a model where the monitored signal is the sum of an incident random process and an attenuated reflected process with a time delay.

The analysis demonstrates that the resulting energy spectra are influenced not only by the incident and reflected amplitudes but also a function of the cosine of the frequency and time delay. The analysis provides a method of separating the incident and reflected spectra. The similarity between this result and that found for equation 54 suggests that the transformations required for Cepstrum Analysis may provide a clearer interpretation of the present experimental data.

Case Example and Attenuation Interpretation

On February 27, 1972 (Run Number 3, 53, g, shown as the last run in Appendix I) a data record was acquired for 35-40 mph winds gusting to 50 mph out of the SSW. The chamber with a solid bottom had a width of seven feet. During the 20 minute record, an observer stood on the working platform, three feet above the still water level. During the same period the water level within the chamber was never greater than three feet above S.W.L. The record log during this observation stated, "the chamber is obviously functioning very well for this wind condition. Waves are passing well overhead on both sides of the chamber along the bridge and yet none of the incident waves are going over the three foot high breakwater porous wall. Another effect which is definitely clear is that the breakwater would completely eliminate the wave runup onto the roadway for this wave condition. There is still a significant amount of wind-blown spray but no wave overtopping." Following digitizing and spectral analysis of this wave record, the attenuation was shown as minus 10.7%. The initial impression from such a result would be that the chamber created rather than attenuated energy. Even aside

from the observed situation, a linear damped oscillator is incapable of altering the frequency of waves impending upon it. Therefore, another explanation is necessary. Careful analysis shows that the term involving the product of the reflected and incident wave heights is an expression which, if the two terms are well correlated, results in a very strong positive or negative influence upon the attenuation. Therefore, the attenuation cannot be used as calculated to judge the performance of the breakwater. It is important to note that the peak frequency occurring in front of the breakwater and at the remote ∞ station were the same for the record under investigation. We can thus conclude that the chamber was operating at its natural frequency and that the actual conversion by the chamber to non-conservative energy was nearly a maximum as indicated by model tests and as observed during the record. The corresponding model results demonstrated an 80% reduction in incident energy for the condition scaling to the record in question. Thus, the difference between the 10% increase in wave energy during reflection shown by the attenuation and the 80% reduction in wave energy in the laboratory are due, at least partially, to this product term. It is therefore necessary to use the random wave data to establish and substantiate the model frequencies for the various conditions. At the same time the frequencies of interest at the test site can be established. Therefore, the efficiency of any given full-scale breakwater condition cannot presently be quantified except by linking it back to the equivalent model data.

Selection of Nyquist Frequency

Figure 39 is a representative spectral plot chosen from Appendix II.

The plot presents a distribution for a five foot chamber with a solid bottom exposed to a 20-25 mph wind/wave condition. The remote spectra shows a peak frequency at approximately .4Hz and a distinct secondary peak at .75Hz. If the Nyquist frequency was chosen incorrectly for the data, i.e., too low, the secondary peak could represent data folded to .75Hz from a frequency above the Hyquist frequency. Figure 39 was obtained from a digital record of 1024 points at equal .328 second intervals; resulting in a 1.52Hz Nyquist frequency. Thus, the secondary peak could represent data that should be assigned to 2.29Hz (1.52 + (1.52 - .75)).

Figure 40 is the spectra for the same breakwater geometry exposed to a 35 mph wind/wave condition. Notice that both the primary and secondary peaks are shifted to a lower frequency. If aliasing had occured the second peak would have shifted toward the Nyquist frequency. Therefore, it is concluded that the aliasing is not a problem and the Nyquist frequency was properly chosen for the data processing.

CHAPTER VI

RESULTS

Scope

The data, taken simultaneously at a fixed location in front of a porous walled breakwater and at a remote station away from the influence of the breakwater, for a matrix of wind conditions and chamber configurations is reduced, using spectral analysis and the resulting spectral plots and calculations are presented. The cautions detailed in the analysis are incorporated and care is taken to interpret the spectra and attenuation results in a manner which separates definite results from less distinct interpretations. The original objective of energy evaluation is not met as quantitatively as would have been possible with a complete separation of the incident and reflected wave components and an assessment of the effects of the chamber on the "effective" distance to the fixed measuring stations. The analyzed data do provide a positive link between the monochromatic wave model studies and the full-scale random wave investigation. In particular, the porous walled breakwater is frequency selective when exposed to wind generated waves; and the natural frequency corresponds to that of a linear damped oscillator as linearly scaled from dimensional analysis of the model studies. The maximum resultant forces exerted on the porous wall are also presented.

Reduction of Wave Runup

The guard rail on the Evergreen Point Bridge is eleven feet above the still water level. Wind conditions in excess of 35 mph produce waves with sufficient energy to runup and overtop the guard rail, creating

a potential hazard to traffic on the bridge (figures 41 and 42). When the same waves impact the porous wall of the breakwater much of the energy goes into turbulent jets passing through the wall into the chamber. For extreme conditions, i.e., winds greater than 40-45 mph, waves overtop the three foot high porous wall and break into the chamber. For the highest observed windspeed of 45 mph, gusting to 55, the maximum wave runup on the back wall of the chamber was four feet and the chamber pumped completely full only once during the forty-five minute observation period. The wind-carried spray from breaking waves a distance from the bridge, is also diminished slightly due to the decrease in reflected wave height.

It can be safely concluded that the application of a resonating chamber with a porous wall five to seven feet in front of the pontoon and extending three feet above S.W.L. would completely eliminate wave runup onto the roadway of the Evergreen Point Floating Bridge. With proper scaling comparable runup reductions could be incorporated into other deep water structures.

Frequency Selective Device

Laboratory studies [16] demonstrated that the porous walled breakwater behaves as a linear damped oscillator when exposed to monochromatic waves. As resonators the models dissipated a maximum energy near the natural frequency of the chamber. Theory demonstrates that the natural frequency can be adjusted by varying the chamber width. In particular, the ratio of the resonant frequencies for breakwater configurations of varying widths equals the square root of the chamber width. One of the major objectives of full-scale investigation was to determine the breakwater

response to random wind generated waves. The full-scale breakwater is shown in operation in figure 43.

Figure 44 demonstrates that the full-scale breakwater is frequency selective when subjected to random waves. If the chamber were not frequency selective the peak frequencies at the two stations over the record periods of approximately six minutes should approximate a one to one correspondence at all wind speeds. As indicated in the figure, the peak frequency in front of the chamber tends toward a central frequency. The location where a line passing through the data crosses the one to one correspondence is the "crossover" frequency. The shift in the "crossover" frequency for the two chamber widths is seen to correspond with the square root of the chamber width; a response predicted by theory for the natural frequency of a linear resonator. The value of the crossover frequency for each chamber width corresponds to the theoretical natural frequency for a linear resonator. The crossover frequency of the five and seven foot, solid bottom, chambers correspond to the peak frequency of incident waves produced by 15-20 and 25-35 mph wind conditions, respectively. The expected crossover frequency for a chamber width of three feet would occur for windspeeds of 10-15 mph. The association of maximum energy dissipation with the natural frequency from laboratory tests and the correspondence of the natural and crossover frequencies were sufficient information to eliminate testing of the three foot chamber width. That is, no matter how effective a three foot chamber is at reducing waves in the 10-15 mph range, if the dominant incident energy at the test site occurs for 25-30 mph winds, a seven foot chamber width would provide a better tuned chamber. The peak frequency inside the

chamber is shown in figures 45 and 46.

Effect of Removing the Chamber Bottom

The removal of the bottom from the breakwater chamber results in a shift of the crossover frequency to a lower value (figure 47). Removing the bottom from a five foot wide chamber produced a crossover frequency shift from .43 cycle/second to approximately .39 cycles/second, which corresponds to a change from matching the peak incident wave frequency produced by a 20 mph wind to that produced by a 25 mph wind. Theory dictates that the resonant frequency is inversely proportional to the chamber depth. Therefore, removing the bottom results in an apparent decrease in chamber depth.

Forces; Magnitude and Frequency

The virtual elimination of wave runup by the porous walled chamber greatly reduces the forces exerted on the solid vertical wall (existing bridge pontoon). With the chamber installed, the maximum force on the solid wall is due principally to the hydrostatic pressure of the water when the chamber is full. For maximum observed wind conditions of 40-45 mph with higher gusts, the chamber never completely pumped to its full height, three feet above still water level. Secondary disturbances superimposed upon the level of the chamber produce an occasional additional height at the wall of at most 1.5 feet. Along the remainder of the bridge for the same windspeed, pontoon walls were subjected to forces due to wave runup containing sufficient energy to overtop the guard rail eleven feet above S.W.L.

By allowing water to pass through the porous front wall of the chamber, it is also subjected to less force than would be exerted on a comparable solid wall. The measured maximum resultant force on the porous wall was 118 pounds per linear foot of wall, measured during a 35-40 mph (gusting to 50) wind condition, and thus was an even greater reduction in force than predicted. Actual finite wave crest lengths would further reduce the average force per unit length acting on a long wall.

The peak frequency of the force is shown in figure 48 to be more nearly related to the chamber crossover frequency than the incident wave frequency. As shown throughout the appendices, the distribution of force with frequency contains only one significant peak which occurs between .35 and .6 cycles/second.

Attenuation

The variance of a record of progressive random wave heights, obtained from spectral analysis, is directly proportional to the average energy per unit surface area (average energy density). Throughout the present study, the signals recorded at two stations, one in front of the breakwater and a second or remote station near by, but away from the influence of the breakwater, were the sum of incident and reflected waves.

The method of data reduction involved computing the variance of the sum of the incident and reflected waves at the two stations. The resulting variances, taken as the sum of average incident and reflected energy densities, were computed over a sufficiently long time period to assure that the incident energy at both stations was the same. Also,

knowing that no energy was transmitted beyond the test site, the differences between the variances were attributed to the average energy dissipation of the reflected waves by the chamber. This difference between the variance at the two stations ratioed to the variance at the remote station was defined as Attenuation (equation 32) and taken to be the average energy density dissipated by the breakwater as a ratio of the average total energy density in front of the solid reflecting barrier.

Attenuation, calculated in this manner, is displayed throughout the appendices for a matrix of chamber configurations and wind speeds. However, the range of calculated Attenuation values did not correspond with visual observation nor reasonable physical expectations. The analysis in Chapter Five demonstrates a discrepancy between the variance and the average energy density. When incident and reflected waves coexist, a "standing" wave envelope results. The time average energy per unit surface area of an incident-reflected wave system measured at a fixed location may differ from the time average energy per unit surface area of the incident-reflected wave system.

This apparent contradiction in terms is due to the fact that actual average energy of a wave is the sum of the time averaged energy of the wave at each point averaged over a wave length. For a progressive wave this average can be obtained at a fixed location. The presence of both incident and imperfectly reflected waves results in a standing wave envelope. As such the time average energy density is not averaged over a wave length. The resulting difference in calculated energy, for each component wave frequency, is shown in equation 54 to be related to the product of the amplitudes of a phase angle between the incident and reflected wave. For waves reflected from the solid wall, the phase

angle is simply related to the distance between the fixed measuring station and the barrier. In front of the breakwater, the expression is complicated by the effect of the breakwater. The porous walled breakwater, a linear resonator, does not affect the frequency of a wave during reflection, but does affect the amplitude and, unlike a solid wall, the phase angle. Due to the alteration in phase angle, the calculated average energy density at the two locations, both the same physical dimension from a wall, can be based on different portions of the standing wave envelope. Thus, even though the physical distance between the two measuring stations and the respective barriers is a constant, they are effectively at different locations. Therefore, energy calculations based on data acquired during the present field test cannot be used directly to analyse the amount of energy dissipated by the breakwater.

Possible alternative methods of analysis are suggested in the analysis section. Attenuation, as calculated, is included in the hope that future work will allow a method of relating the calculated spectra and variances to the actual average energy density. The attenuation calculated for various wind conditions is summarized in figures 49 and 50. The occurence of a negative attenuation corresponding to frequencies near the predicted natural frequency demonstrate the strong influence of the chamber on shifting the phase angle of the wave during reflection at frequencies near resonance. The calculation of an apparent energy increase in front of the chamber near the resonant frequency can be noted throughout the appendices. It must be remembered that this value is due to the effects enumerated in the analysis and is not representative of the average energy density at that frequency.

CHAPTER VII

CONCLUSION AND RECOMMENDATIONS

Conclusion

The porous walled breakwater behaves as a linear damped oscillator, or resonator, when exposed to random wind generated waves. The cross-over frequency of the system occurs at the frequency predicted by theory to be the natural frequency of a linear resonator and the frequency response of the full-scale device exposed to random waves scales properly from the results of models exposed to monochromatic waves. The model resonators produce a maximum reduction in reflected wave energy near the natural frequency. If the full-scale chambers correspondingly dissipate the maximum energy near the natural frequency, the five and seven foot chamber widths investigated produce a maximum energy dissipation for random waves resulting from 15-20 and 25-35 mph storm conditions, respectively.

The runup and overtopping onto the roadway are completely eliminated by the porous walled chamber with an associated reduction in force exerted on the pontoon wall. The magnitude of the force on the porous wall is less than predicted and its frequency distribution appears to correspond well with the peak frequency recorded in front of the breakwater.

It is concluded that the porous wall resonating chamber, a device which can easily be appended to an existing structure or incorporated into a new structure, does reduce the reflected wave energy and the force exerted on the structure without requiring any power to drive it.

Though observation verifies that the breakwater works well, the

amount of energy dissipated by the chamber cannot be quantified at this time. As enumerated in the analysis, the time average energy density of co-existing incident and reflected waves at a given point is not only a function of the wave heights, as is the case for progressive waves, but is also a function of the distance to the barrier, the product of the incident and reflected amplitudes, and the random phase angle. For a constant physical distance to a barrier, the change in phase angle during reflection caused by the breakwater produces an effectively different distance to the porous wall than to a solid wall. Thus, the energy density calculated during this investigation at two fixed stations, one in front of the breakwater and another in front of a solid wall cannot be directly compared. However, the performance of the chamber exposed to random wind generated waves is like that of the models in monochromatic wave systems in several respects. The effect of changing the chamber width; the match with predicted resonant frequencies; the result of removing the chamber bottom; and the observed attenuation at the resonant frequency, are consistant between model and full-scale results. Therefore, it is concluded that the two systems are indeed hydraulically similar.

Recommendations

The porous walled resonating chamber provides many benefits for application to floating structures. The units are light wieght, require no power, and can be pre-fabricated and appended to existing structures or can be an integral and structural part of new structures. For

applications to existing floating bridges the porous walled chamber could be easily incorporated into cantilevered lanes on existing pontoons, while at the same time reducing the structural loads upon the pontoons by the wave action. Dimensions can be selected from the parameters developed in the study. A seven foot chamber width with a solid chamber bottom is recommended for an exposure like the one at the Evergreen Point Bridge. In a permanent installation large spill ports should be provided above the top of the porous wall to allow spillage of exceptionally large waves into the chamber. Occasional perforations between compartments would equalize loads on supports.

The amplification of the force on solid end panels noted during this investigation can be eliminated in a permanent full length installation by using porous end plates. The mass transport into the chamber results in an accumulation of surface debris. A permanent installation should allow for easy removal of this debris.

Academically, the possible alternative data analysis methods suggested should be pursued to provide a means of quantifying the energy dissipated by the breakwater.

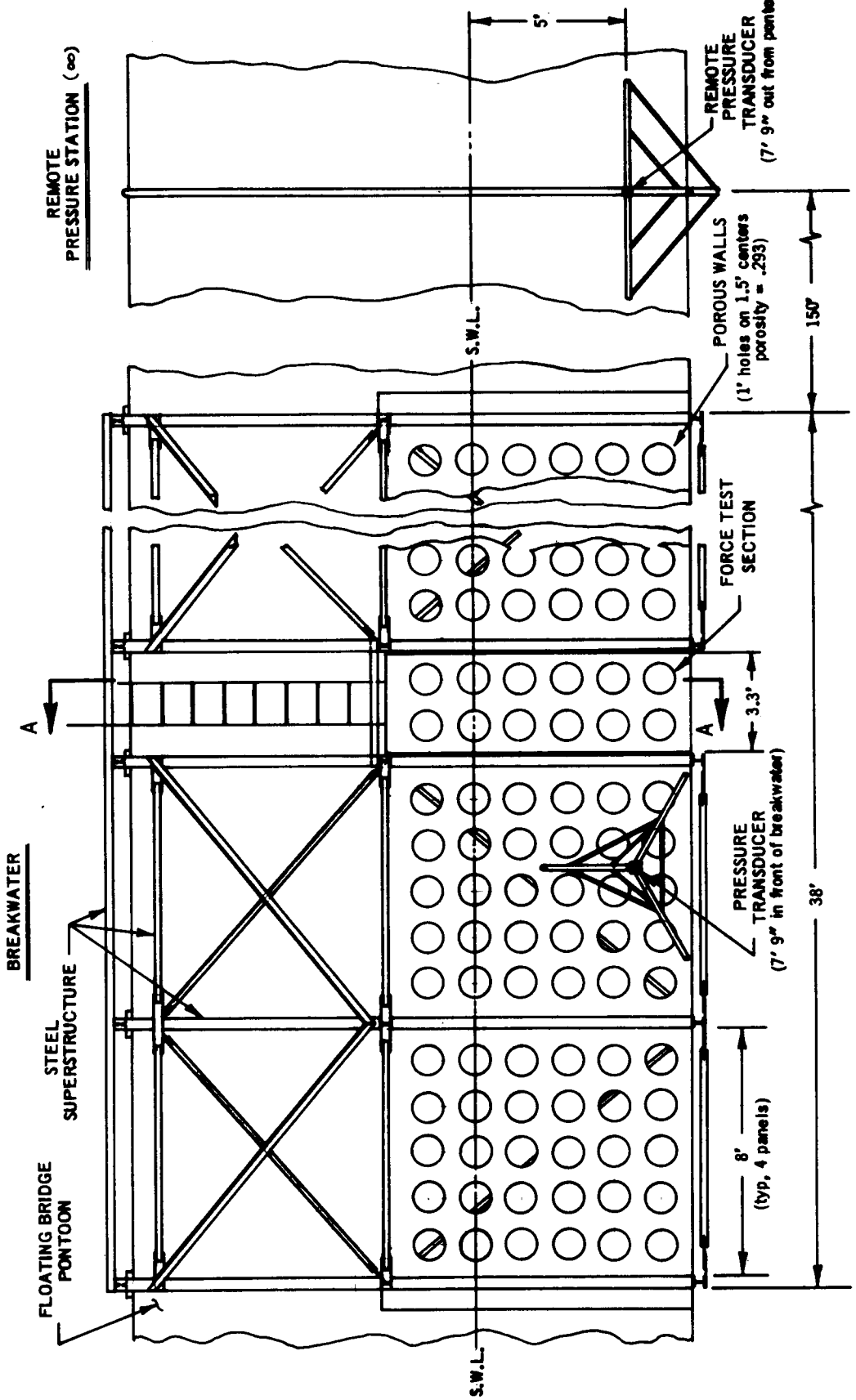

FIGURE 1. Porous Walled Breakwater; Front View.

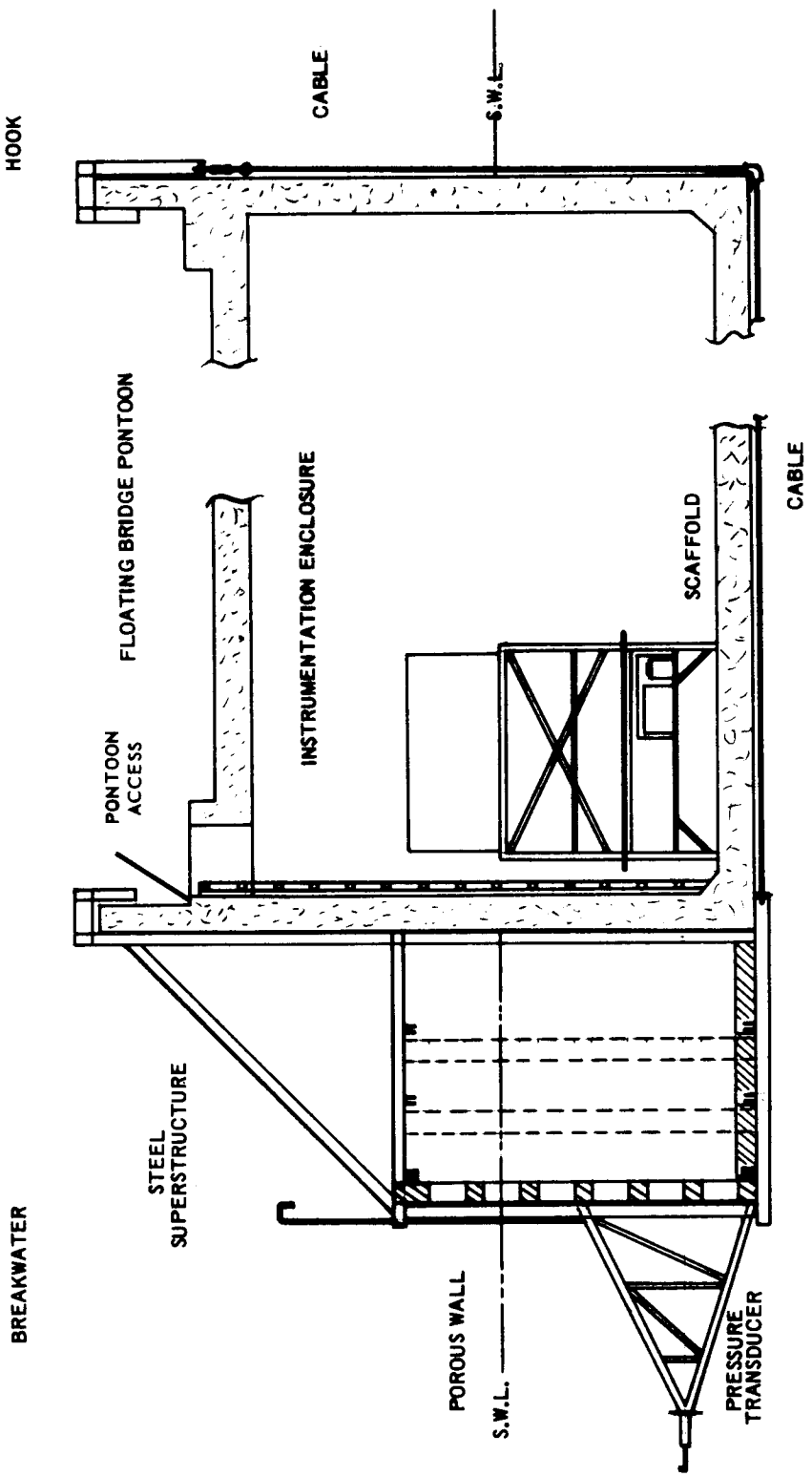

FIGURE 2. Cross-Section A-A Of Breakwater Attached To Floating Bridge Pontoon.

FIGURE 3. TEST SITE

DEEP WATER WAVE SPEED AND LENGTH AS A FUNCTION OF WAVE PERIOD OR FREQUENCY (SMALL AMPLITUDE THEORY)

T (sec)	f (cycle sec)	Co (ft/sec)	Co (knots)	Lo (feet)
0.6	1.66	3.07	1.82	1.84
0.7	1.43	3.58	2.12	2.51
0.8	1.25	4.09	2.42	3.28
0.9	1.11	4.61	2.73	4.15
1.0	1.00	5.12	3.03	5.12
1.1	.91	5.63	3.33	6.19
1.2	.83	6.14	3.64	7.37
1.3	.77	6.65	3.94	8.65
1.4	.71	7.17	4.24	10.0
1.5	.67	7.68	4.55	11.5
1.6	.63	8.19	4.85	13.1
1.7	.58	8.70	5.15	14.8
1.8	.56	9.21	5.45	16.6
1.9	.53	9.72	5.76	18.5
2.0	.50	10.2	6.06	20.5
2.1	.48	10.7	6.36	22.6
2.2	.45	11.2	6.67	24.8
2.3	.43	11.8	6.97	27.1
2.4	.42	12.3	7.27	29.5
2.5	.40	12.8	7.58	32.0
2.6	.38	13.3	7.88	34.6
2.7	.37	13.8	8.18	37.3
2.8	.36	14.3	8.48	40.1
2.9	.34	14.8	8.79	43.0
3.0	.33	15.4	9.1	46.1
3.1	.32	15.9	9.4	49.2
3.2	.31	16.4	9.7	52.4
3.3	.30	16.9	10.0	55.8
3.4	.29	17.4	10.3	59.2
3.5	.29	17.9	10.6	62.7
3.6	.28	18.4	10.9	66.4
3.7	.27	18.9	11.2	70.1
3.8	.26	19.4	11.5	73.9
3.9	.26	20.0	11.8	77.9
4.0	.25	20.5	12.1	81.9
4.5	.22	23.0	13.6	104
5.0	.20	25.6	15.2	128

FIGURE 4. Range Of Deep Water Wave Parameters Applicable To Test Site .

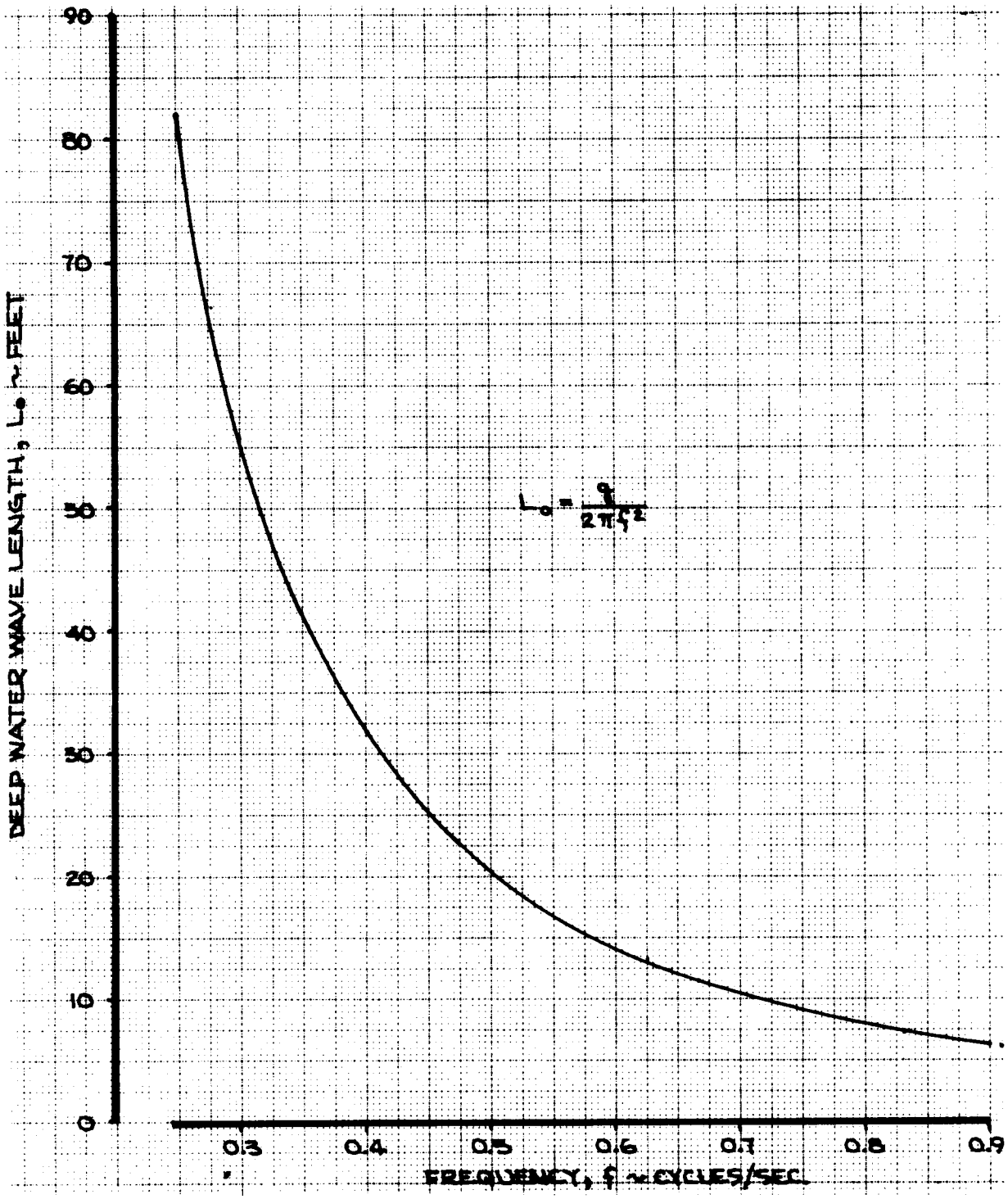

FIGURE 5. Deep Water Wave Length Versus Frequency.

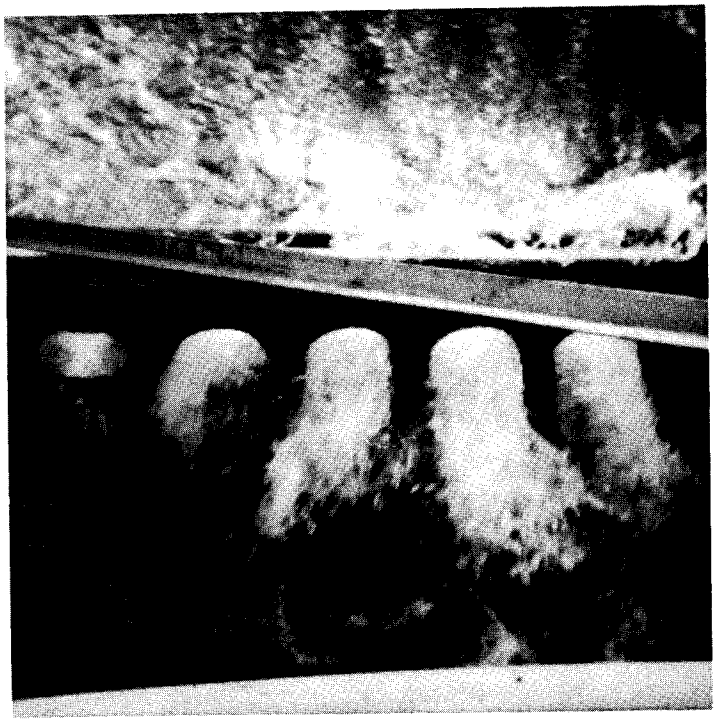

Figures 6 & 7 Breakwater Operation.
(Incident wave energy converted to kinetic energy [jets] and dissipated through turbulent mixing and diffusion.)

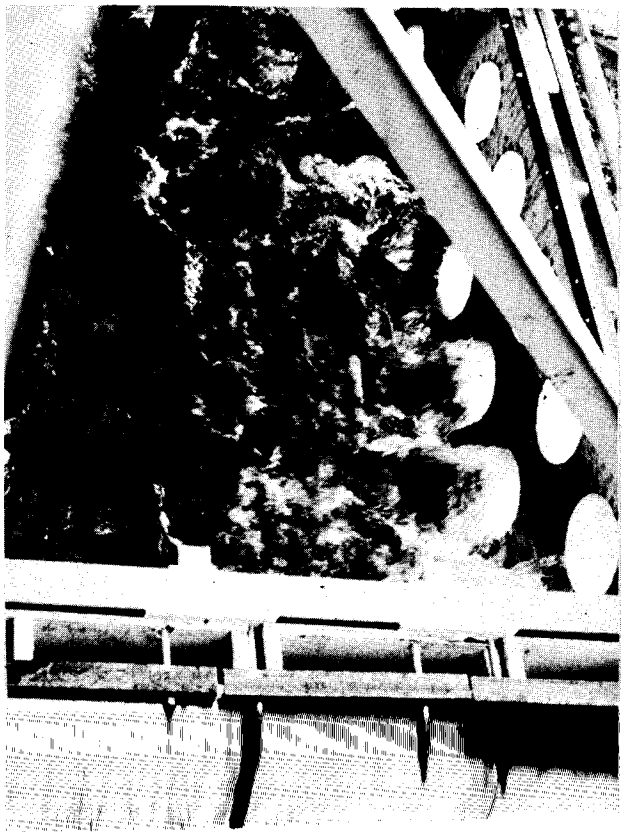

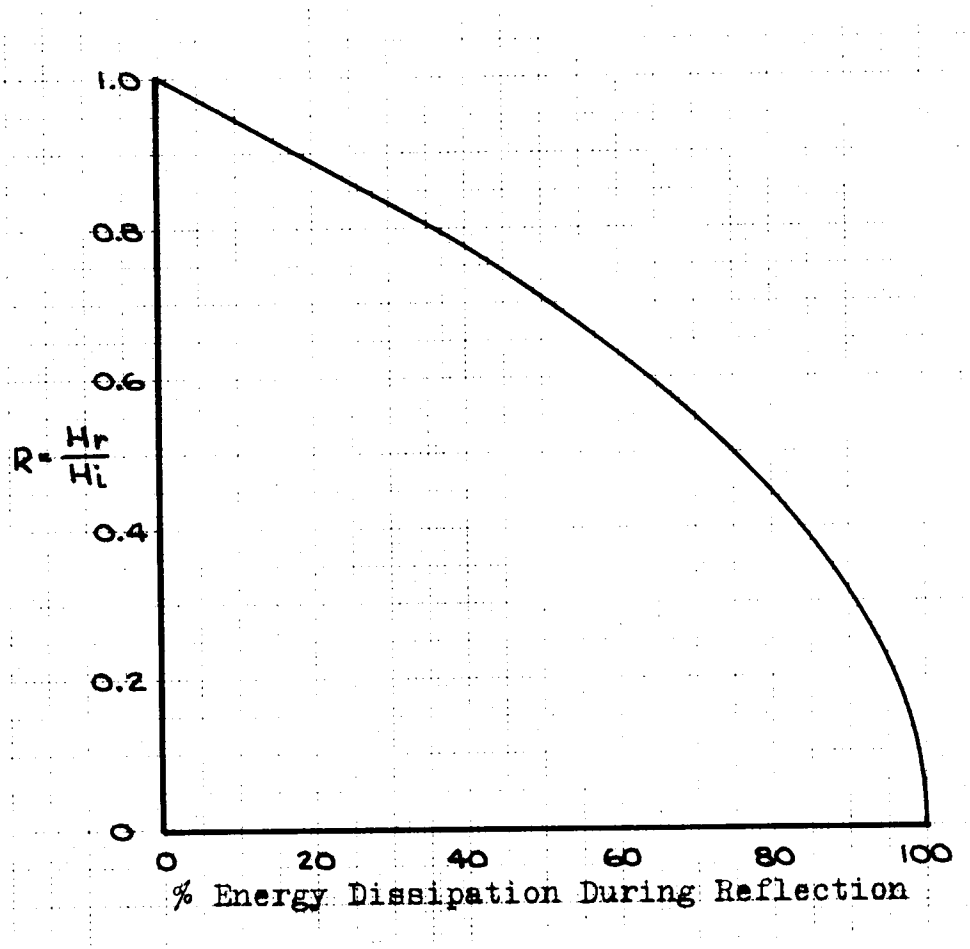

FIGURE 8 . Relationship Between Energy Dissipation and Reflection Coefficient.

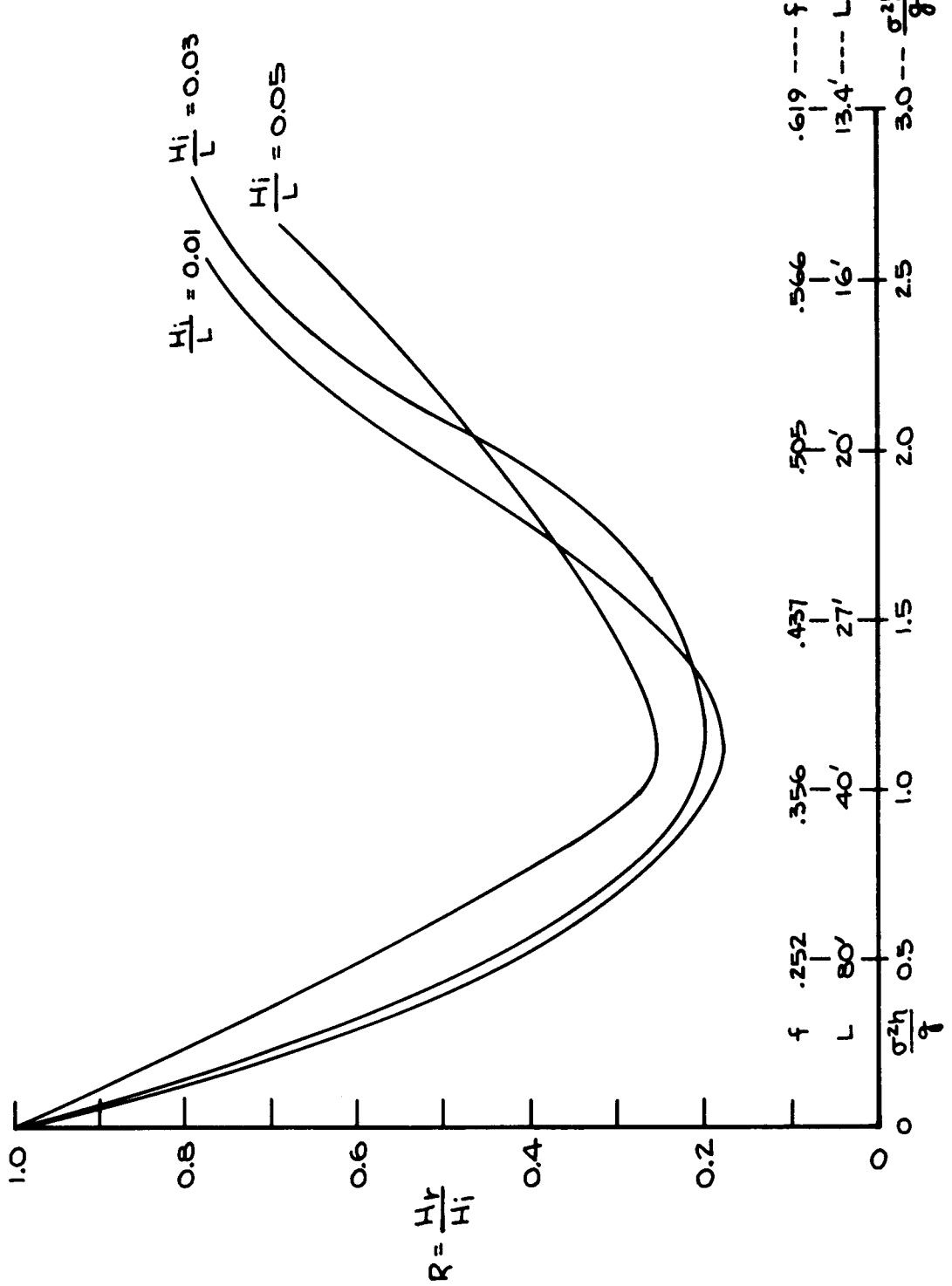

FIGURE 9. EXPERIMENTAL REFLECTION COEFFICIENT; MODEL BREAKWATER CORRESPONDING TO 4' CHAMBER WIDTH, POROSITY = .196, SOLID BOTTOM

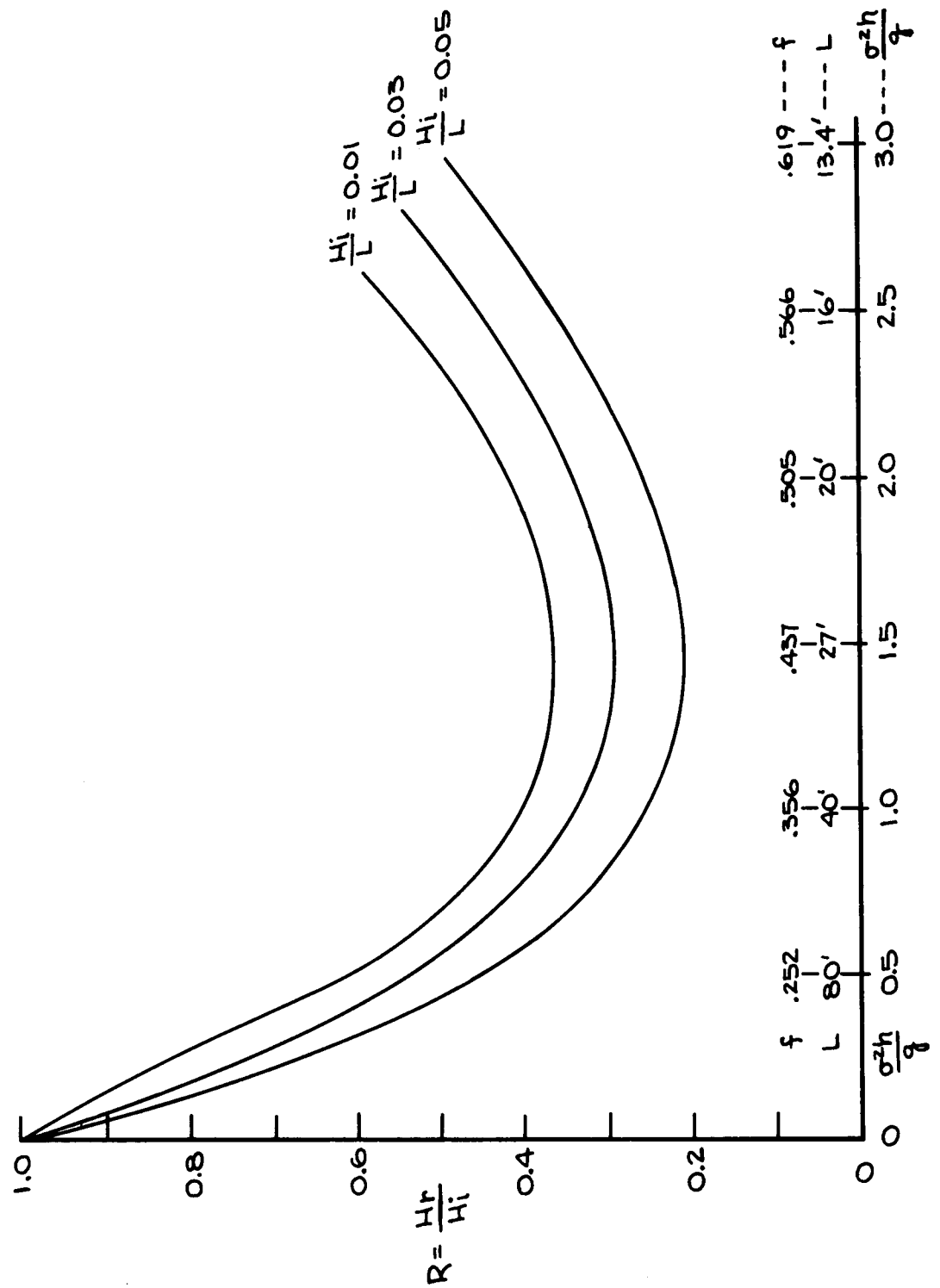

FIGURE 10. EXPERIMENTAL REFLECTION COEFFICIENT ; MODEL BREAKWATER CORRESPONDING TO 4' CHAMBER WIDTH, POROSITY = .333, SOLID BOTTOM

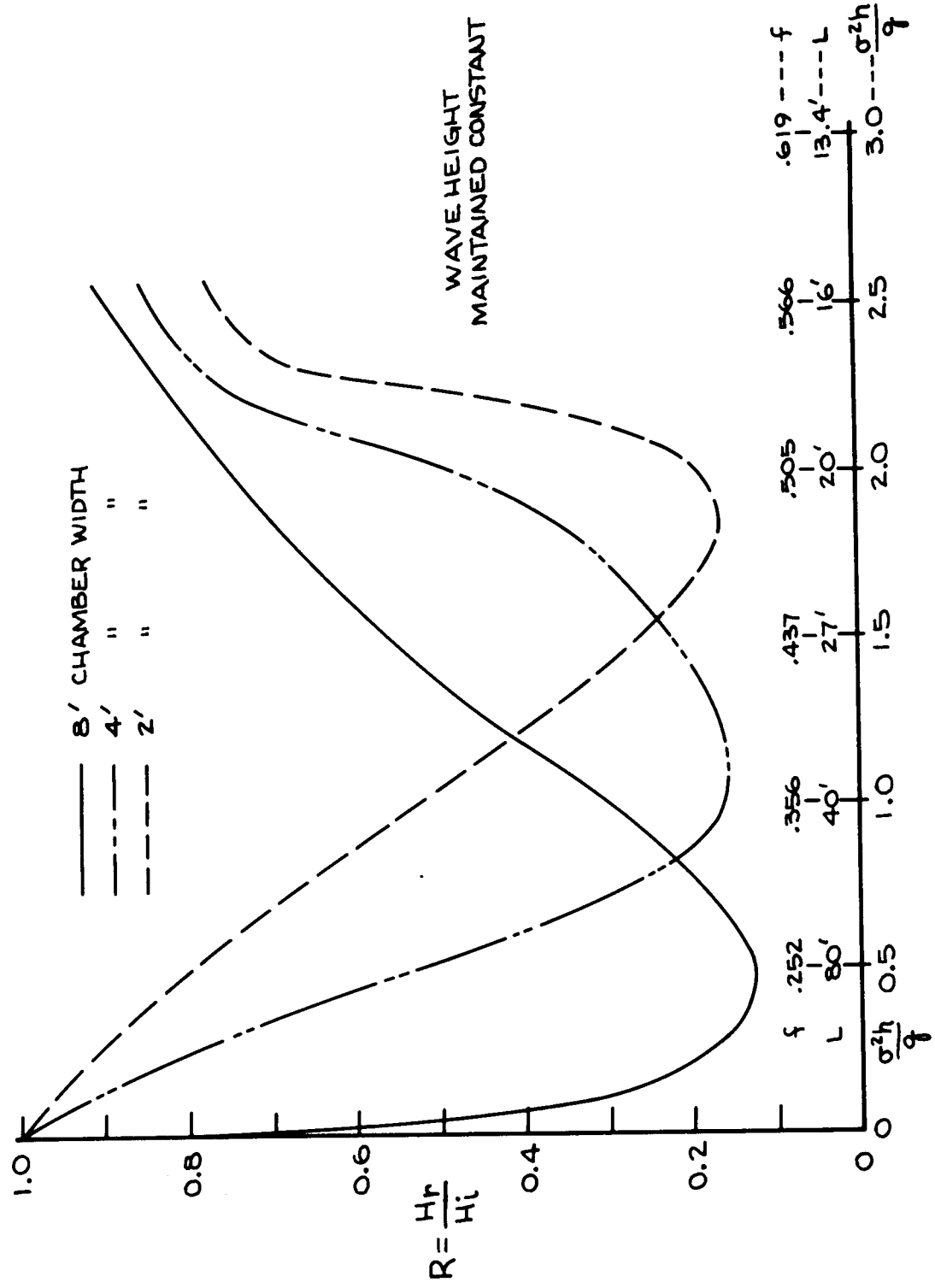

FIGURE 11. EXPERIMENTAL REFLECTION COEFFICIENT DEPENDENCE ON BREAKWATER WIDTH; MODEL SCALE, POROSITY = .196, SOLID BOTTOM

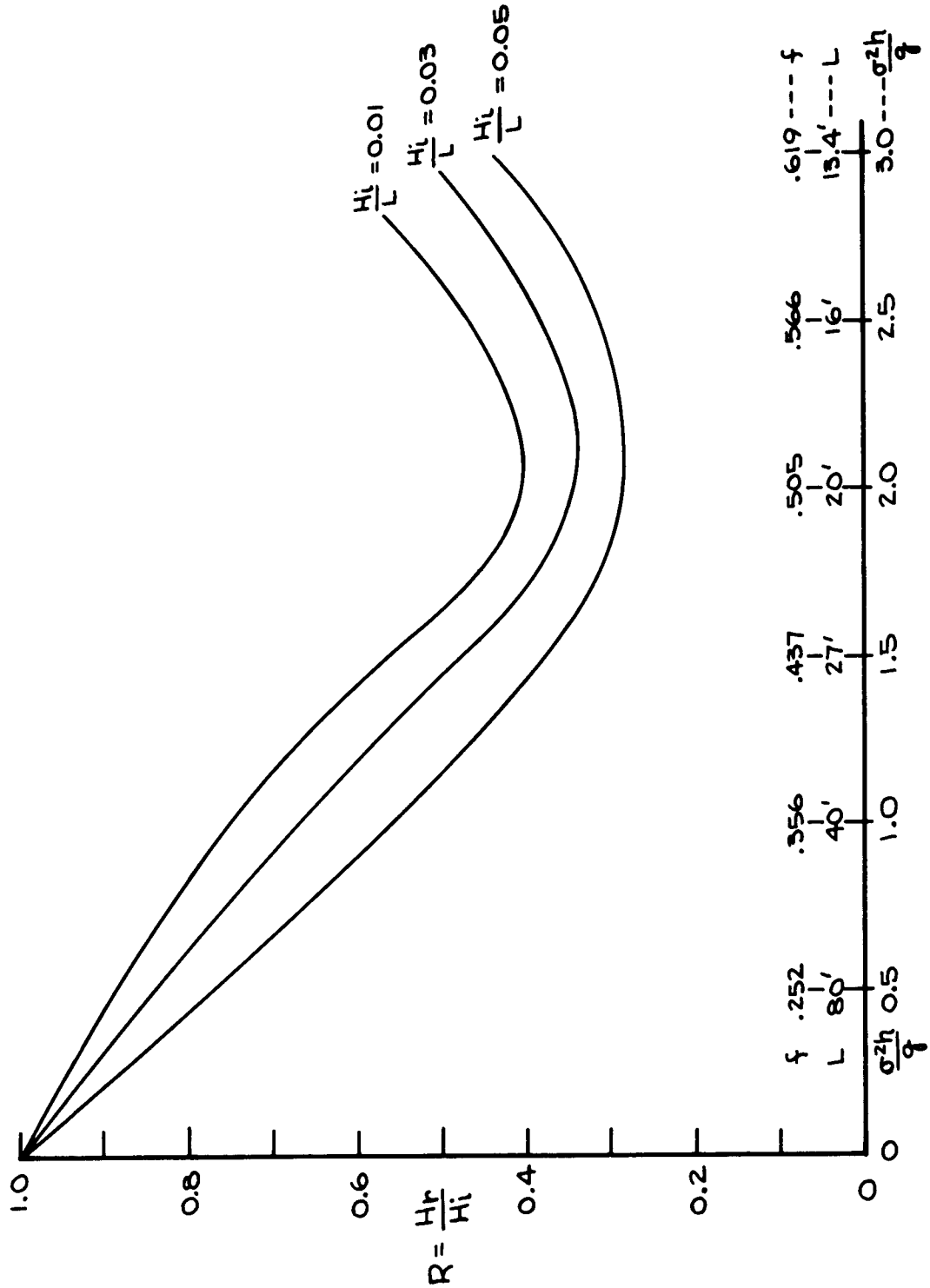

FIGURE 12. EXPERIMENTAL REFLECTION COEFFICIENT; MODEL BREAKWATER CORRESPONDING TO 4' CHAMBER WIDTH, POROSITY = .333, BOTTOM REMOVED

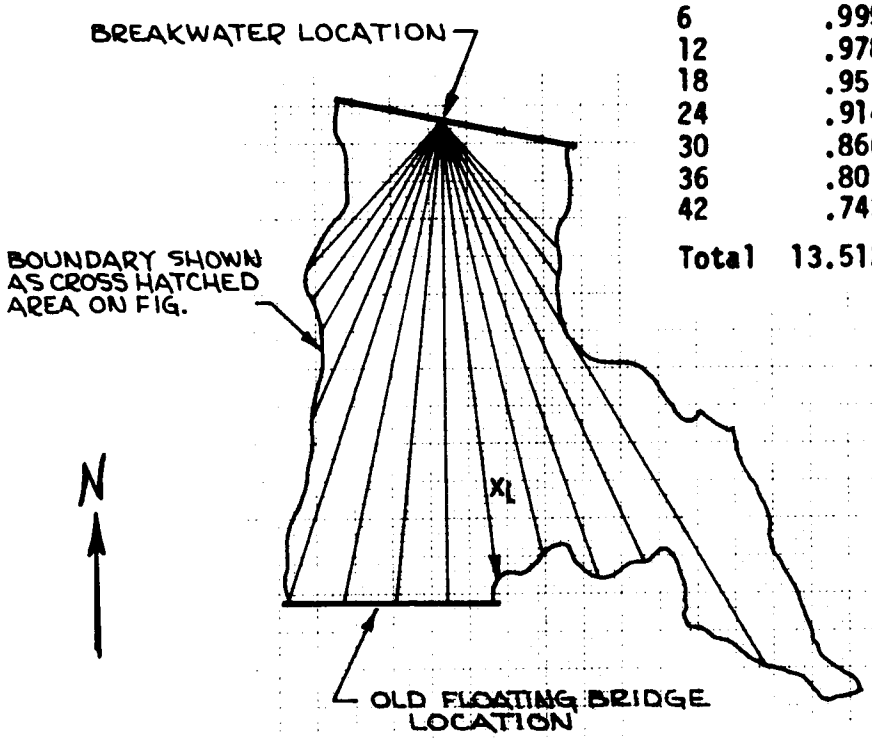

	cos α	X_i^n	X_i cos α
42	.743	1.09"	.81
36	.809	1.15	.93
30	.866	1.28	1.11
24	.914	1.72	1.57
18	.951	2.65	2.52
12	.978	2.57	2.51
6	.995	2.54	2.53
0	1.000	2.52	2.52
6	.995	2.40	2.39
12	.978	2.30	2.25
18	.951	2.53	2.41
24	.914	2.54	2.32
30	.866	2.60	2.25
36	.809	1.00	.81
42	.743	.88	.65
Total	13.512		27.58

$$F_{EFF} = \frac{\Sigma X_i \cos\alpha}{\Sigma \cos\alpha}$$

$$= \frac{27.58}{13.512}$$

$$= 2.04 \text{ UNITS}$$

2.18 MILES = 3 UNITS

$\therefore F_{EFF} = 2.8$ MILES

FIGURE 13. COMPUTATION OF EFFECTIVE FETCH FOR SOUTHERLY WIND

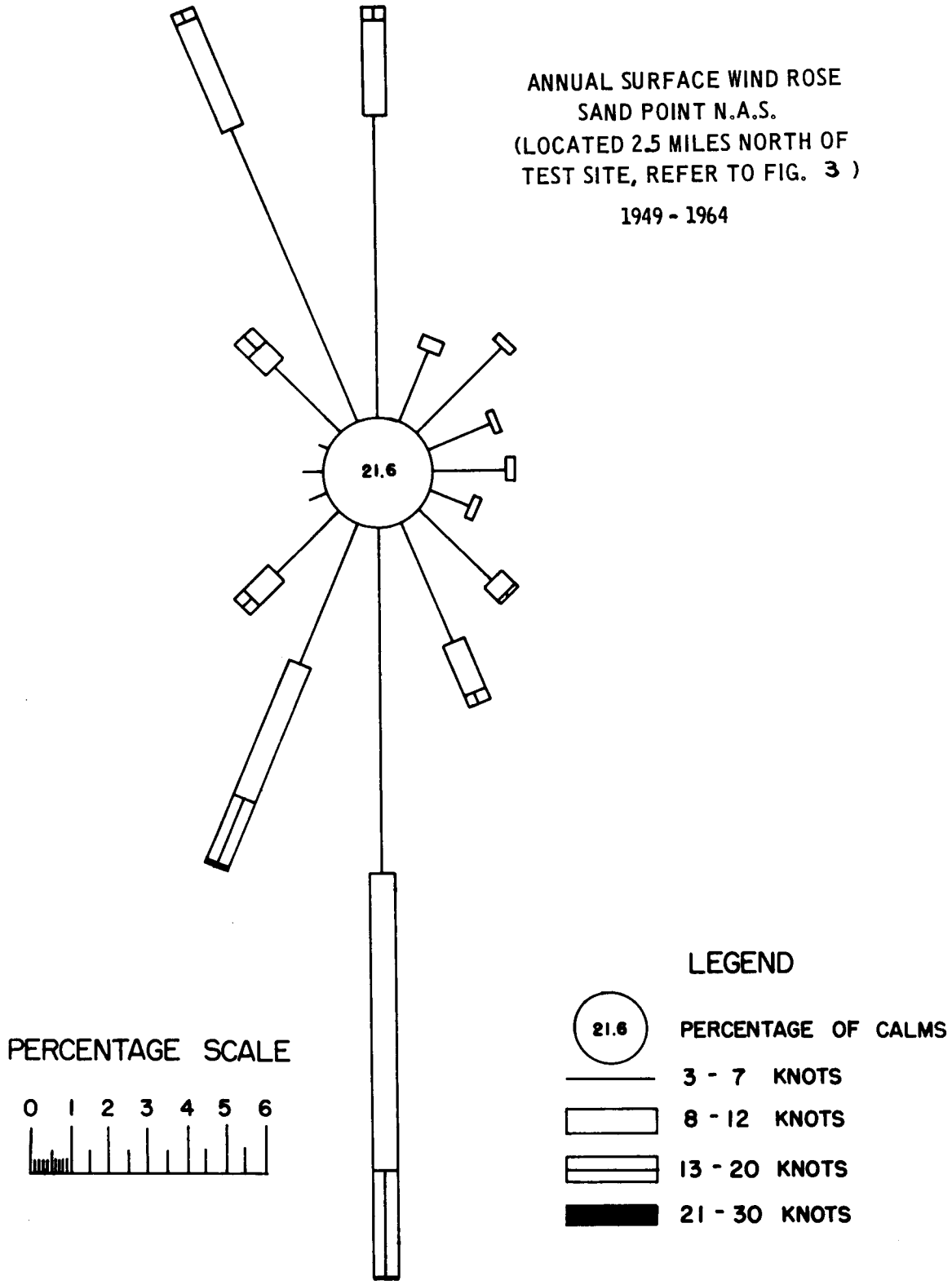

FIGURE 14. APPROXIMATE ANNUAL WIND ROSE FOR TEST SITE

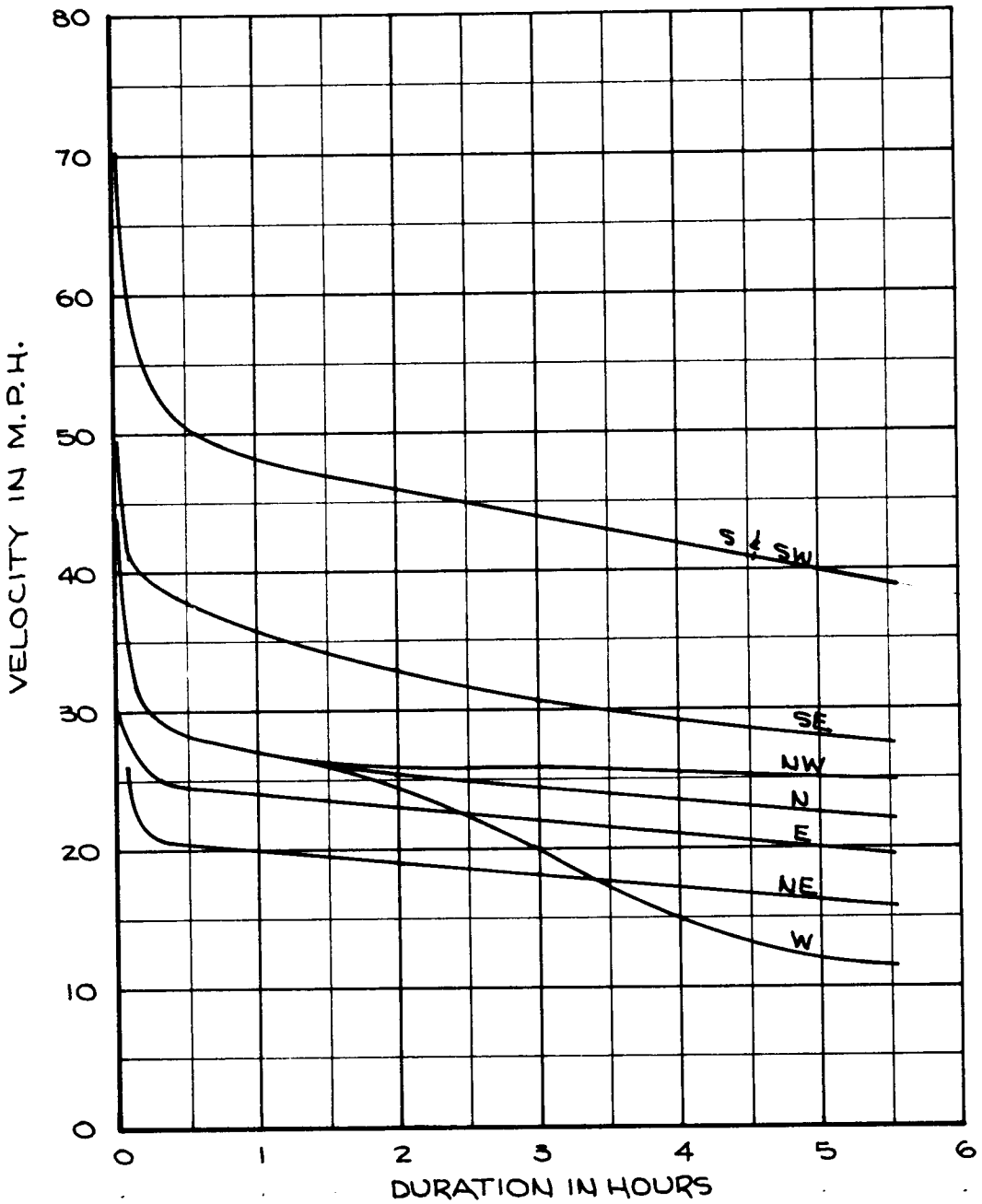

NOTE: BASED ON MAXIMUM RECORDED WIND MOVEMENT FOR DURATIONS TO 5 HRS. FOR SEATTLE CITY OFFICE, U.S. WEATHER BUREAU. PERIOD OF RECORD 1900-1955

FIGURE 15. WIND VELOCITY DURATION CURVE AT TEST SITE

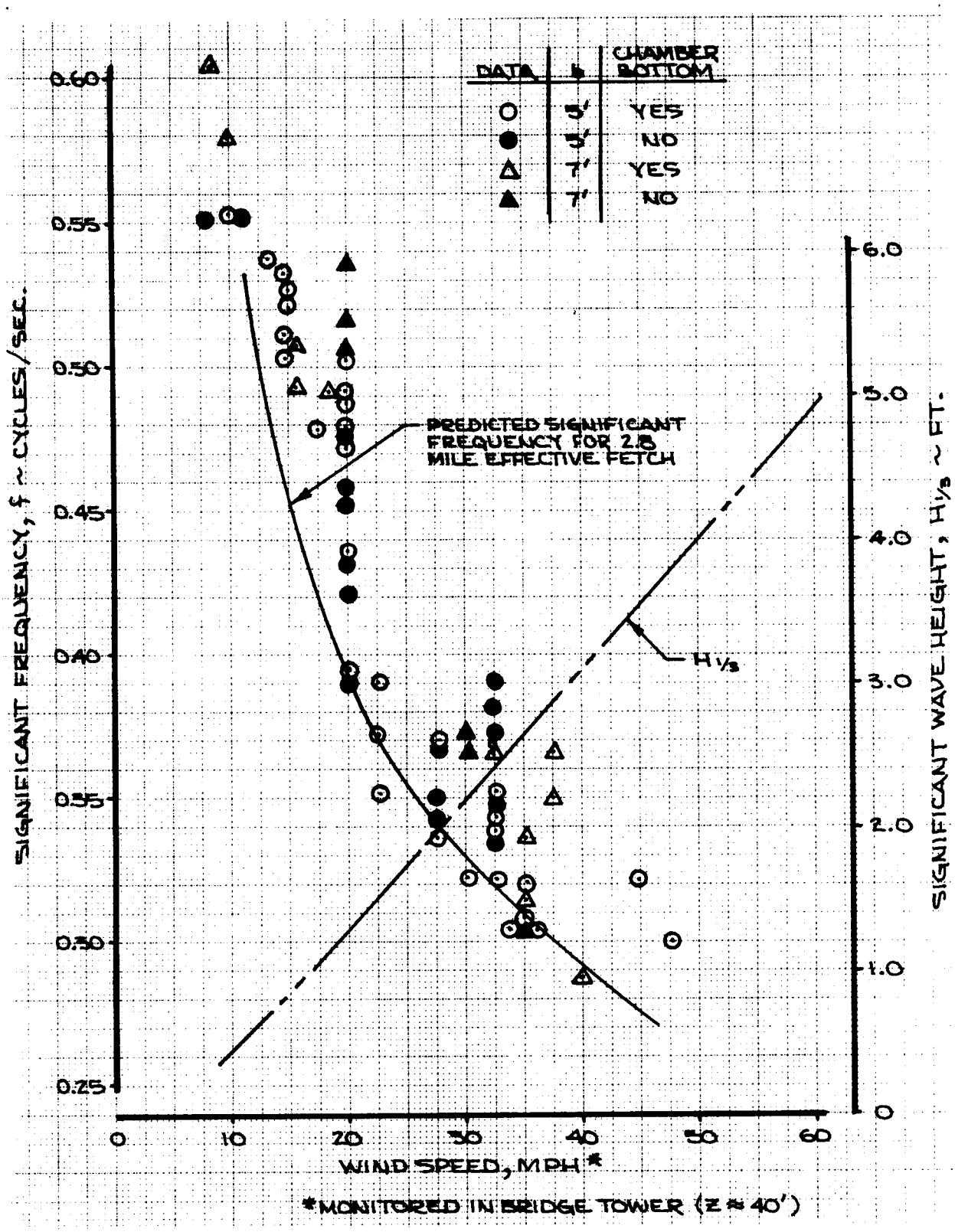

FIGURE 16. SIGNIFICANT FREQUENCY AS A FUNCTION OF WINDSPEED; PREDICTION AND DATA

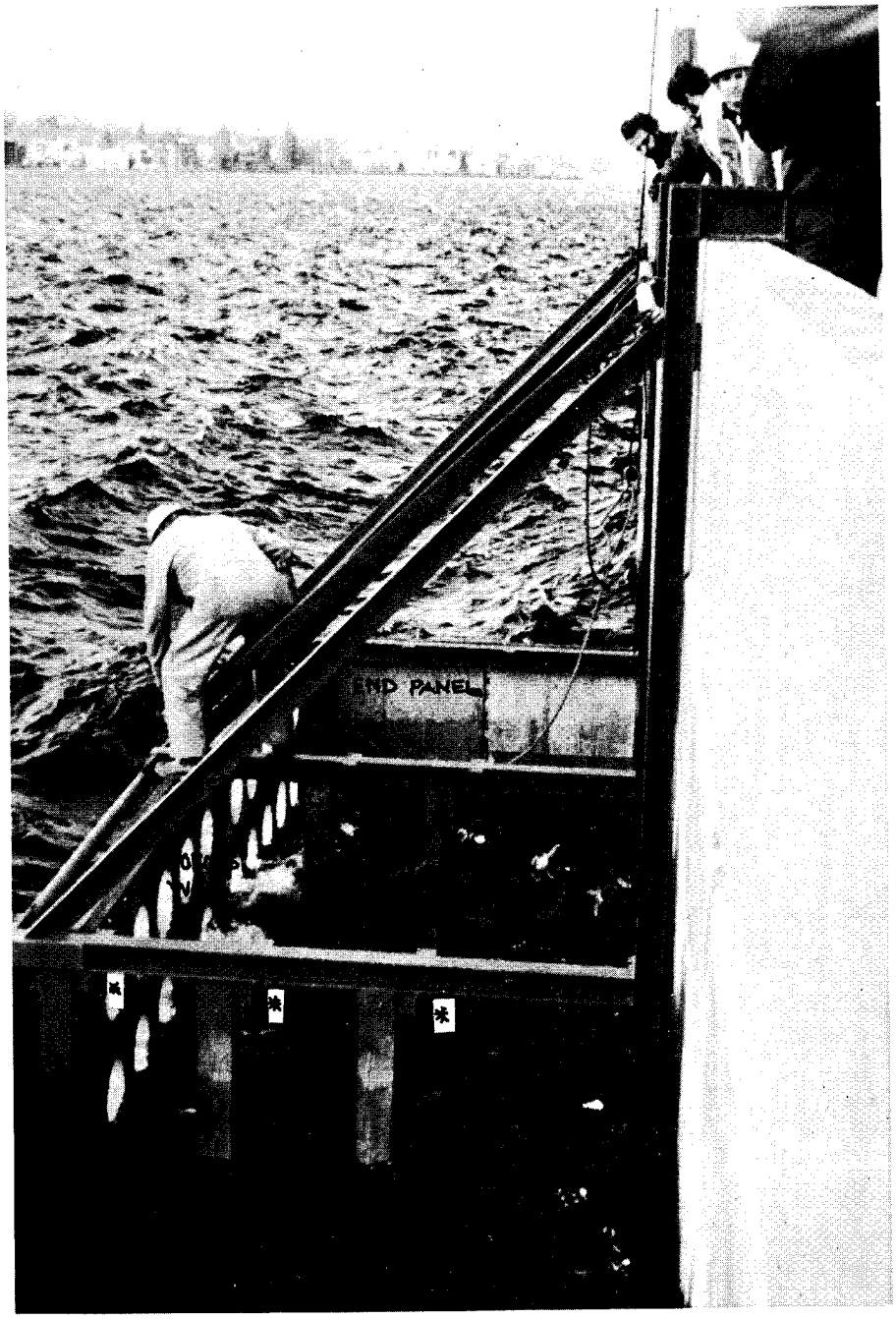

Figure 17 Breakwater Module Installed on the Evergreen Point Floating Bridge.

Seven foot chamber width shown.

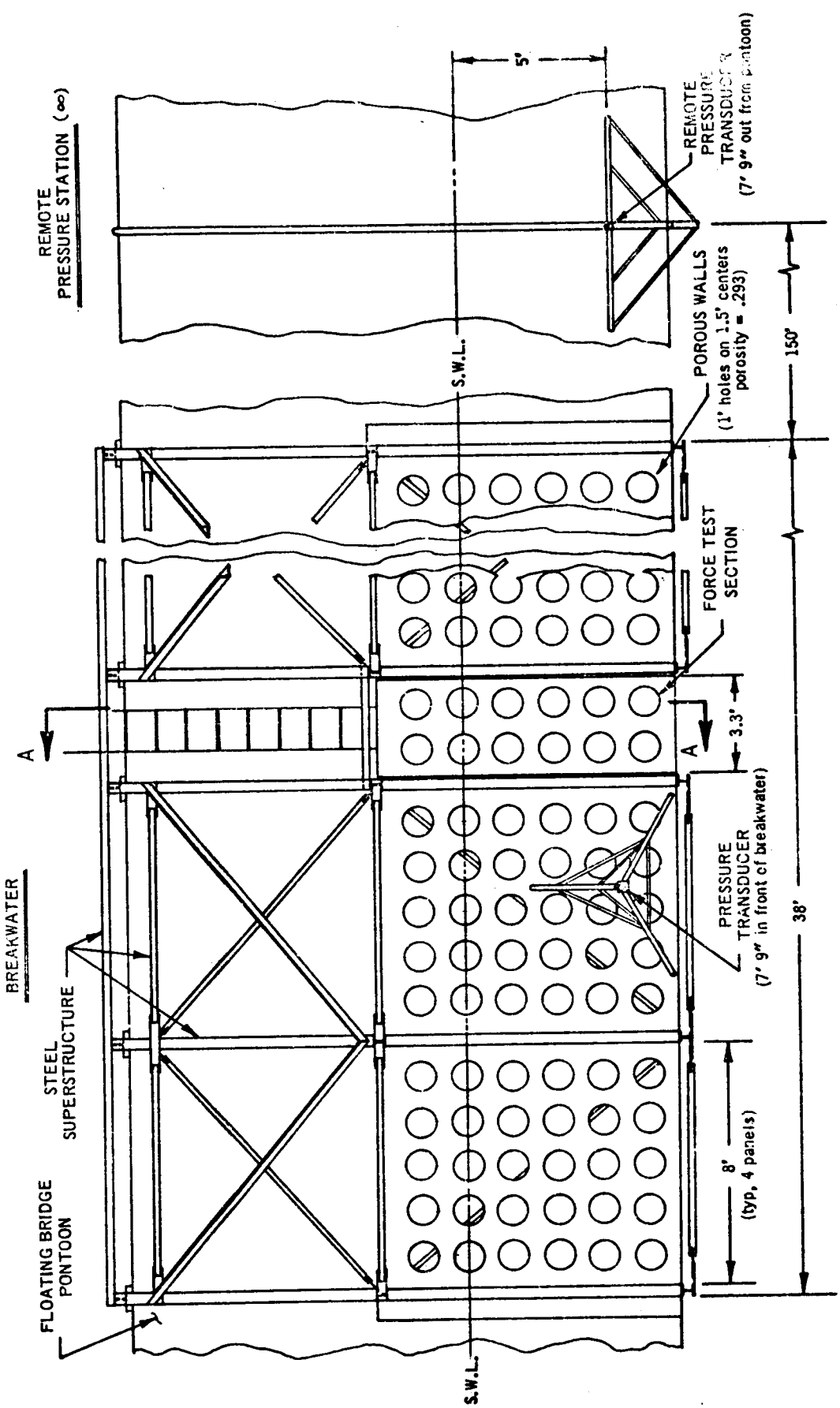

FIGURE 18. Porous Walled Breakwater and Remote Station; Front View.

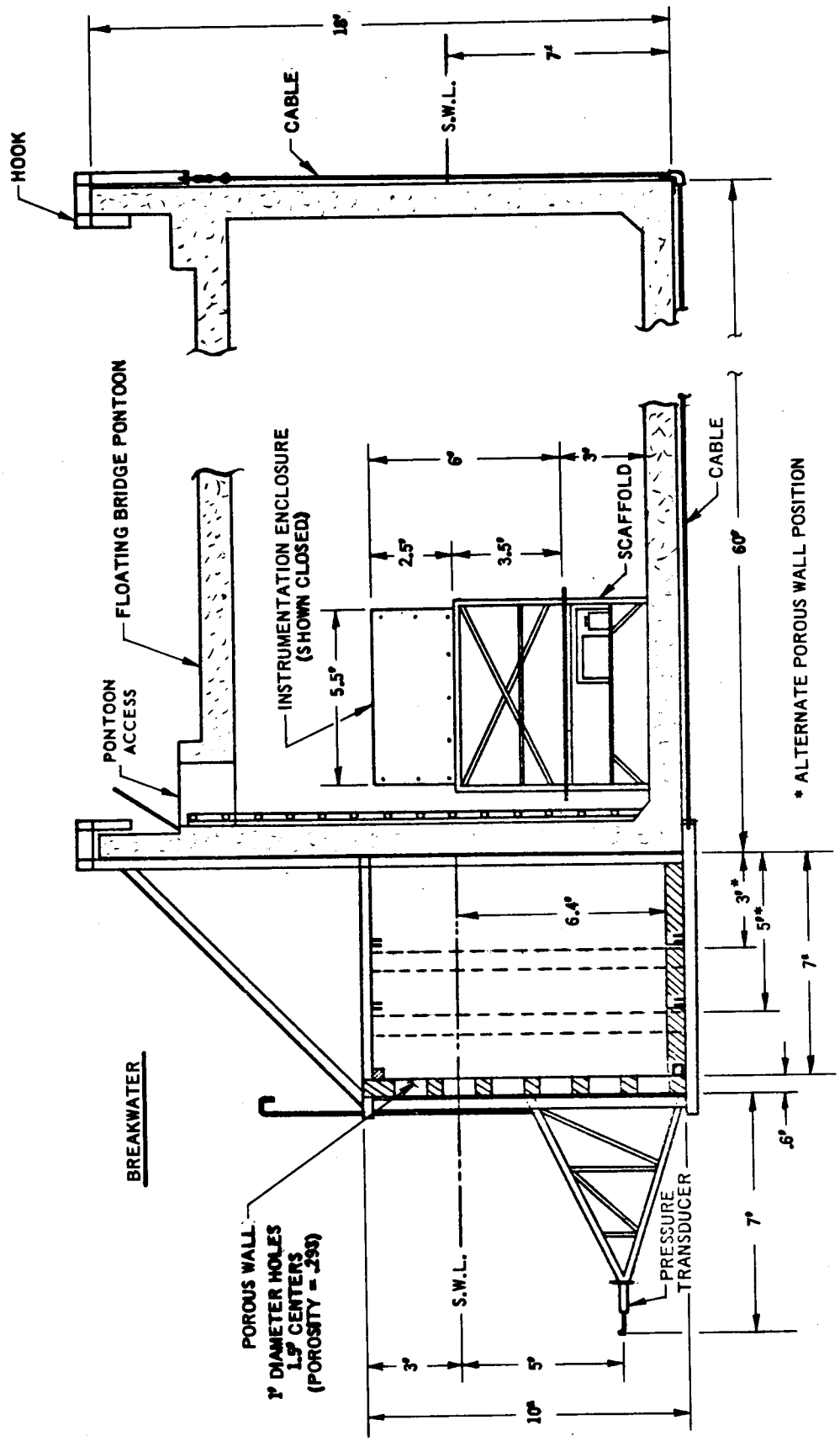

FIGURE 19. BREAKWATER SCHEMATIC (SECTION VIEW) INCLUDING KEY DIMENSIONS.

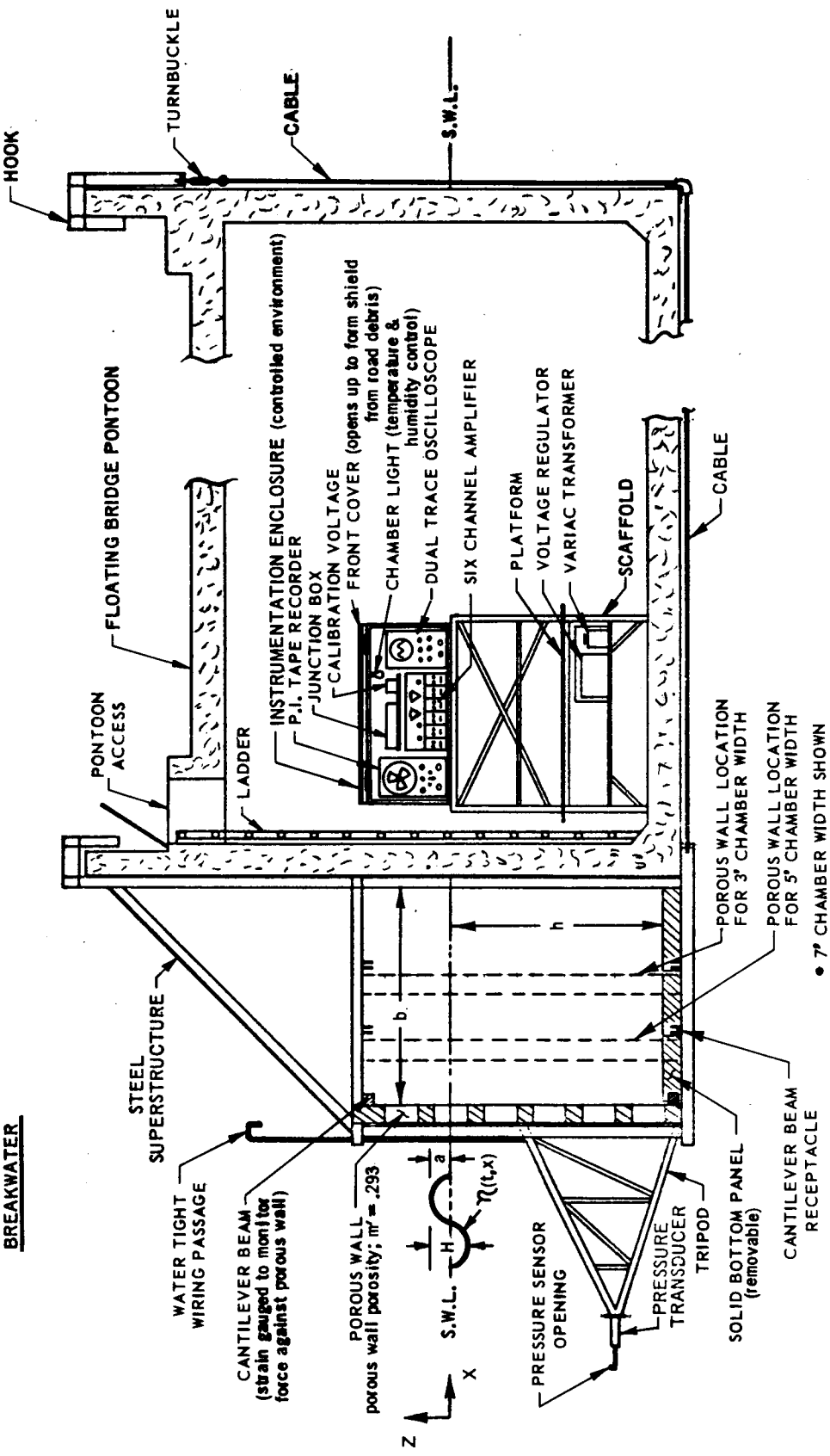

FIGURE 20. NOMENCLATURE (SECTION VIEW A - A)

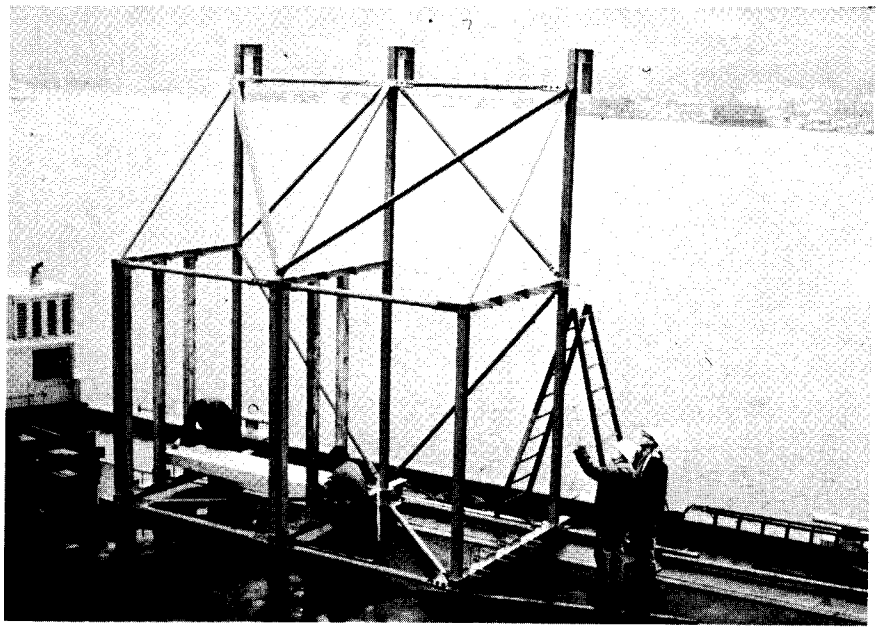

Figure 21 Steel Superstructure. One Module Shown. Removable bottom panel being installed.

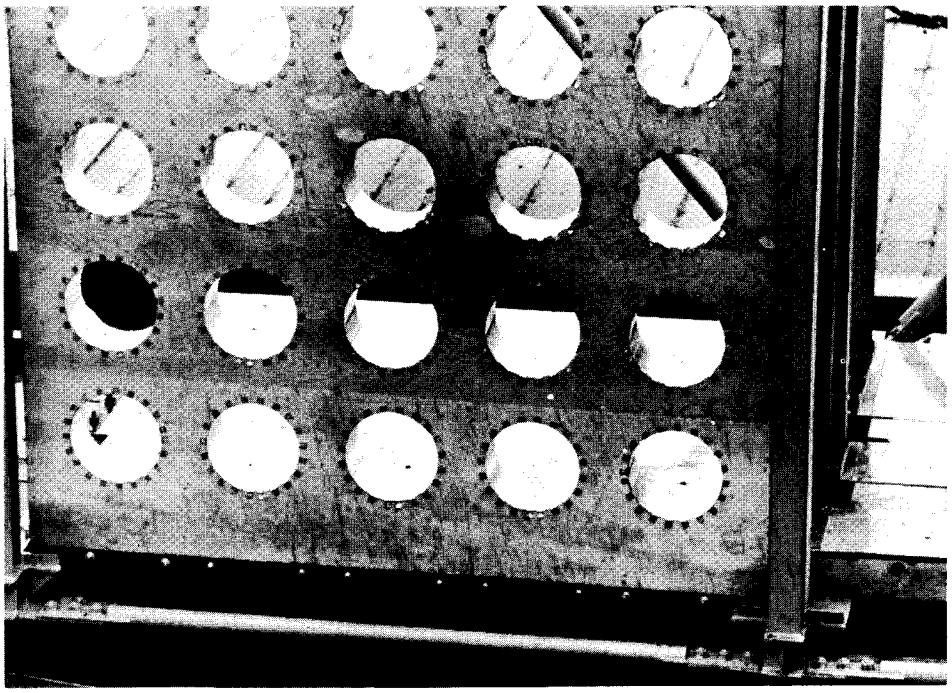

Figure 22 Porous Wall

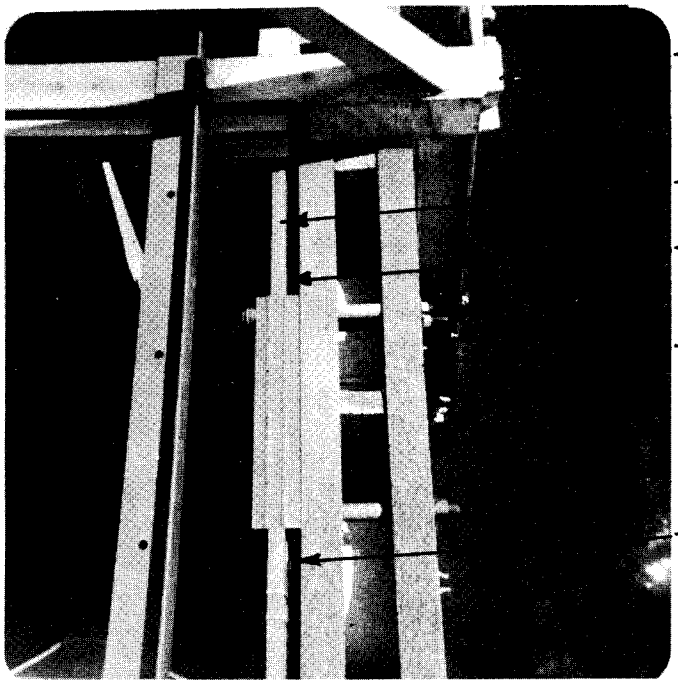

Figure 23 Test Section and Cantilever Beam Assemblies

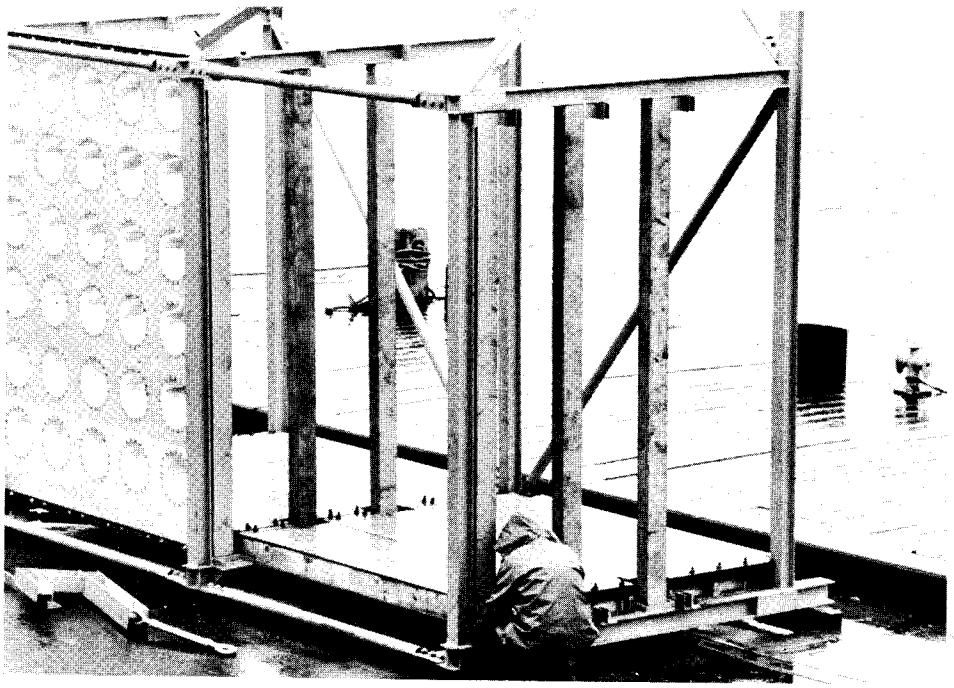

Figure 24 Removable Chamber Bottom Installed on one Module.
(One porous wall panel removed; hook and turnbuckle in foreground).

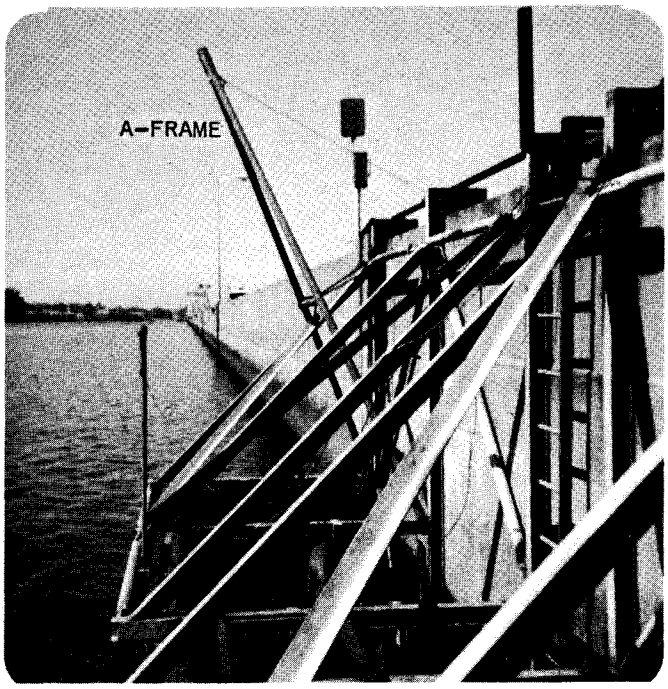

Figure 25 A-Frame; Allowing Self-contained Chamber Width Variations.

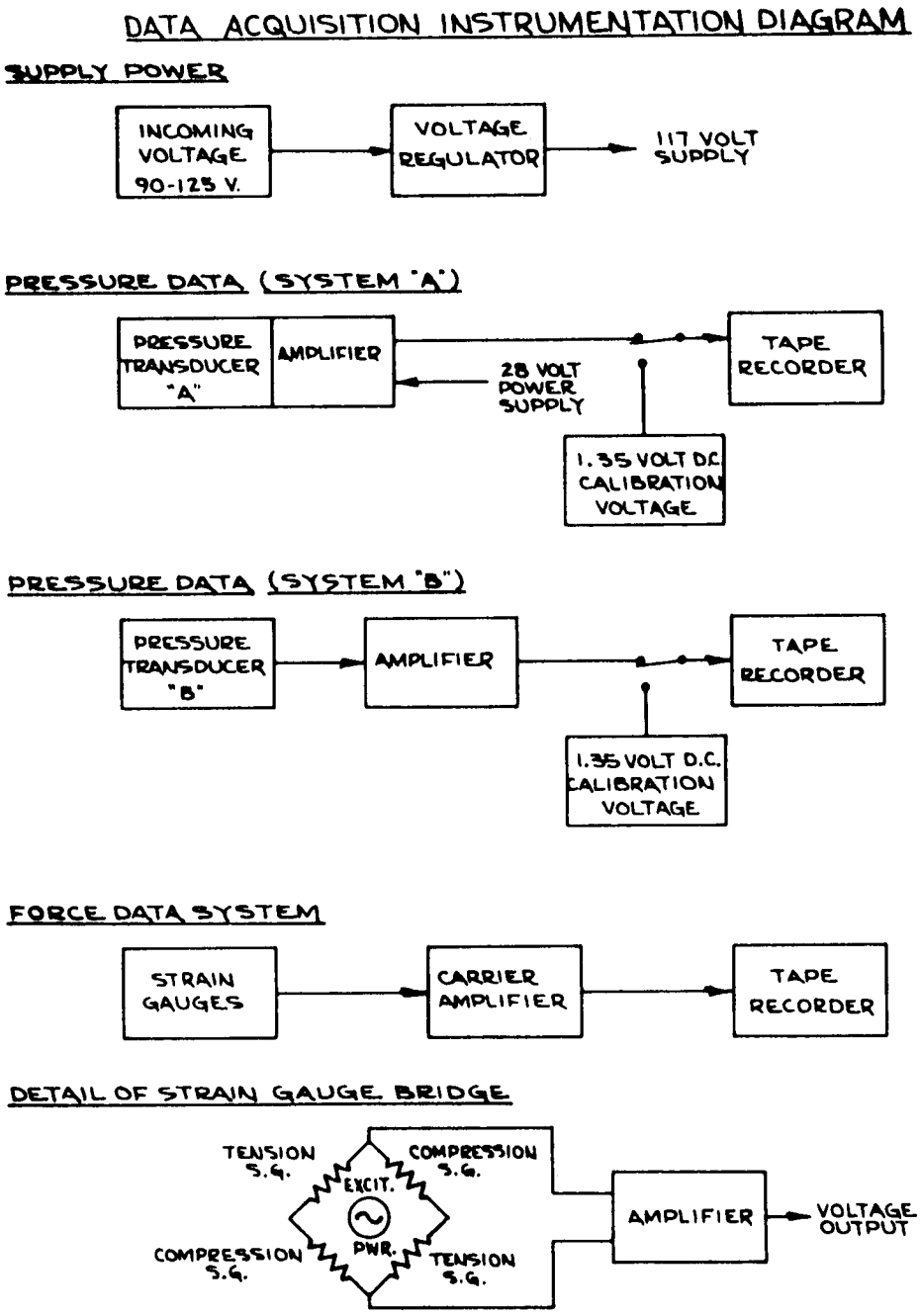

FIGURE 26. DATA ACQUISITION INSTRUMENTATION DIAGRAM

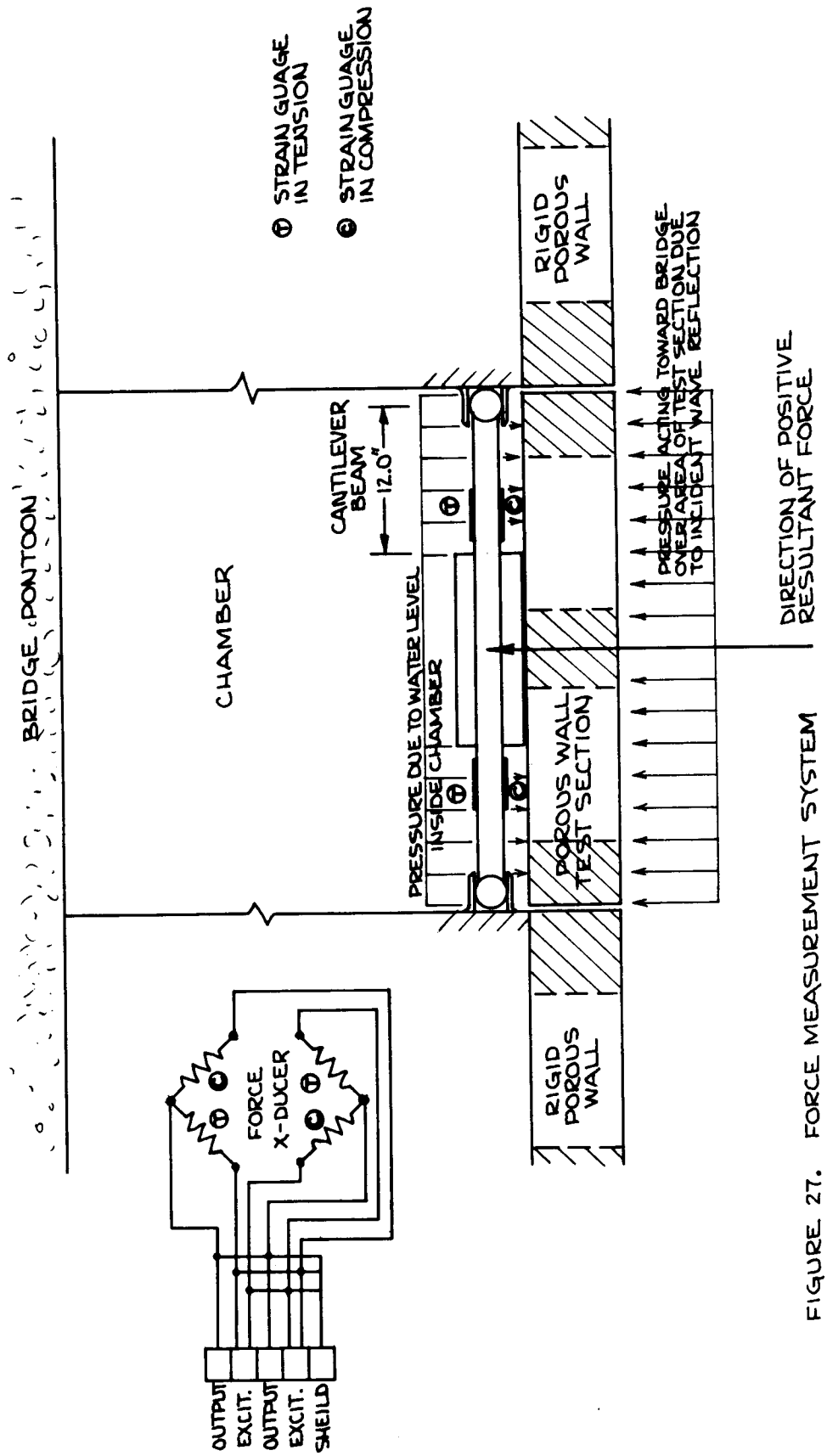

FIGURE 27. FORCE MEASUREMENT SYSTEM

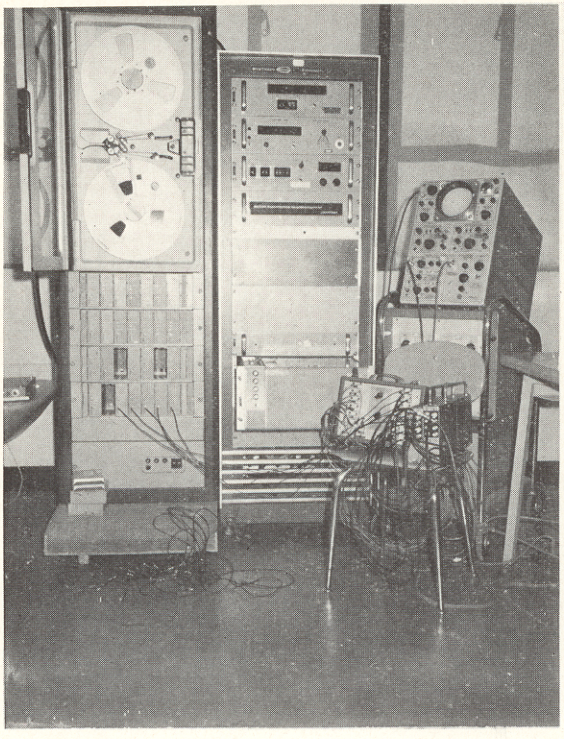

Figure 28 Data Reduction Instrumentation

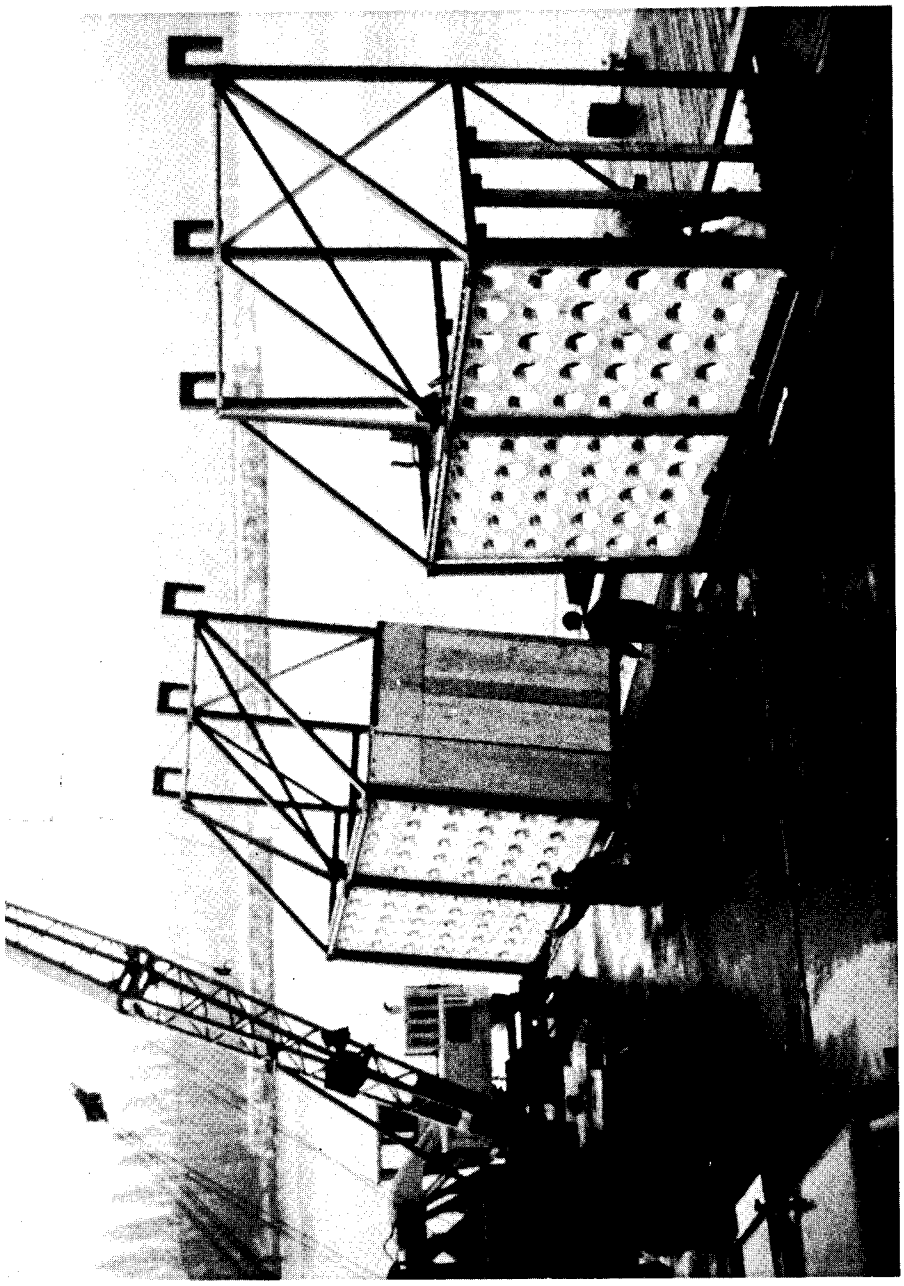

Figure 29 Assembled Breakwater Modules Before Installation

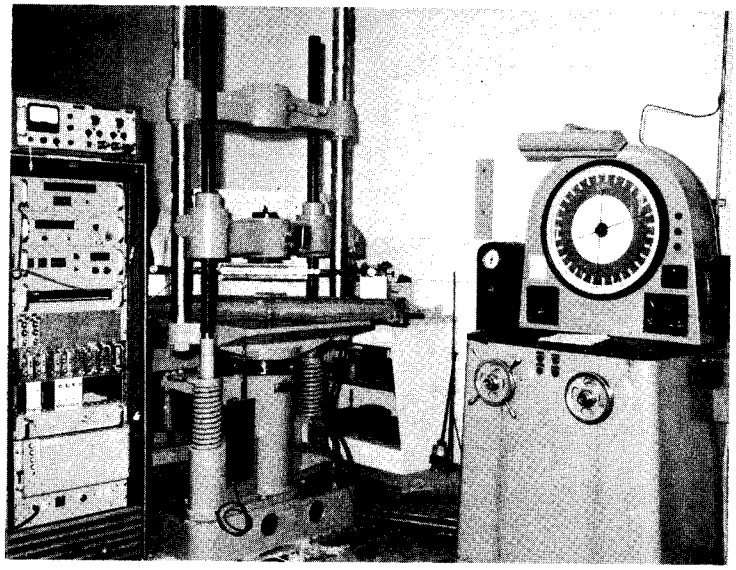

Figure 30 Cantilever Beam Calibration:
Known Force Input vs. Strain Gauge Output.

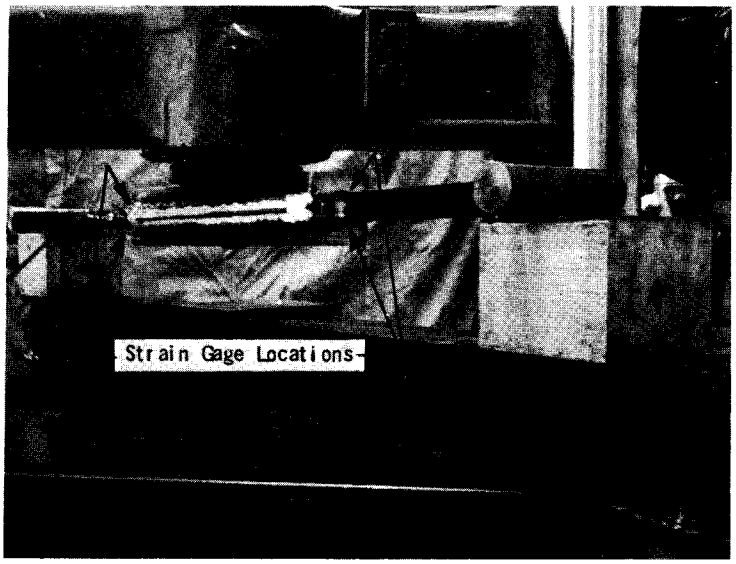

Figure 31 Close-up of Cantilever Beam Assembly.

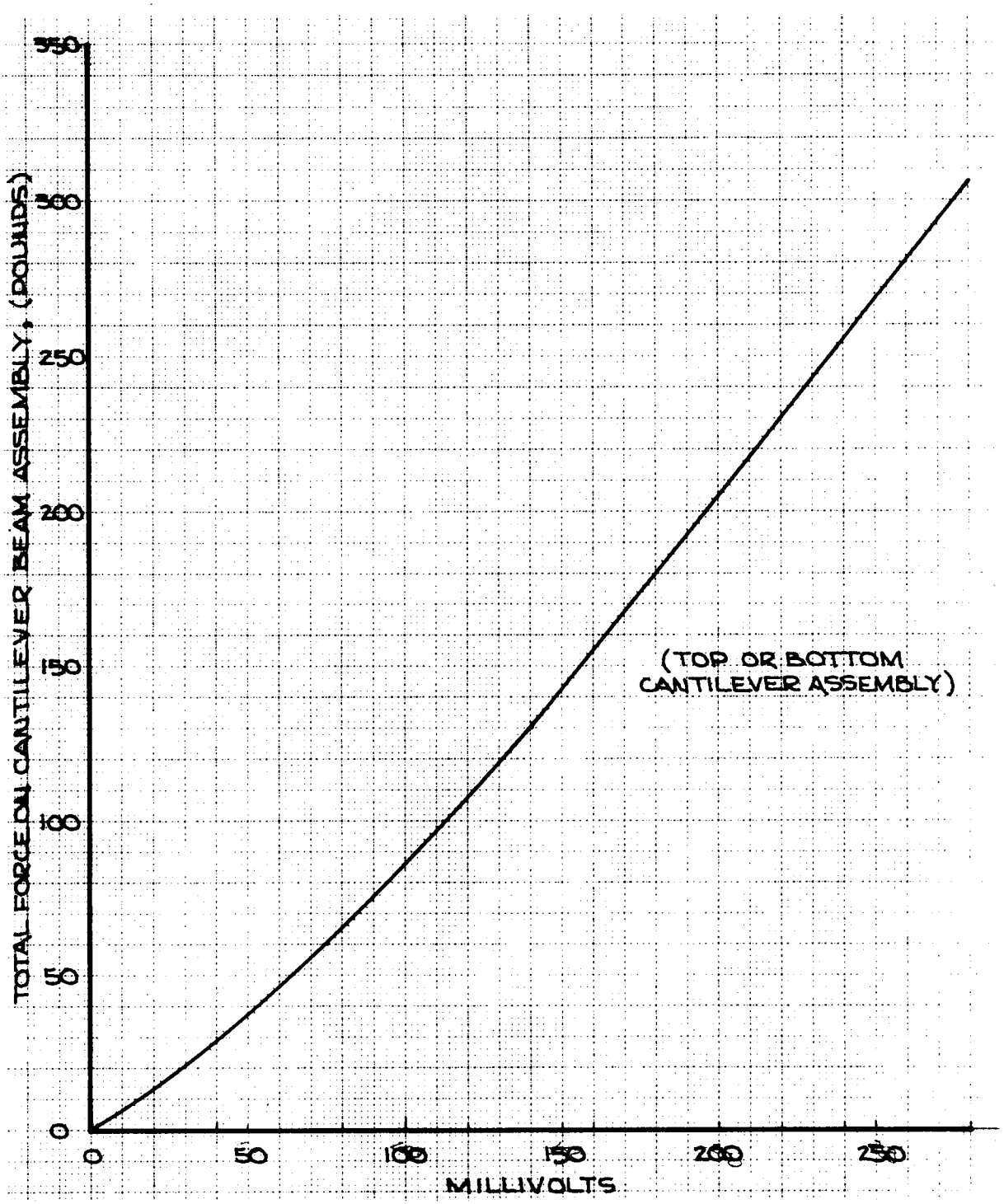

FIGURE 32. FORCE CALIBRATION CURVE (1 of 2)

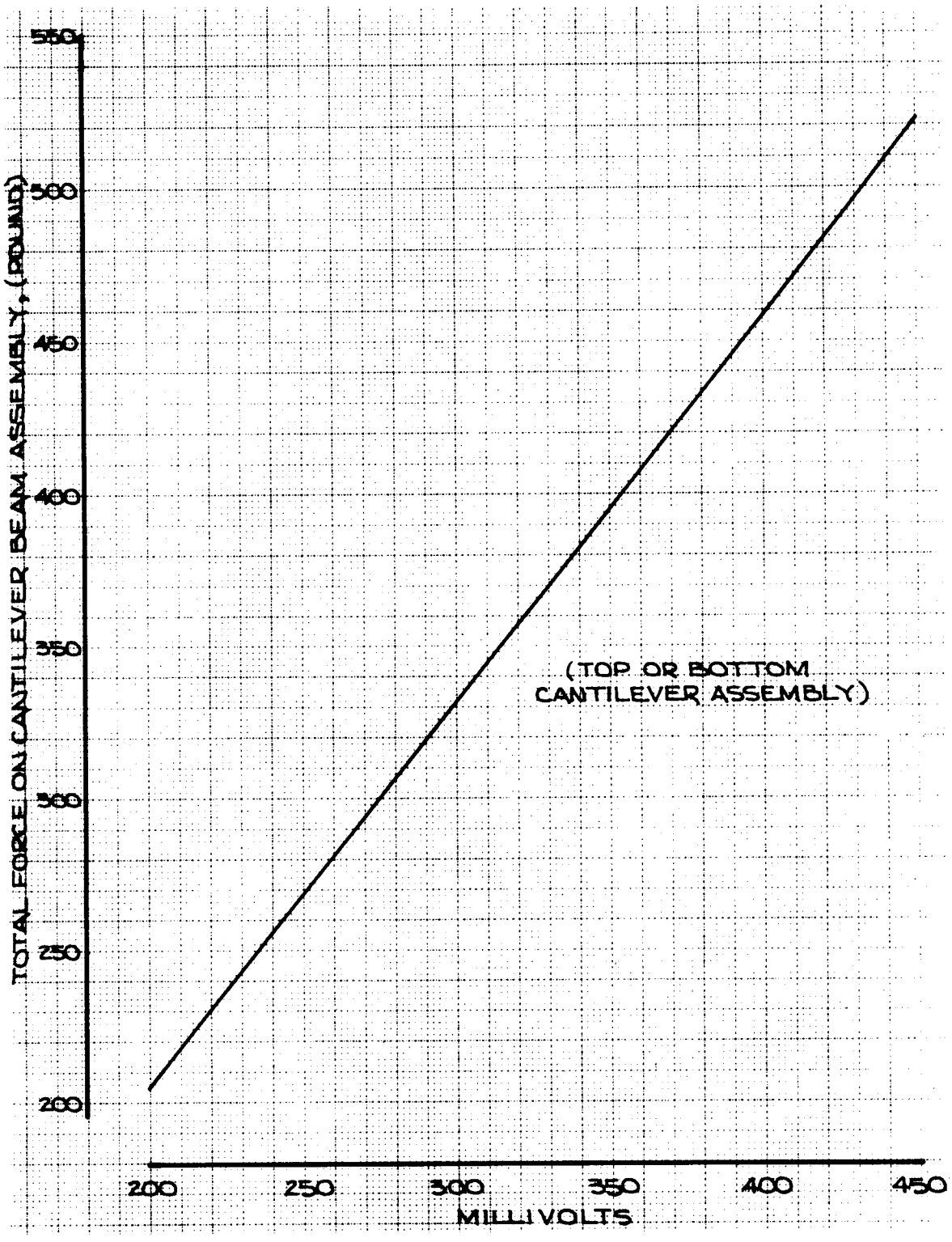

FIGURE 33. FORCE CALIBRATION CURVE (2 of 2)

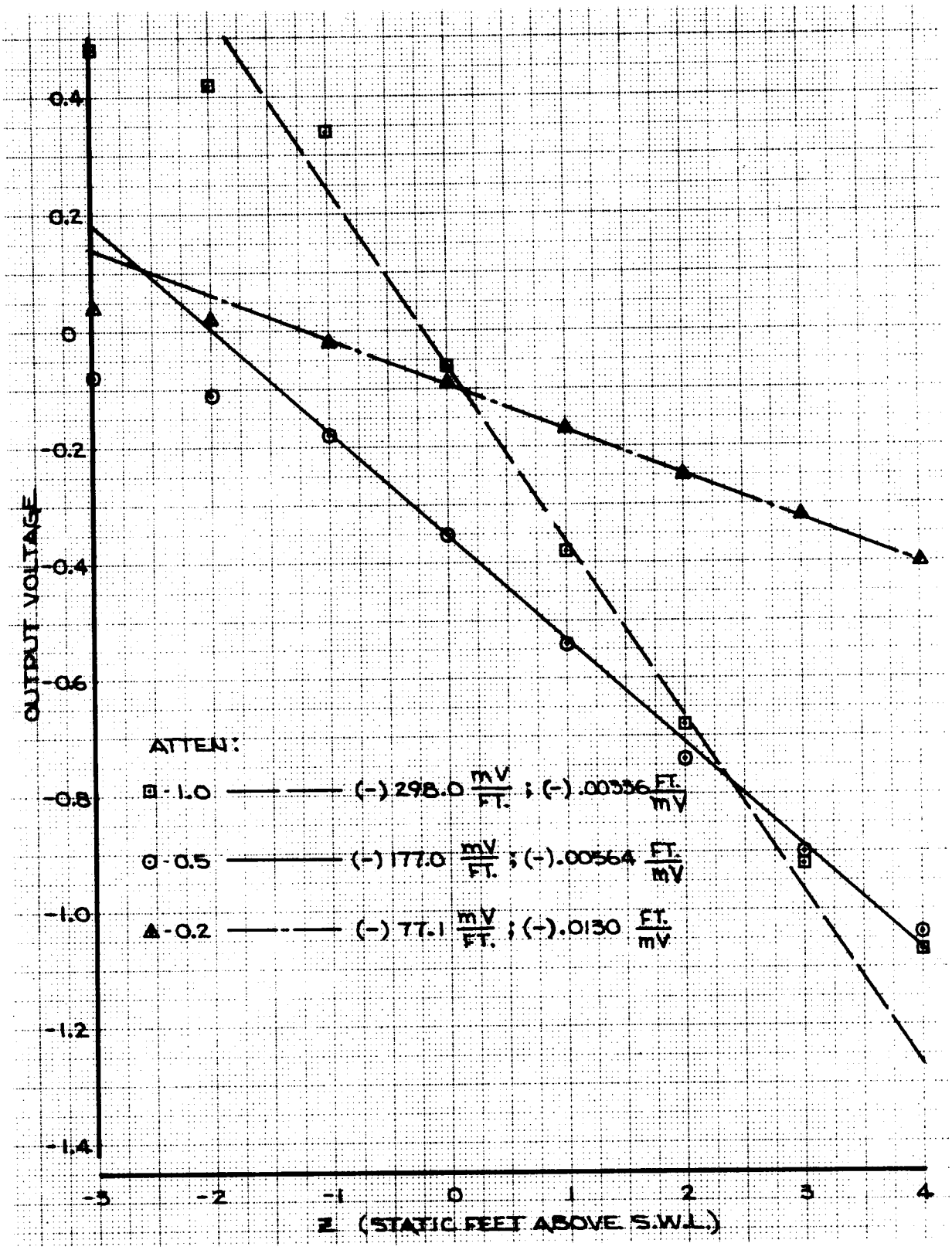

FIGURE 34. REMOTE (∞) TRANSDUCER CALIBRATION CURVE (CHANNEL # 3)

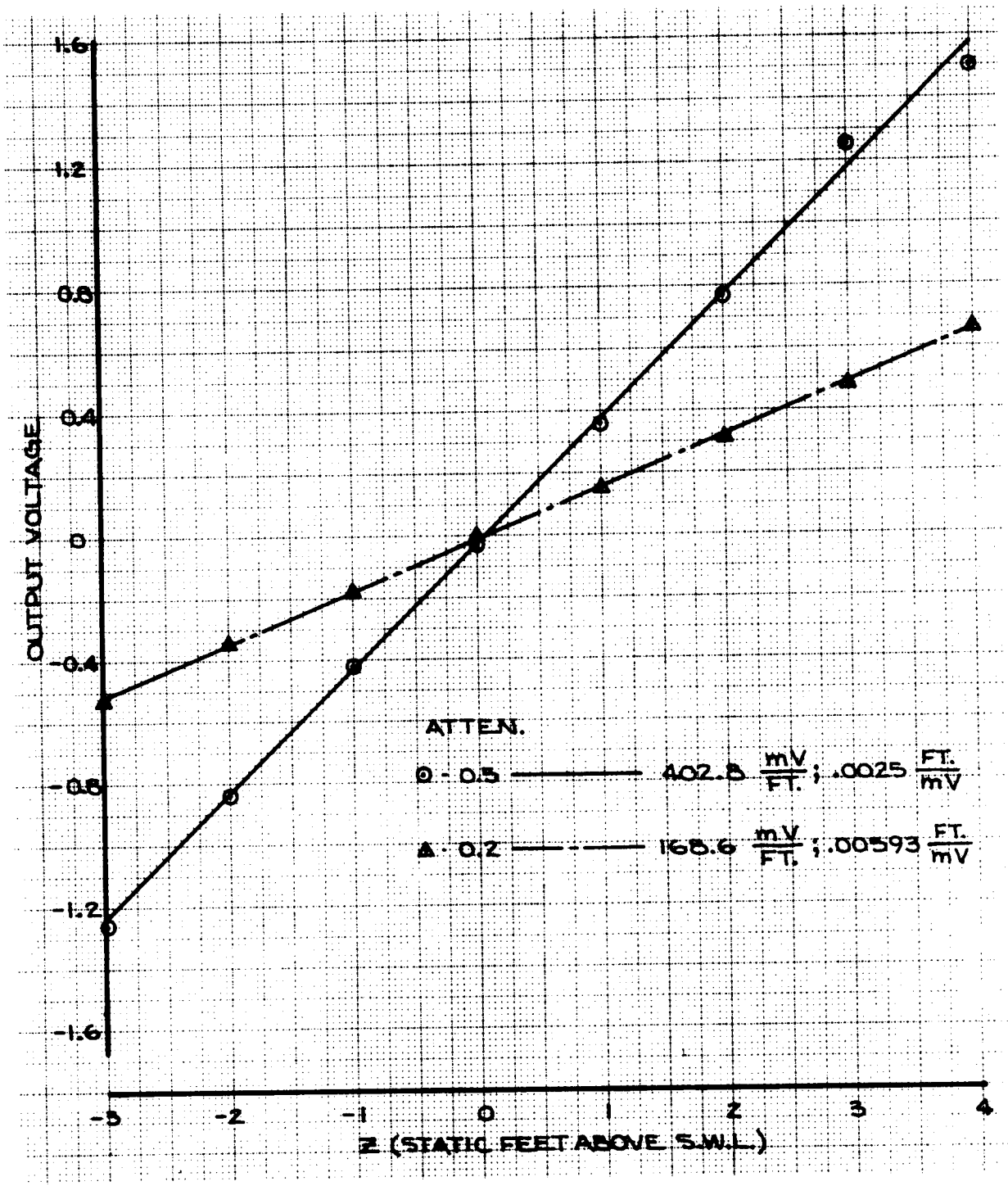

FIGURE 35. CALIBRATION CURVE FOR TRANSDUCER IN FRONT OF BREAKWATER (CHANNEL #4)

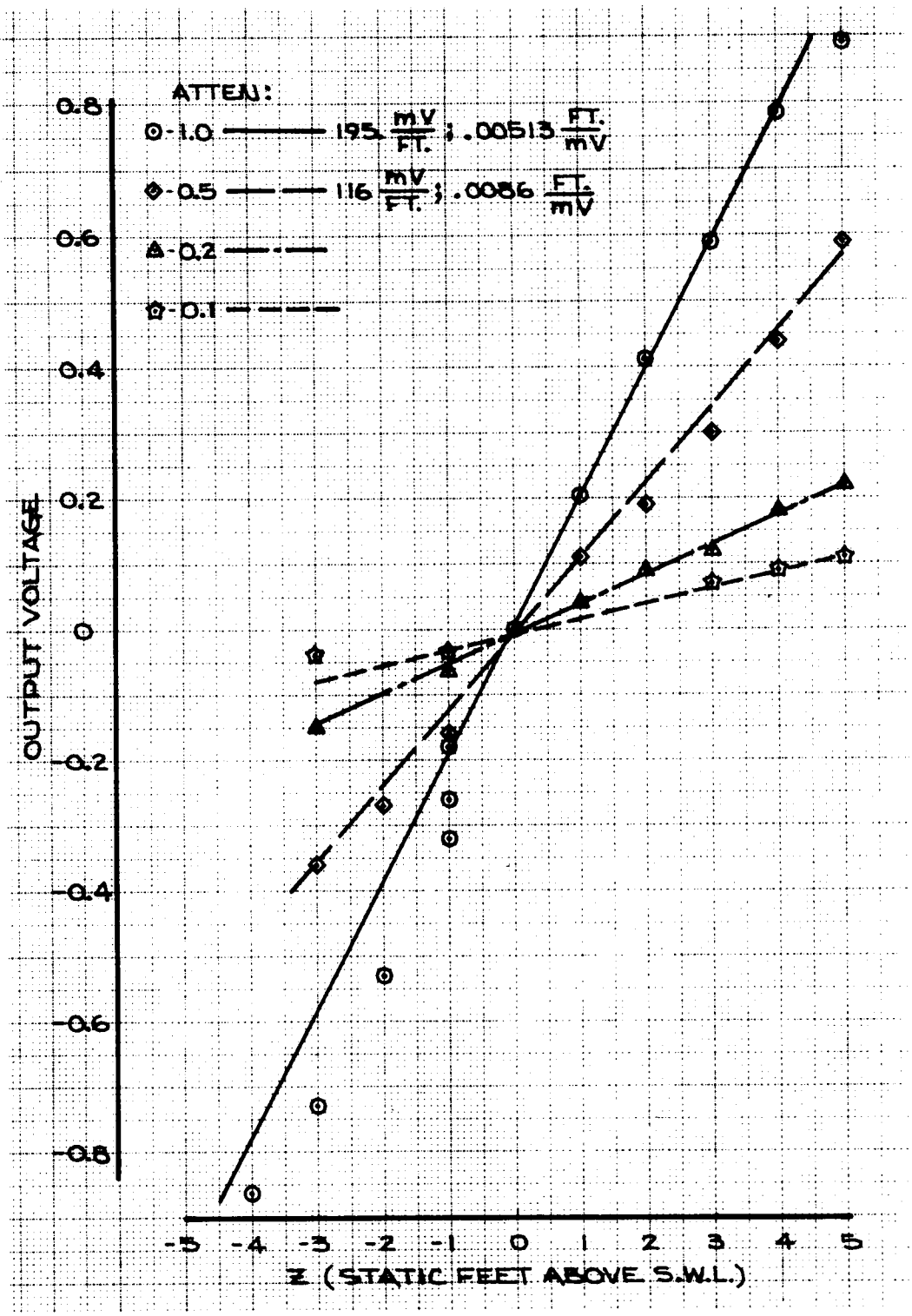

FIGURE 36. CALIBRATION CURVE FOR TRANSDUCER INSIDE CHAMBER (CHANNEL #5)

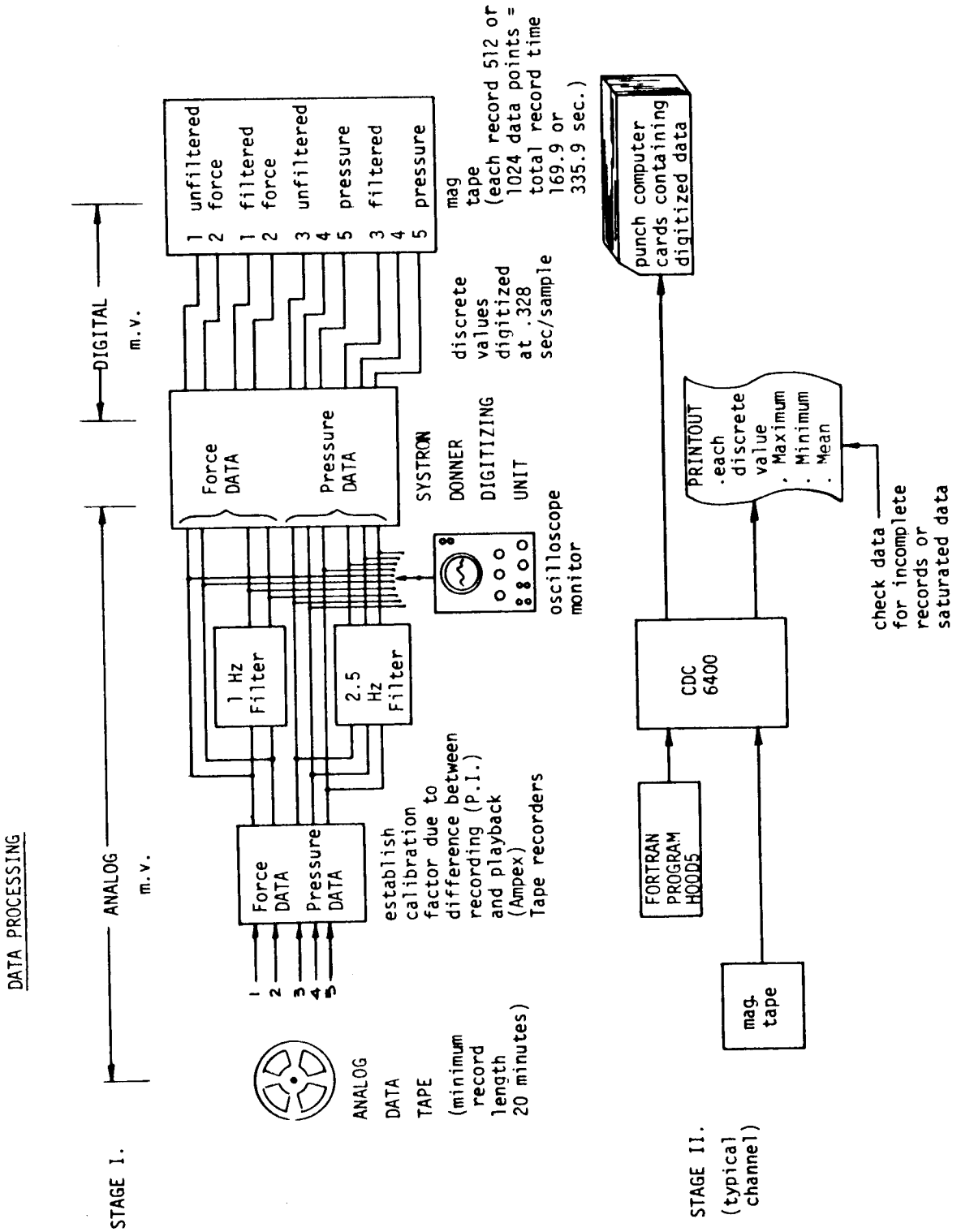

FIGURE 37 . Initial Data Processing

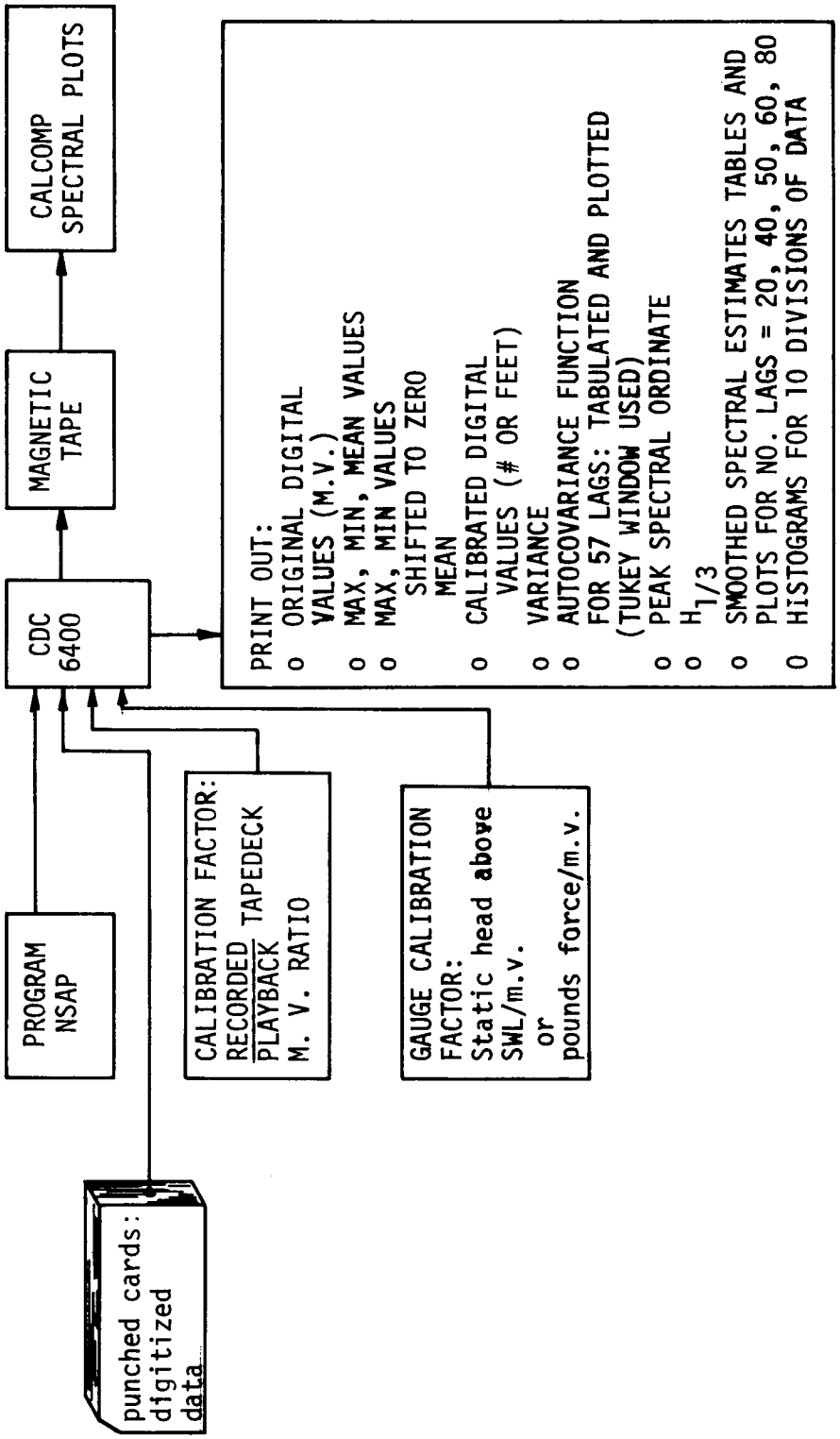

FIGURE 38. FINAL DATA PROCESSING

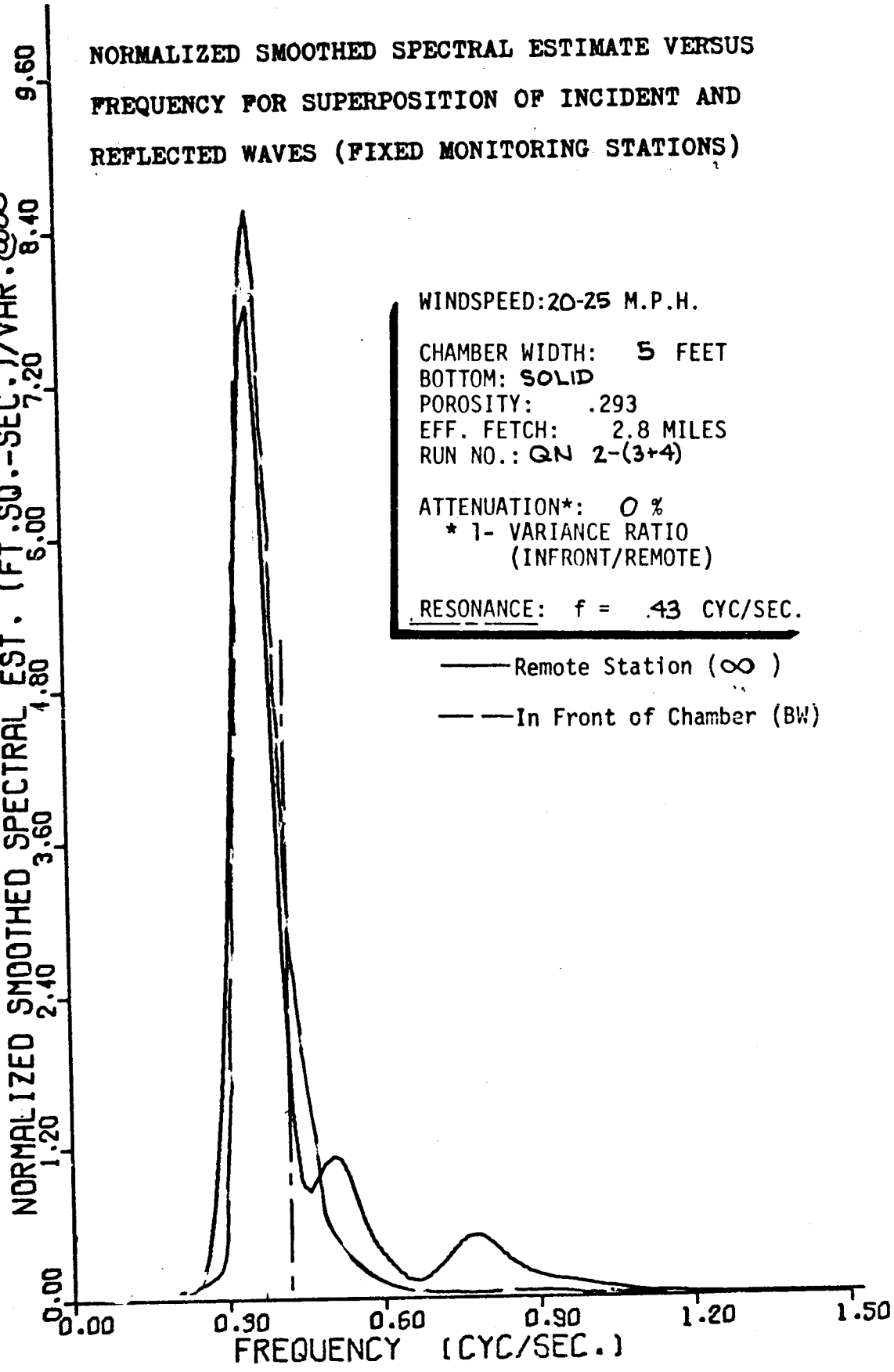

FIGURE 39. SPECTRAL PLOT FOR NYQUIST FREQUENCY EXAMPLE

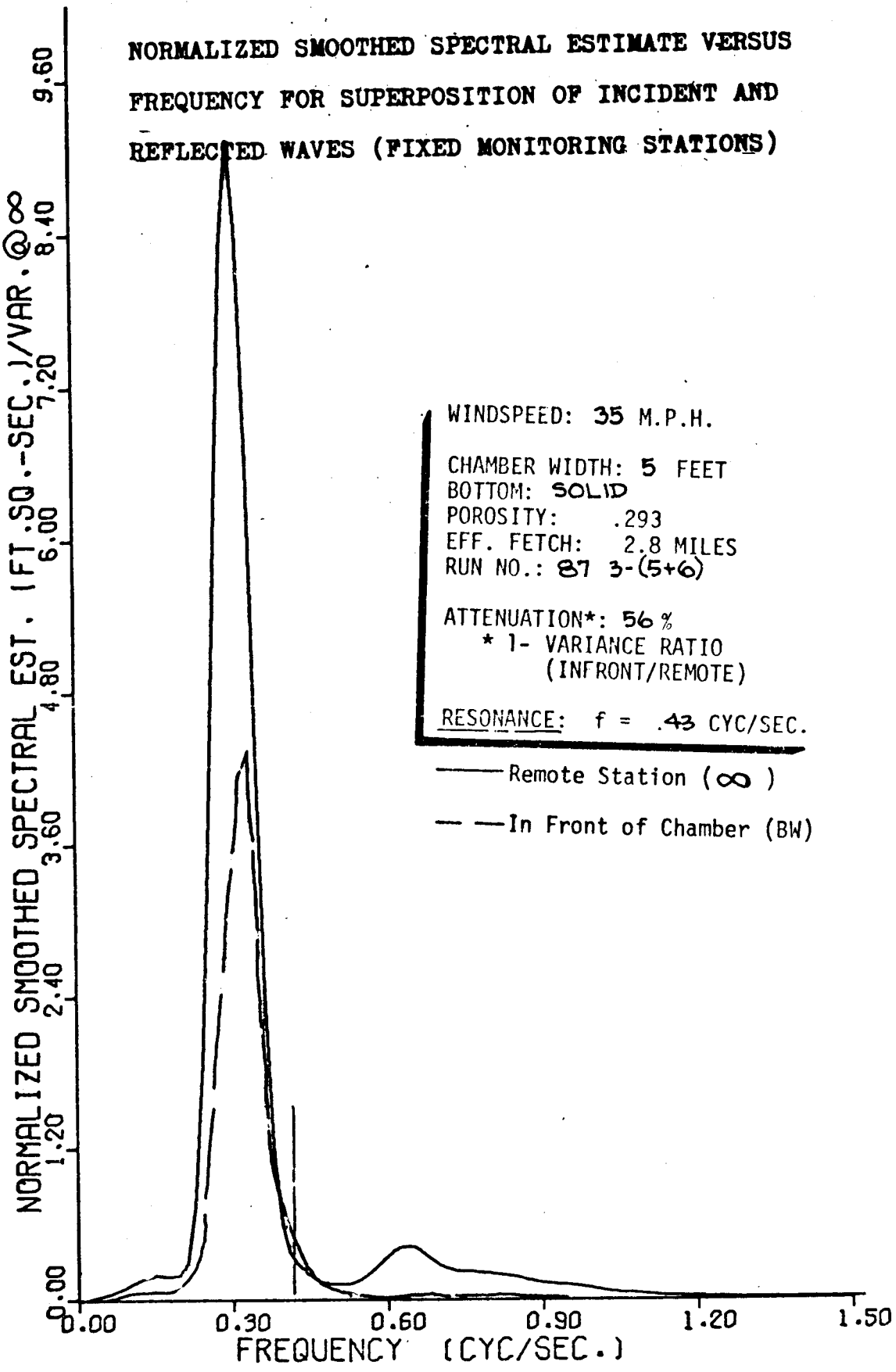

FIGURE 40. SPECTRAL PLOT FOR NYQUIST FREQUENCY EXAMPLE

FIGURE 43 Breakwater Operation. Energy Conversion To Non-Conservative Forms.

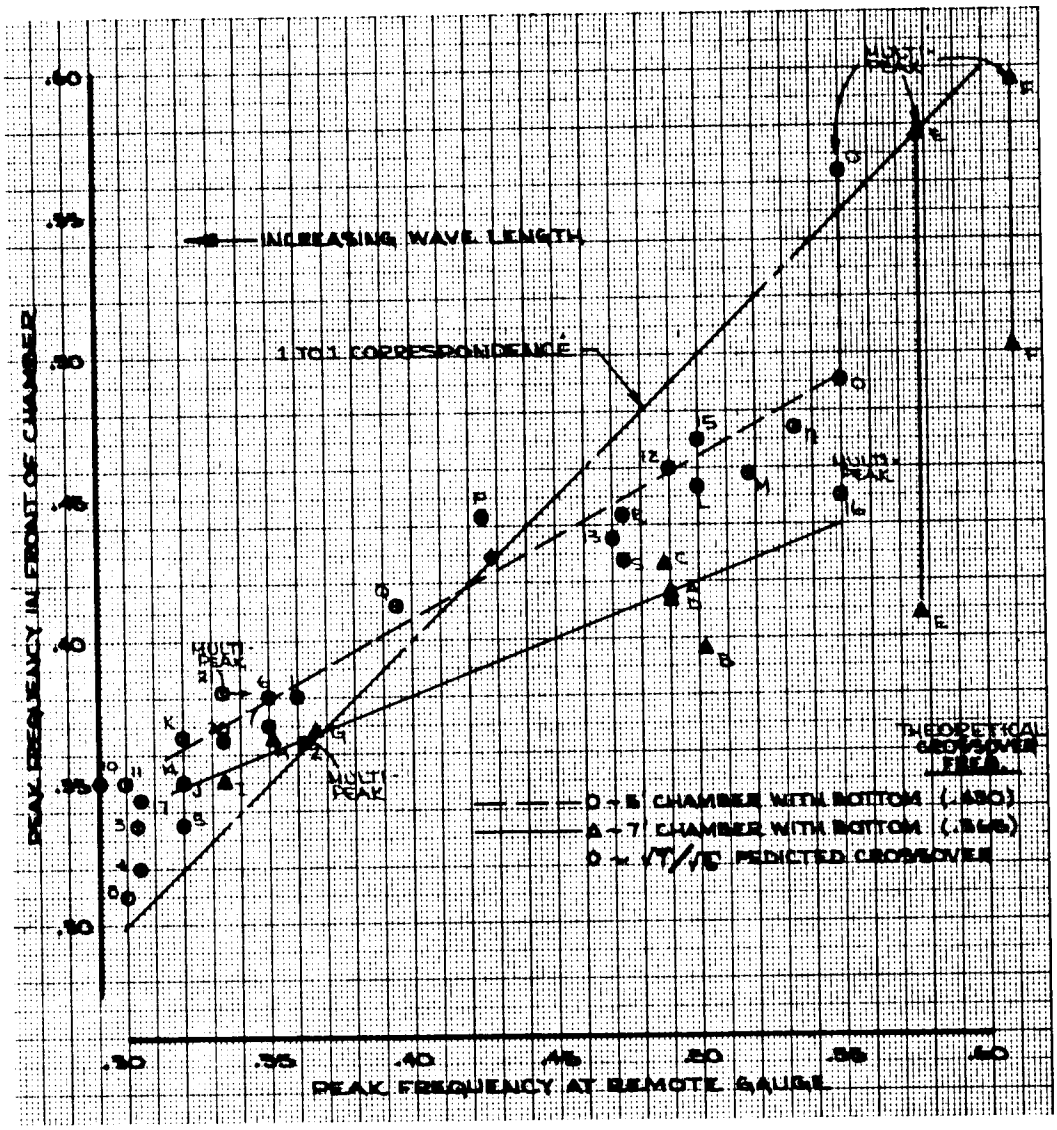

FIGURE 44. Effect of Chamber Width on Peak Frequency; Data and Predicted Crossover Frequencies.

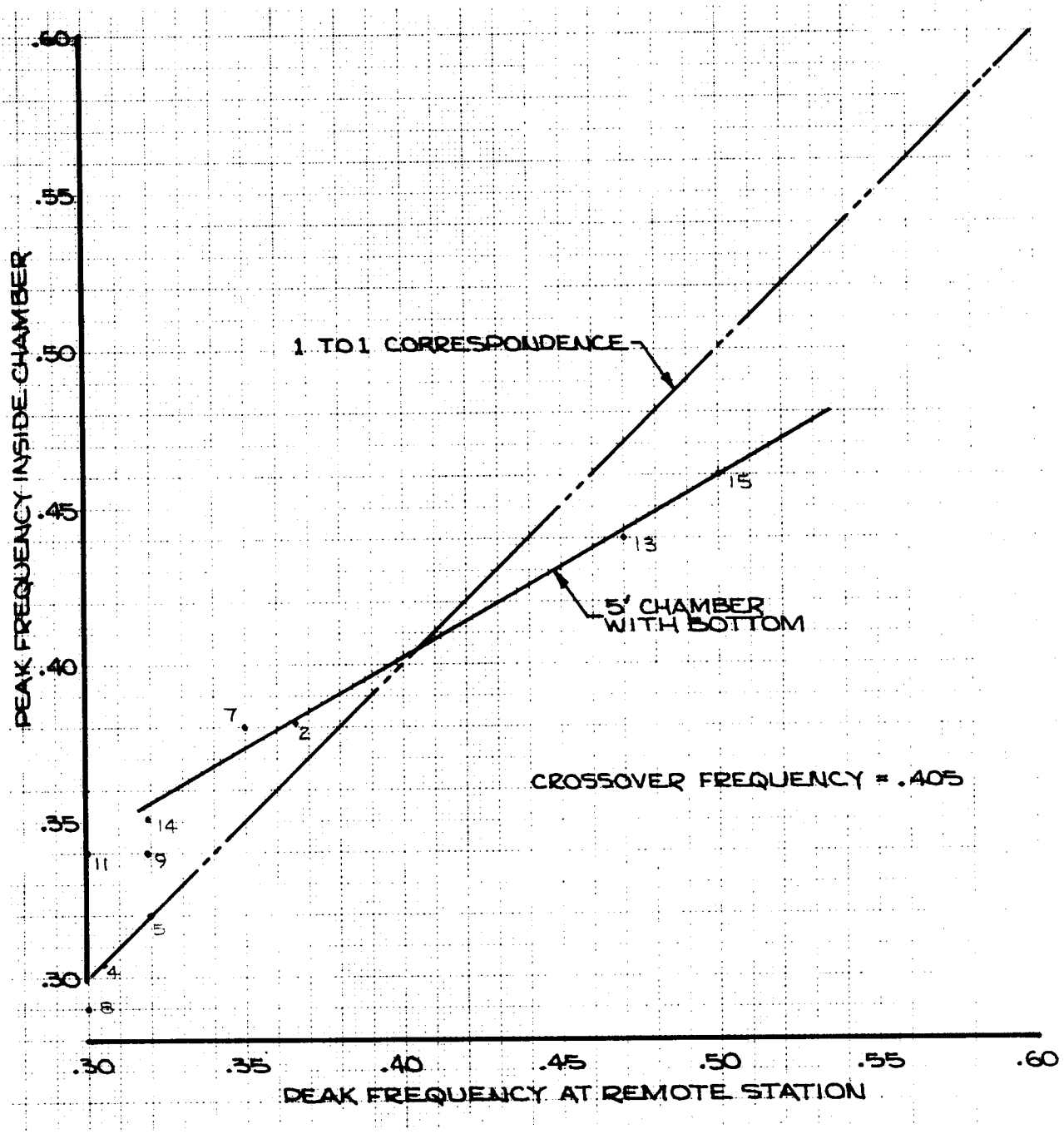

FIGURE 45. PEAK FREQUENCY DISTRIBUTION INSIDE OF FIVE FOOT WIDE CHAMBER WITH SOLID BOTTOM

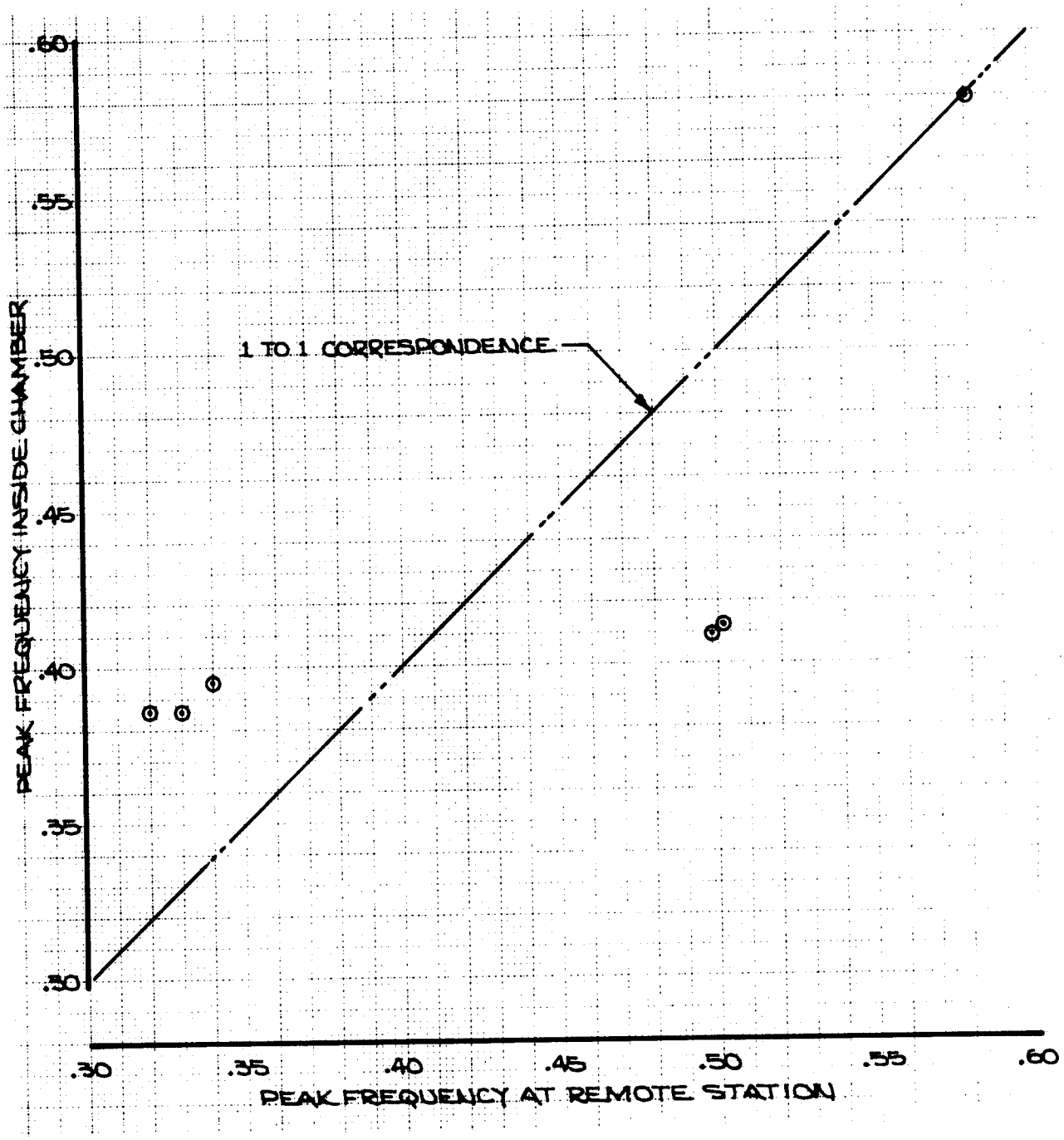

FIGURE 46. PEAK FREQUENCY DISTRIBUTION INSIDE SEVEN FOOT WIDE CHAMBER WITH SOLID BOTTOM

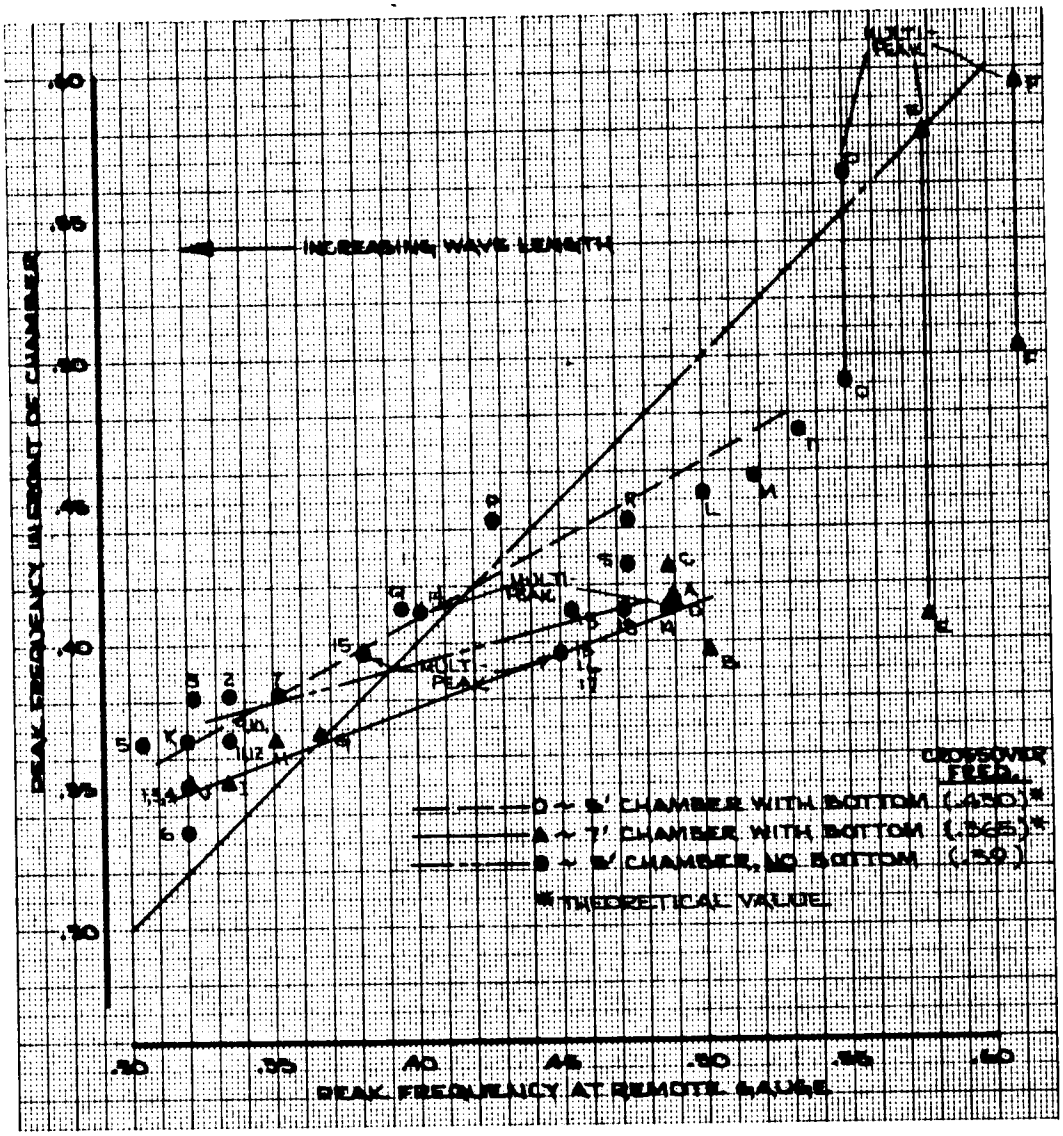

FIGURE 47. Effect of Bottom Removal on Peak Frequency.

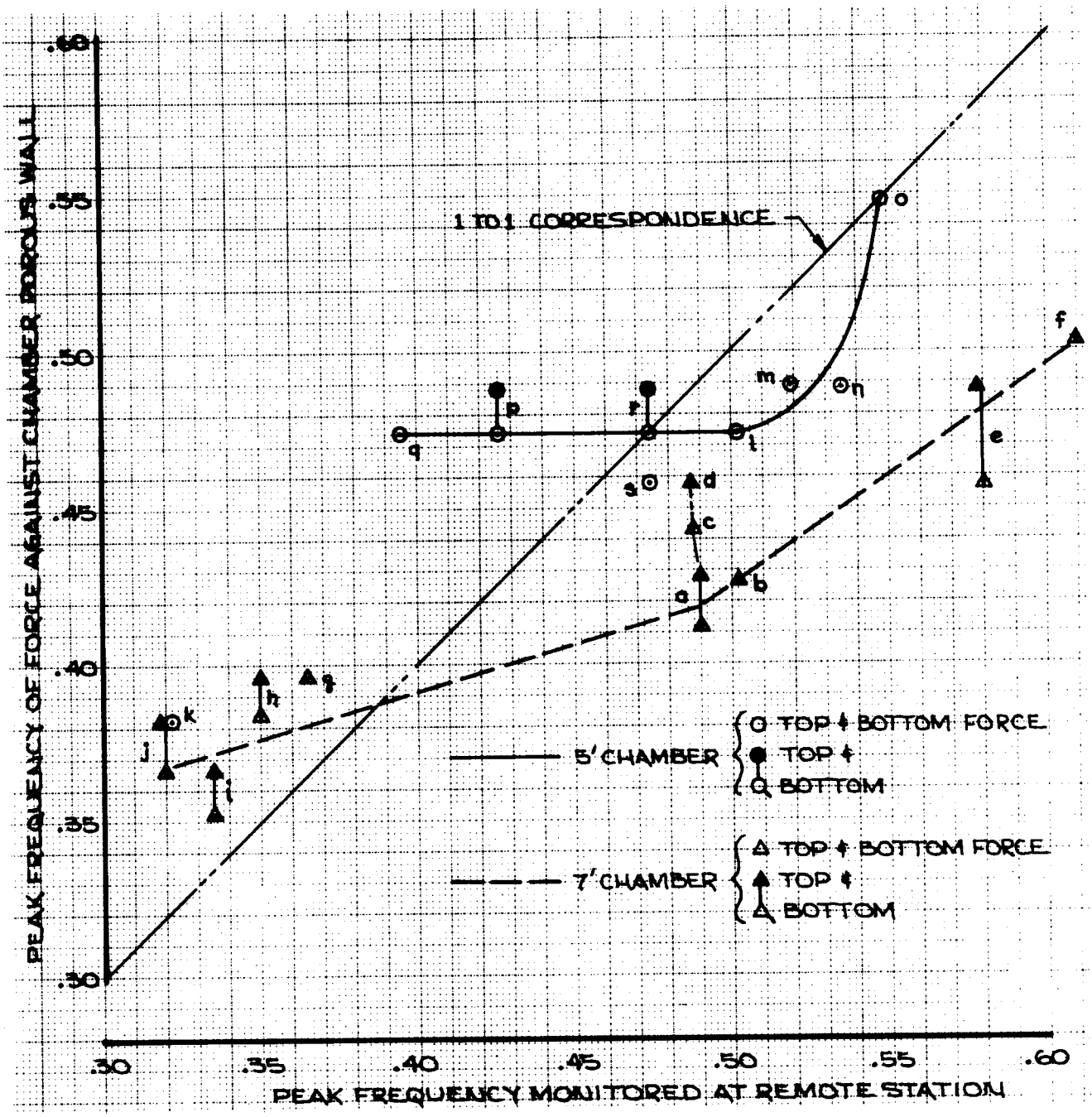

FIGURE 48. PEAK FREQUENCY DISTRIBUTION OF FORCE

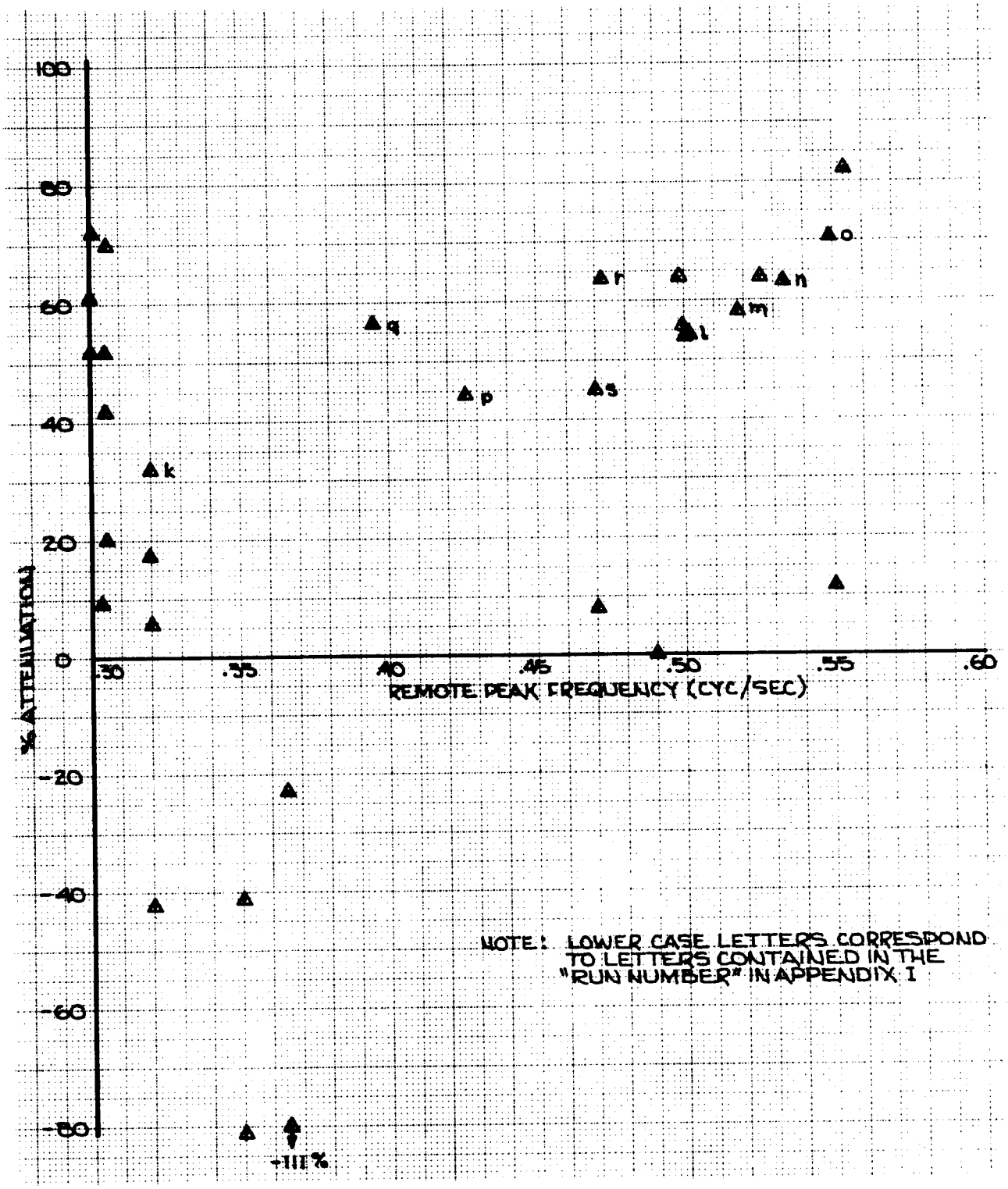

FIGURE 49. % ATTENUATION VS. PEAK FREQUENCY MONITORED AT THE REMOTE STATION FOR CHAMBER WIDTH EQUAL TO FIVE FEET

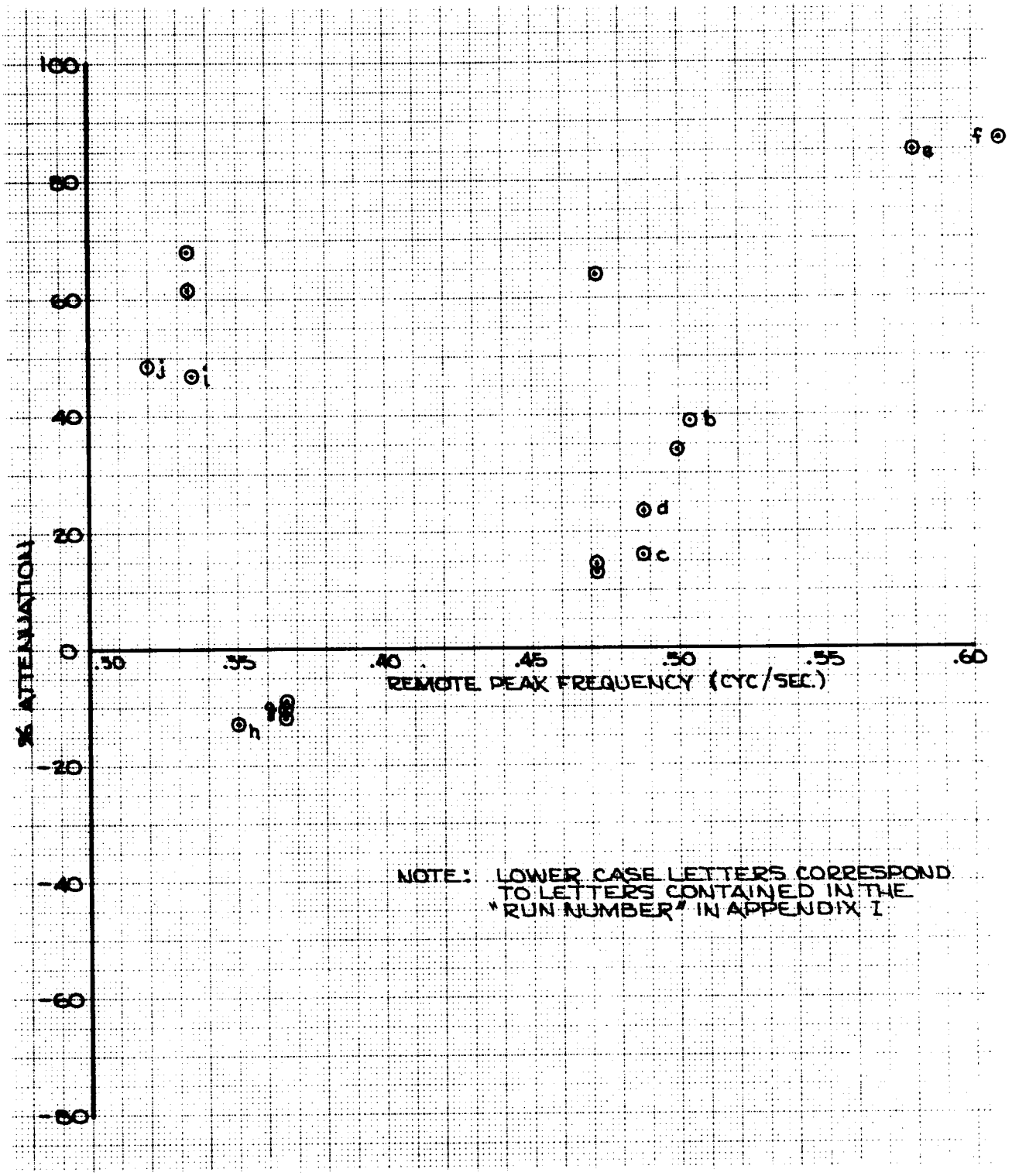

FIGURE 50. % ATTENUATION VS. PEAK FREQUENCY MONITORED AT THE REMOTE STATION FOR CHAMBER WIDTH EQUAL TO SEVEN FEET.

REFERENCES

1. Hudson, R., "Model Tests of Portable Breakwaters for D-Day Invasion Harbors", Civil Engineering, New York, Vol. 15, No. 9, September, 1945, pp. 405-8.

2. Minikin, R., "Floating and Foundationless Breakwaters", Engineering, Vol. 166, No. 4325, December, 1948, pp. 577-9.

3. Laurie, A., "Pneumatic Breakwaters", The Dock and Harbor Authority, Vol. 33, No. 379, May, 1952, pp. 11-13.

4. Nece, R.E., Richey, E.P., and Rao, V.S., "Dissipation of Deep Water Waves by Hydraulic Breakwaters", Conference on Coastal Engineering, London, Vol. 2, September, 1968, pp. 1032-48.

5. Garrison, C.J., "Interaction of an Infinite, Shallow Draft Cylinder Oscillating at the Free Surface with a Train of Regular Waves", Unpublished Ph.D. Dissertation, University of Washington, 1968.

6. Lawson, J.D., "Model Studies of Wave Absorbing Devices", The Dock and Harbor Authority, Vol. 33, No. 379, 1952, pp. 11-13.

7. Bourodimos, E.L., and Ippen, A.T., "Characteristics of Open Tube Wave Attenuation System", ASCE Proceedings, Vol. 94, Journal of Waterways and Harbors Division, November, 1968, pp. 465-87.

8. Jarlan, G.E., "A Perforated Vertical Wall Breakwater", The Dock and Harbor Authority, April, 1961, pp. 394-398.

9. Jarlan, G.E., "The Application of Acoustic Theory to the Reflective Properties of Coastal Engineering Structures", National Research Council of Canada, Report No. DME/NAE 1965(1) pp. 23-65.

10. Marks, W., "Perforated Mobile Breakwater for Fixed and Floating Application", Proceedings of the Tenth Conference on Coastal Engineering, Tokyo, Japan, Vol. 2, September, 1966, pp. 1079-1129.

11. Marks, W. and Jarlan, G.E., "Experimental Studies on Fixed Perforated Breakwaters", Proceedings of the Eleventh Conference of Coastal Engineering, London, Vol. 2, September, 1968, pp. 1121-40.

12. "Phillips Ekofisk Million Barrel Oil Storage Tank Nears Completion", Ocean Engineering, Vol. 7, Gulf Publishing Co., July, 1972, pp. 33-5.

13. Morse, W.L., "The Challenge of North Sea Oil", Machine Design, Vol. 45, No. 14, Penton Publications, June 14, 1973, pp. 16-25.

14. James, W., "Rectangular Resonators for Harbor Entrances", Proceedings of the Eleventh Conference on Coastal Engineering, Vol. 2, September, 1968, pp. 1512-30.

15. Tanaka, S., "Researches on Double Curtain Wall Breakwater", Proceedings of the Tenth Conference on Coastal Engineering, 1966, pp. 913-31.

16. Richey, E.P. and Sollitt, C.K., "Attenuation of Deep Water Waves by a Porous Walled Breakwater", Technical Report No. 25, C.W. Harris Hydraulics Laboratory, University of Washington, 1969.

17. Lean G.H., "A Simplified Theory of Permeable Wave Absorbers", Journal of Hydraulic Research, Vol. 5, No. 1, 1967, pp. 15-30.

18. Robertson, J.M., Hydrodynamics In Theory and Application, Prentice-Hall, Inc., Englewood Cliffs, N.J., 1965, pp. 169-70.

19. Burrows, F.G.A., "Wave Force Study", Unpublished Report, C.W. Harris Hydraulics Laboratory, University of Washington, 1969.

20. Richey, E.P. and Nece, R.E., "Reflected Waves on Lake Washington", Technical Report No. 19, C.W. Harris Hydraulics Laboratory, University of Washington, 1966.

21. Jenkins, G.M. and Watts, D.G., Spectral Analysis and its Applications, Holden-Day, Inc., San Francisco, 1968.

22. Lamb, H.B., Hydrodynamics, Dover Publications, New York, 1932.

23. Ippen. A.T., ed., Estuary and Coastline Hydrodynamics, Engineering Societies Monographs, McFraw-Hill Book Co., 1966.

24. "Shore Protection, Planning and Design", Technical Report No. 4, U.S. Army Coastal Engineering Research Center, 3rd ed., 1966.

25. Shapiro, A.H., The Dynamics and Thermodynamics of Compressible Fluid Flow, Vol. 1, The Ronald Press Company, New York, 1953, pp. 100, 359.

26. Thornton, E.B. and Calhoun, R.J., "Spectral Resolution of Breakwater Reflected Waves", ASCE Proceedings, Vol. 98, Journal of Waterways, Harbors and Coastal Engineering Division, November, 1972, pp. 443-460.

27. Kemsait and Childers, "Signal Detection and Extraction of Cepstrum Technique", IEEE Transactions on Information Theory, Vol. II-15, No. 16, November, 1972.

BIBLIOGRAPHY

Alster, M., "Improved Calculation of Resonant Frequencies of Hemholtz Resonators," Journal of Sound and Vibration, 1972, pp. 63-85.

Gibson, G.E., "Pressure Distribution on a Rigidly Supported, Partially Submerged, Structure subjected to Waves in Deep Water", unpublished M.S. Thesis, University of Washington, 1969.

Hogan, D.F., Nece, R.E., and Richey, E.P., "Floating and Other Breakwaters", Unpublished Report, Departments of Civil Engineering and Ocean Engineering, University of Washington, August 1971.

Hom-ma, M., Horikawa, K., Mochizuki, H., "Experimental Studies on Floating Breakwaters", Coastal Engineering in Japan, Vol. 7, 1964. pp. 85-94.

Hom-ma, M., Horikawa, K., "Experimental Study on Total Wave Force Against Sea Wall", Coastal Engineering in Japan, Vol. 8, 1965, pp. 119-29.

Hom-ma, M., Horikawa, K., and Komori, S., "Response Characteristics of Underwater Wave Gauges," Coastal Engineering, Vol. 1, 1966, pp. 99-114.

Johnson, E.R., "Horizontal Forces Due to Waves Acting on Large Vertical Cylinders in Deep Water," Trans. of the ASME, Journal of Basic Engineering, December 1972, pp. 862-866.

Kamel, A.M., "Water Wave Pressures on Seawalls and Breakwaters", U.S. Waterways Experimental Station Research Report 2-10, February 1968, pp. 39.

Murk, W.H., Snodgrass, F., and Tucker, M.J., "Spectra of Low-Frequency Ocean Waves", Scripps Institution of Oceanography Bulletin, 1959, pp. 283-361.

Muraki, Y., "Field Observations of Wave Pressure, Wave Run-Up, and Oscillation of Breakwater," Coastal Engineering, Vol. 1, 1966, pp. 302-321.

Stoker, J., Water Waves, Pure and Applied Mathematics, Vol. 4, Interscience Publishers, New York, N.Y., 1951.

Thornton, E.B., "Spectral Resolution of Breakwater Reflected Waves," Journal of Waterways, Harbors and Coastal Engineering Division, ASCE, November 1972, pp. 443.

Tucker, E.O., "Transmission of Water Waves Through Small Apertures", Journal of Fluid Mechanics, 1971, pp. 65-74.

Wiegel, R.L., Oceanographical Engineering, Prentice-Hall, Inc., 1964.

Note: Appendices I through IV of this report, pages 132-236,containing tabulations and CalComp plots of representative records of various chamber widths and wind conditions, have not been included in the main report. Copies have been filed with the State of Washington, Washington State Highway Commission, Department of Highways, Olympia, Washington.